Reliability-Based Design Optimization of Nonlinear Beam-Columns

Zhongwei Li

Dissertation submitted to the faculty of the Virginia Polytechnic Institute and State University in partial fulfillment of the requirements for the degree of

Doctor of Philosophy
in
Aerospace Engineering

Mayuresh Patil, Chair
Alan J. Brown
Rakesh K. Kapania
Kevin G. Wang

Mar. 23, 2018
Blacksburg, Virginia

Keywords: Ultimate Strength, Nonlinear Beam-Column, Sensitivity Analysis, Structural Optimization, Structural Reliability, Reliability-Based Design Optimization

Reliability-Based Design Optimization of Nonlinear Beam-Columns

Zhongwei Li

ABSTRACT

This dissertation addresses the ultimate strength analysis of nonlinear beam-columns under axial compression, the sensitivity of the ultimate strength, structural optimization and reliability analysis using ultimate strength analysis, and Reliability-Based Design Optimization (RBDO) of the nonlinear beam-columns. The ultimate strength analysis is based on nonlinear beam theory with material and geometric nonlinearities. Nonlinear constitutive law is developed for elastic-perfectly-plastic beam cross-section consisting of base plate and T-bar stiffener. The analysis method is validated using commercial nonlinear finite element analysis. A new direct solving method is developed, which combines the original governing equations with their derivatives with respect to deformation matric and solves for the ultimate strength directly. Structural optimization and reliability analysis use a gradient-based algorithm and need accurate sensitivities of the ultimate strength to design variables. Semi-analytic sensitivity of the ultimate strength is calculated from a linear set of analytical sensitivity equations which use the Jacobian matrix of the direct solving method. The derivatives of the structural residual equations in the sensitivity equation set are calculated using complex step method. The semi-analytic sensitivity is more robust and efficient as compared to finite difference sensitivity. The design variables are the cross-sectional geometric parameters. Random variables include material properties, geometric parameters, initial deflection and nondeterministic load. Failure probabilities calculated by ultimate strength reliability analysis are validated by Monte Carlo Simulation. Double-loop RBDO minimizes structural weight with reliability index constraint. The sensitivity of reliability index with respect to design variables is calculated from the gradient of limit state function at the solution of reliability analysis. By using the ultimate strength direct solving method, semi-analytic sensitivity and gradient-based optimization algorithm, the RBDO method is found to be robust and efficient for nonlinear beam-columns. The ultimate strength direct solving method, semi-analytic sensitivity, structural optimization, reliability analysis, and RBDO method can be applied to more complicated engineering structures including stiffened panels and aerospace/ocean structures.

Reliability-Based Design Optimization of Nonlinear Beam-Columns

Zhongwei Li

GENERAL AUDIENCE ABSTRACT

This dissertation presents a Reliability-Based Design Optimization (RBDO) procedure for nonlinear beam-columns. The beam-column cross-section has asymmetric I shape and the nonlinear material model allows plastic deformation. Structural optimization minimizes the structural weight while maintaining an ultimate strength level, i.e. the maximum load it can carry. In reality, the geometric parameters and material properties of the beam-column vary from the design value. These uncertain variations will affect the strength of the structure. Structural reliability analysis accounts for the uncertainties in structural design. Reliability index is a measurement of the structure's probability of failure by considering these uncertainties. RBDO minimizes the structural weight while maintaining the reliability level of the beam-column. A novel numerical method is presented which solves an explicit set of equations to obtain the maximum strength of the beam-column directly. By using this method, the RBDO procedure is found to be efficient and robust.

Acknowledgement

First of all, thanks to late Dr. Owen Hughes for offering me the opportunity of studying at the Aerospace and Ocean Engineering department of Virginia Tech. Under his supervision I first started this research on ultimate strength. May he rest in peace.

My advisor, Dr. Patil has provided the most valuable guidance throughout the research in this dissertation. His knowledge, vision and detailed explanation have helped me understand and solve the problems in the research. His passion in research and teaching, effective way of conveying knowledge, his patience and kindness will keep him as a role model in my future career.

My committee members, Dr. Brown, Dr. Kapania and Dr. Wang gave useful comments on this dissertation. I have learned practical skills and knowledge from the courses they offered at Virginia Tech.

In the past year, I received assistantship from the Aerospace and Ocean Engineering department of Virginia Tech. Dr. Canfield's Structural Optimization course is helpful for my research on optimization and reliability analysis. Thanks to everyone in the AOE department.

When I graduated from college in China, my former advisors, Dr. Yousheng Wu and Dr. Weicheng Cui offered me the guidance and training opportunity to start the career as a researcher and engineer. In those two years I gained the skills and experiences that I have been relying on ever since. I wish them the best.

It is a long journey completing this PhD dissertation. From the beginning to end, I appreciate the help and support coming from friends, colleagues and many others on countless occasions. Thanks to everyone who has helped me in the past.

Finally, my parents, my brother and all other family members are always supportive of me pursuing my goals. Thanks to all for the understanding.

Contents

List of Figures

List of Tables

1 Chapter One

Introduction

Deterministic structural design using yield criteria is a common practice for aerospace, ocean and land-based structures. Ships and offshore structures operate in the harsh ocean environment under large amount of uncertainties, including random wave/wind loads, nondeterministic structural properties and unpredictable human errors. These uncertain factors have to be considered in the design for structural safety.

Traditionally in ocean structural design, the rare extreme cases like one-hundred/thousand-year storm, were often used as the design load depending on the structural type. Ship design usually uses working stress design (WSD) method which applies a safety factor to the yield stress (American Bureau of Shipping, 2017). In offshore industry the load resistance factor design (LRFD) method is commonly used (Det Norsk Veritas, 2014). LRFD applies different levels of safety factors to different loads. LRFD method is a reliability-based design method because it accounts for some of the uncertainties in the design (Hughes and Paik, 2010). Offshore industry is relatively new which and has developed since the mid-twentieth century compared to the over-hundred-year history of modern ship industry. So the more advanced design methodology is adopted more broadly. Other more accurate reliability analysis methods like the first order, second order method and stochastic design take consideration of more uncertain factors than the partial safety factor method (Hughes and Paik, 2010).

Structural optimization is important for ocean structural design, especially for high speed ships. Lower structural weight means lower material cost. Cargo ships or passenger ships can carry more live load by reducing self-weight. For high speed ships lower structural weight is also important in reducing the resistance leading to higher efficiency. However, lower weight requires thinner and less strong structural members. There is a trade-off between structural weight and structural

strength. The objective of structural optimization is to achieve the balance of the two goals, i.e. to reduce structural weight while maintaining a strength level.

If yield criteria and extreme design loads are used for elasto-plastic materials like aluminum and steel, the structural deformation is only allowed in the elastic range. However, the extreme load case will be encountered rarely. Most of the time the working load during operation is much lower than the design load. In rare occasions the working load may exceed the design load. Under these extreme circumstances, the structure may have plastic deformations at some local area but still maintain structural integrity. Once the extreme load is not in effect, these permanently deformed local structures can be repaired or replaced during maintenance. Thus, if plasticity is allowed, design by yield criteria will be over conservative because the structure can still take additional load after yielding occurs and before reaching the ultimate strength. Ultimate strength design uses the maximum load carrying capacity as the limit by allowing plasticity. Therefore, design by ultimate strength criteria is more rational for structures that allow plastic deformation.

These are three aspects of rational structural design. Firstly, ultimate strength criterion is used for structural analysis. Secondly, reliability analysis is used to account for the design uncertainty. Thirdly, structural optimization is used to find the minimum weight design that satisfies the strength requirement. The goal of this dissertation is to develop Reliability-Based Design Optimization (RBDO) methodology that combines these three aspects. The structure in consideration is the commonly used stiffener-plate combination made of elasto-plastic material. The objective is to find the minimum weight design with reliability index constraint under ultimate limit state.

1.1 ULTIMATE STRENGTH

Research on ultimate strength of stiffened panels started as early as mid-20th century. Various forms of empirical formulas have been proposed based on test results and numerical analysis (Zhang, 2016). In the past few decades, the development of nonlinear finite element tools and increasing computational power have made it easier to perform full structure ultimate strength

analysis. For example, there is research on ultimate strength analysis of ship structures using nonlinear finite element analysis (FEA) (Paik et al, 2008c).

For large ships and offshore structures, full scale test is not realistic. Full nonlinear finite element analysis is too costly and the numerical convergence for large model is difficult. Moreover, during the design cycle structural properties are constantly changing, so a large number of analyses will be repeated. The research of ultimate strength has been focused on the basic structural units: stiffened panels or so called 'grillage' which is the combination of base plate and attached stiffeners (Paik et al, 2008b).

One common approach in large structure's strength analysis is to break down the structure into hierarchical models (Hughes and Paik, 2010). A coarse global finite element model is used for the entire structure. The coarse elements of ship structures are usually cross-stiffened panels bounded by strong members like girders and bulkheads. From the global analysis, the global loads can be transferred onto individual panels. In detailed engineering, the ultimate strength analysis is applied to the stiffened panels under the local loads which is the combination of axial compression, bending moment, shear force, torsional force and lateral pressure.

The stiffened panels under large loads will fail due to the development of plasticity at various locations and in various deformed modes. There are several factors affecting the failure modes, including the load combination, initial imperfection and structural scantlings. There are six typical failure modes for cross-stiffened panels (Paik and Thayamballi, 2003). These failure modes normally interact with each other and cannot be clearly separated. Due to the complexity of material and geometric nonlinearities, there is no analytic solution for the stiffened panel ultimate strength analysis. Some semi-analytic methods have been developed for some of the failure modes. For example, orthotropic plate theory can be applied to panels with small stiffeners under axial compression (Paik and Lee, 2005). Beam-column model can be used for panels with large stiffeners under uniaxial compression (Chen, 2003). These methods have been integrated into finite element analysis packages as the local ultimate strength analysis module (MAESTRO Marine, 2016).

IACS (International Association of Classification Societies) Common Structure Rule has included the incremental iterative method to calculate the ultimate strength of ship mid-section (IACS, 2005). It is inefficient and the results are approximate due to some assumptions. Numerical methods like nonlinear finite element analysis have shown accuracy when compared to structural test results (Ghavami and Khedmati, 2006). Some simple ultimate strength design formulas are based on data from nonlinear FEA and structural tests (Cho et al, 2013). In general, these formulas have practical use because of the simplicity but the accuracy is not ideal. Some influential design variables, like initial imperfection, are not included in the formula. Nonlinear FEA is reliable for ultimate strength analysis if the model is set up properly but the cost of modeling and computation is high. FEA results of stiffened panels under various load combinations have been used as the benchmark for ultimate strength analysis method (Xu and Soares, 2013). Recent works has used nonlinear FEA for the ultimate strength analysis of cracked, pitted or damaged panels, and panels of innovative or unconventional design (Wang et al, 2015; Paik and Kumar, 2006; Badran et al, 2013; Brubak et al., 2013).

Beam-column model has been successfully used to predict the ultimate strength of stiffened panels under uniaxial compression (Hughes et al., 2004). A beam-column model consists of the stiffener and the attached plate strip. The cross-section has asymmetric I shape. The nonlinear beam-column model is the structure focused in this dissertation.

Chapter 2 presents beam-column ultimate strength load-incremental analysis method based on nonlinear beam theory. The nonlinear constitutive equations for the asymmetric I cross-section and elasto-plastic material are developed.

1.2 STRUCTURAL OPTIMIZATION

Structural optimization had a long history and the optimization techniques have advanced with fast pace during the last a few decades with the development of modern computers (Haftka and Gurdal, 1992). The two main branches of structural optimization, mathematic programming and optimality criteria, have been applied to various size, shape and topological optimization problems (Palizzolo,

2004; Bielski and Bochenek, 2008; Ohsaki and Pan, 2009). Finite element method is often used for structural analysis in the optimization. The iterations of optimization algorithms usually require large number of structural analysis (Lamberti et al., 2003). In order to improve the efficiency for large and complex structures, various techniques like adjoint method, constraint/force approximation, design variable linking, have been developed to reduce the number of design variables and structural analysis (Haftka and Gurdal, 1992). A robust optimizer requires accurate design variable sensitivity. Finite difference sensitivity is often used for convenience but the numerical errors from small step size can be significant and can affect the convergence of the optimization algorithm. Complex step sensitivity is very accurate if it can be calculated from the structural analysis. Analytic sensitivity requires extra effort to be derived from the structural analysis but it significantly improves the efficiency and the robustness of the optimization.

Chapter 3 presents deterministic beam-column structural optimization with ultimate strength constraint. The beam-column ultimate strength direct solving method is used to calculate finite difference sensitivity which is more accurate than the sensitivity calculated by load-incremental analysis method. The nonlinear beam-column gradient-based optimization converges faster and is more robust than non-gradient-based algorithm.

1.3 STRUCTURAL RELIABILITY ANALYSIS

All parameters in structural design are non-deterministic in reality. The material properties, structural scantlings and initial imperfection have probabilistic distributions. The mean of the variable is the design value and the variance depends on the quality of manufacturing and fabrication (Xu et al., 2015). In ocean environment, the short term wave loads follow Raleigh distribution and long term wave loads follow Weibull distribution (Hughes and Paik, 2010). Oceanographic data also provides the scatter diagram for specific sea area in different seasons. The scatter diagram provides the probability of waves in different direction and of various significant wave height, which is often used for structural fatigue analysis. Besides the parameters that can be described by probabilistic distributions, some other factors like meteorological phenomenon, extreme waves, accidents and human factors, are epistemic or cannot be

characterized by a mathematical distribution. For example, the squall wind is completely random with unpredictable and constantly changing magnitude and direction. By ignoring the variation of random variables, the deterministic designs always have an unknown chance of structural failure even with imposed safety factors. Reliability is a better measurement of structural safety as it accounts for the uncertainties that can cause structural failure.

Partial safety factor design has basic reliability consideration compared with the deterministic design which has a single safety factor on the working stress. In partial safety factor design different levels of safety factors are applied to different aspects of the design so the randomness of variables is addressed. If all the random variables can be described by mathematical distributions, first order and second order reliability methods are quite accurate in predicting the probability of failure provided the failure surface is not highly nonlinear. The first order second moment method has been widely used in practice (Ba-abbad et al., 2003). With more complicated mathematical approach, full probabilistic analysis can be performed in the reliability calculation (Hughes and Paik, 2010). Sampling method is usually used to validate the reliability analysis. Monte Carlo Simulation is often very costly and time consuming because large samples of structural analysis is required. Some techniques like Importance Sampling and Latin Hypercube Sampling can improve the efficiency (Choi, Grandhi & Canfield, 2007). When the failure probability is small, sampling method becomes unrealistic. For designs having epistemic variables, uncertainty quantification analysis can be used for reliability estimation (Hale, 2016).

Chapter 4 presents structural reliability analysis for nonlinear beam-columns with ultimate strength constraint. First Order Reliability Method (FORM) is used to calculate the reliability index by optimization technique and beam-column ultimate strength direct solving method is used as the limit state function. Complex step sensitivity of ultimate strength with respect to random variables is calculated for the reliability analysis. The complex step sensitivity is more robust than finite difference sensitivity and as accurate as the analytic sensitivity.

1.4 RELIABILITY-BASED DESIGN OPTIMIZATION

Reliability-Based Design Optimization (RBDO) adds reliability constraint to optimization thus accounting for the uncertainties in the analysis and design parameters. RBDO considers the cost, performance and safety of the design under uncertainties at the same time. In structural design, RBDO is usually solved as a double loop optimization problem. In the outer loop, the objective of structural optimization is to minimize the weight and the main constraint is to limit the reliability index. The inner loop of RBDO calculates the reliability index at the current design point. First Order Reliability Method (FORM) is accurate in calculating the reliability index if the structure's failure surface is not highly nonlinear near the design point. The reliability index of FORM is the distance from the origin to the Most Probable Point (MPP) in the normalized random variable space. The search for MPP can be solved by an optimization procedure that finds the minimum distance from the origin to the failure surface. Thus RBDO using FORM is represented by a double loop optimization problem (Choi, Grandhi & Canfield, 2007). Sensitivity analysis is important for gradient-based optimization algorithms. Semi-analytic sensitivity calculates the sensitivity from linear sensitivity equations with analytic coefficient matrix and numerical structural residuals. Semi-analytic sensitivity has less computational cost as compared to complex step sensitivity. It is as accurate as the analytic sensitivity and is more robust than finite difference sensitivity as it eliminates the subtractive cancellation error at small step size.

Chapter 5 demonstrates Reliability-Based Design Optimization procedure for nonlinear beam-columns by using the ultimate strength direct solving method, semi-analytic sensitivity and gradient-based optimization algorithm.

2 Chapter Two

Ultimate Strength of Steel Beam-Columns under Axial Compression

2.1 TITLE

Ultimate Strength of Steel Beam-columns under Axial Compression

By: Zhongwei Li, Mayuresh Patil and Xiaochuan Yu

2.2 ABSTRACT

This paper presents a semi-analytical method to calculate the ultimate strength of inelastic beam-columns with I-shaped cross-section by using geometrically-exact beam theory. A computer code based on this method has been applied to beam-columns under axial compression. The results agree with nonlinear finite element analysis. Compared with previous step-by-step integration approach, this new method is more efficient and can be extended to multi-span beam-columns and other load combinations including lateral pressure. The presented beam-column model is ideally suited for ultimate strength prediction of stiffened steel panels of ships and offshore structures.

2.3 INTRODUCTION

Stiffened panels are widely used in ships and offshore structures. Cross stiffened panel is usually called “grillage”. The strength of these grillages is important to structural safety. When the hull deforms in ocean waves, the stiffened panels is subjected to axial compression along with other loads including lateral pressure. In recent years, the ultimate strength of stiffened panels under these loading conditions has drawn significant interest in ocean structural design, especially for high performance ships (Paik and Thayamballi, 2003).

A typical grillage has bulkheads and frames in transverse direction. In longitudinal direction there are stiffeners built up or rolled up on the plates. Buckling analysis is important to the design of stiffened panels. Besides structural tests (Mukherjee and Yao, 2006), the ultimate strength of grillage can be calculated using analytical methods based on beam-column model or orthotropic plate model and numerical methods like finite difference method and finite element method. Due to the cost of tests, usually the results from nonlinear finite element analysis are benchmarks for ultimate strength analysis (Ghavami and Khedmati, 2006). Using commercial nonlinear finite element analysis software is time-consuming in terms of setting up and calibrating the analysis using tests, and creating finite element models and running numerous load cases. On the other hand, simple design formulas are not always accurate for all the cases (Paik, 2007).

Paik et al. have done intensive research on the ultimate strength of beam-columns, plates and cross stiffened panels. The loads include uniaxial compression, biaxial compression and additional lateral pressure and edge shear (Paik et al, 2008a, 2008b, 2008c). The developed methods have been integrated in a program ULSAP and have been used in ship structural design (Paik et al, 2008d) and optimization (Ma et al, 2013). Details of the approach can be found in a recently published book (Hughes and Paik, 2010). Plasticity is accounted for by using empirical formulations to avoid difficulties of solving the governing equations with both geometric and material nonlinearities. The empirical formulas are based on the results of nonlinear finite element analysis. Zhang (2016) reviewed the current state of panel ultimate strength research and presented another set of formulas. Cho et al. (2013) developed an ultimate strength formulation for stiffened panel subject to combined loading. The unknown coefficients in the formulation are obtained by regression analysis based on numerical solution.

The empirical formulas are approximations to either test data or numerical method. However, test data are limited and the initial imperfections of the test specimens are uncontrollable. Most of the formulas have already included a range of initial imperfection. Similarly, numerical analysis like nonlinear FEM also has applied initial deformed shape and deflection on the model. The fitted formulas may likely differ from numerical solutions if the initial imperfection changes.

Brubak et al. (2013) developed a semi-analytical method to predict the ultimate strength for stiffened panels. Plasticity in the stiffeners is accounted for by reducing the cross-sectional area.

Chen and Lui (1987) have done comprehensive research on beam-column buckling problems. Based on this, Chen (2003) developed a modified step-by-step integration method to calculate the ultimate strength of inelastic beam-columns under axial compression. Furthermore, the beam-column ultimate strength was used to predict the ultimate strength of stiffened panels and the results agreed with ABAQUS nonlinear analysis. When solving three span beam-column problems, this approach assumes that the end bay remains elastic under axial compression. This method becomes inefficient for beam-columns with three or more spans without this assumption because of additional inner supports. The step-by-step integration is iterative and has to converge at each support point. Each additional support leads to additional iteration cycle. It is also difficult to converge if lateral pressure is added.

The research in this paper presents a semi-analytical method of inelastic beam-column buckling analysis. Based on geometrically-exact beam theory (Hodges, 2006), the solution is obtained directly by numerical method without step-by-step integration. The efficiency and accuracy enables this approach be used for stiffened panel ultimate strength prediction by beam-column method under various loading conditions. The beam-column ultimate strength results are compared with nonlinear finite element buckling analysis (by using ABAQUS and ANSYS) for validation. This method can be used on beams of other cross-sectional shape and of various materials as long as the nonlinear constitutive law is correctly established.

2.4 ULTIMATE STRENGTH

Ultimate limit-state design is based on the criteria of structural plastic collapse or ultimate strength. Figure 2-1 illustrates the nonlinear behavior of a material versus that of a structure. The limit of elastic range of the structure is far from the peak load carried by the structure. Unlike in a material, load redistribution in a structure allows for this ability to carry higher loads. The true margin of

structural load-carrying capacity is thus the ultimate strength and its calculation requires an accurate and efficient nonlinear structural analysis method.

2.4.1 Models of Stiffened Panels

A beam-column model (Chen and Atsuta, 1976) cross section is shown in Figure 2-2. It is different from plate-stiffener separation model or orthotropic plate model. A beam-column model is more suitable for stiffened panels with medium or medium to large size stiffeners.

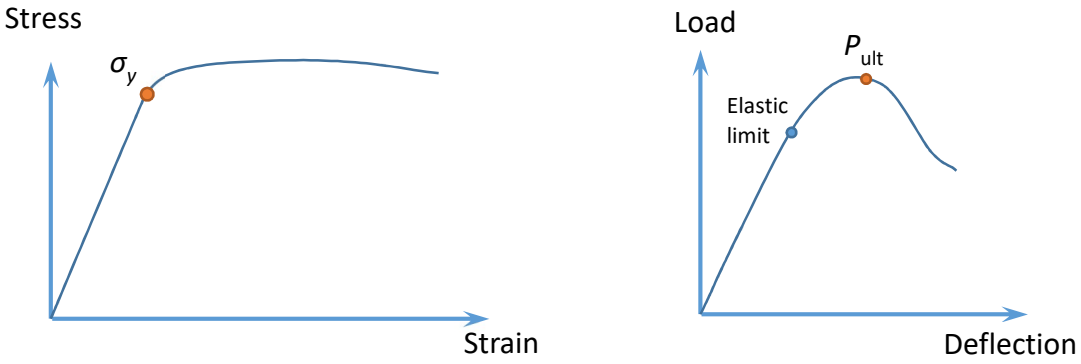

Figure 2-1. Stress-strain relationship of steel and ultimate limit-state of structures (load – deflection).

Figure 2-2. Beam-column model of stiffened panels.

The beam-column ultimate strength approach of this paper is based on geometrically-exact beam theory. The nonlinear intrinsic dynamic equations are written in a matrix form without any geometrical approximation. Since the ultimate strength analysis of beam-columns is quasi-static, dynamic terms can be removed. Hodges developed a simple discretization scheme of geometrically-exact beam equations for a static case (Hodges, 2003) which is used in the present

paper. The research of this paper uses a simplified version of these equations based on several assumptions.

2.4.2 Methodology

When a geometrically perfect beam-column is under compression, the critical load is either the eigenvalue buckling load or squash load, depending on the slenderness.

In ocean structures like ships and offshore platforms, initial imperfections are unavoidable during manufacturing. Therefore, lateral deflection occurs as soon as the beam-column is loaded. Considering the plasticity of steel material, some portion of the cross section will yield first. Consequently, only the portions that remain elastic are capable of carrying additional load. Buckling will occur when the stress level is beyond elastic range of the whole cross-section. This type of buckling is usually referred to as nonlinear buckling. The maximum load carrying capability of inelastic beam-column is the ultimate strength.

2.4.3 Governing Equations

The original equations of motion of geometrically-exact beam theory have dynamic terms (Hodges, 2006). Equations 2.1 to 2.9 are the governing equations of equilibrium of a 2-D geometrically-exact beam. Coordinate system is shown in Figure 2-3 and Figure 2-4. **x** direction is along the beam length. **y** direction is along the axis of symmetry for the I-shaped beam cross section. **z** direction is along the neutral axis of the I-shaped beam cross section. Origin can be chosen at the beam end for convenience.

$$F_x' - (k_z + \kappa_z)F_y + f_x = 0 \qquad (2.1)$$

$$F_y' + (k_z + \kappa_z)F_x + f_y = 0 \qquad (2.2)$$

$$M_z' + (1 + \gamma_x)F_y - \gamma_y F_x + m_z = 0 \qquad (2.3)$$

$$\gamma_x = \cos\theta_z(1 + u_x' - k_z u_y) + \sin\theta_z(u_y' + k_z u_x) - 1 \qquad (2.4)$$

$$\gamma_y = -\sin\theta_z(1 + u_x' - k_z u_y) + \cos\theta_z(u_y' + k_z u_x) \qquad (2.5)$$

$$\kappa_z = \theta_z' \qquad (2.6)$$

$$F_x = c_x(\gamma_x, \gamma_y, \kappa_z) \qquad (2.7)$$

$$F_y = c_y(\gamma_x, \gamma_y, \kappa_z) \qquad (2.8)$$

$$M_z = c_z(\gamma_x, \gamma_y, \kappa_z) \qquad (2.9)$$

In equations 2.1 to 2.9, subscripts *x*, *y* and *z* indicate the components of the variables, parameters, and functions. *F* is the cross-sectional stress resultant force. *M* is the cross-sectional stress resultant moment. *u* is the deflection. k_z and κ_z are the pre-twist/pre-curvature and deformed twist/curvature respectively. *f* is the applied force per unit length and *m* is the applied moment per unit length. θ_z is the rotational angle. γ is the beam generalized strain. c_x, c_y and c_z are nonlinear functions of strain and curvature which determines the stress resultants via the beam cross-sectional integral of the constitutive law for the material. The terms with prime are the derivatives in the direction of beam length (**x** direction).

These equations and the corresponding terms have been explained in detail by Hodges (2006). Equations 2.1 to 2.3 are equilibrium equations. Equations 2.4 to 2.6 are kinematics equations. Equations 2.7 to 2.9 are effective constitutive equations.

Equations 2.1 to 2.9 have 6 differential equations and 3 algebraic equations. There are also 9 unknown variables. Therefore 6 boundary conditions are required to solve the equations.

For half of a simply supported beam in Figure 2-4, with only axial compressive load *P* the boundary conditions will be:

Center: $F_x = -P$; $F_y = 0$; $\theta_z = 0$.

Left End: $u_x = 0$; $u_y = 0$; $M_z = 0$.

For quasi-static beam-column buckling problems, some assumptions can be adopted to reduce the number of unknown variables and equations. If forces are applied only at the end of the beam or additional supports, then $f_x = m_z = 0$. For more complicated load cases with distributed load, these terms can be added into the equations when needed.

2.4.3.1 Shear Assumption

Euler-Bernoulli beam theory is assumed to be applicable here. Euler-Bernoulli assumption leads to infinite shear rigidity (zero shear flexibility) and thus the cross section remains plane after bending, and remains undeformed in the cross sectional plane. It should be noted that there is shear stress in the beam cross section. The shear force can be calculated from equilibrium. Zero shear strain leads to $\gamma_y = 0$.

2.4.3.2 Small Deformation Assumption

The lateral deflection of typical beam-columns in ship structures is small compared with beam length, even in the plastic range. Usually the deflection is less than 1% of the beam length. If δ is a small value which means $\delta << 1$ and L is the beam length, then we have following relationships:

$$\frac{u_x}{L} \sim \delta, \frac{u_y}{L} \sim \delta, \theta_z \sim \delta, \kappa_z \sim \frac{\delta}{L}, k_z \sim \frac{\delta}{L}$$

If there is only axial compressive force acting on the beam-column but no lateral pressure, shear force can be assumed to be a small value compared with axial force, i.e. $F_y \sim \delta \times F_x$ .Equations 2.1 to 2.9 therefore can be further simplified with small deformation assumption by ignoring the second-order small terms.

Equation 2.1 then will only have one variable F_x after the simplification. Actually for the beam-column under only axial compression, F_x equals to the axial compressive force P. u_x will only appear in Equation 2.4 after the simplification. Therefore, Equation 2.1 and 2.4 can be removed from the set. P replaces F_x and u_x can be calculated during post process after the equation set is solved.

If there is only axial compressive force as external load, the simplified version of Equation 2.1 to 2.9 is following:

$$F_y' - \kappa_z P - k_z P = 0 \qquad (2.10)$$

$$M_z' + F_y = 0 \qquad (2.11)$$

$$-\theta_z + u_y' = 0 \qquad (2.12)$$

$$\theta_z' - \kappa_z = 0 \qquad (2.13)$$

$$c_x(\gamma_x, \kappa_z) + P = 0 \qquad (2.14)$$

$$c_z(\gamma_x, \kappa_z) - M_z = 0 \qquad (2.15)$$

2.4.3.3 Nonlinear Constitutive law

In Equation 2.14 and 2.15, c_x and c_z are functions of beam strain γ_x and beam curvature κ_z. c_x and c_z calculate the internal axial force and moment respectively. Let σ, ε be the material stress and strain. The nonlinear constitutive law is derived here for a beam of the I-shaped cross section.

To simplify the problem, elastic-perfectly-plastic steel material model is used in this research as shown by Figure 2-1. In the elastic range while the stress is less than yield stress, linear Hooke's law is used: $\sigma = E\varepsilon$ where, E is Young's modulus of steel, and also the slope of the elastic stress-

strain part in Figure 2-1. In the plastic range, stress is assumed to remain equal to yield stress while strain can keep increasing as seen in the zero slope part in Figure 2-1.

2.4.3.4 Constitutive Law of I-Shaped Cross-section

Figure 2-3 shows the cross section geometry properties of a T type stiffener with attached plating (acting as the bottom flange), representing an asymmetric I-shaped cross section, which is of interest in the present paper.

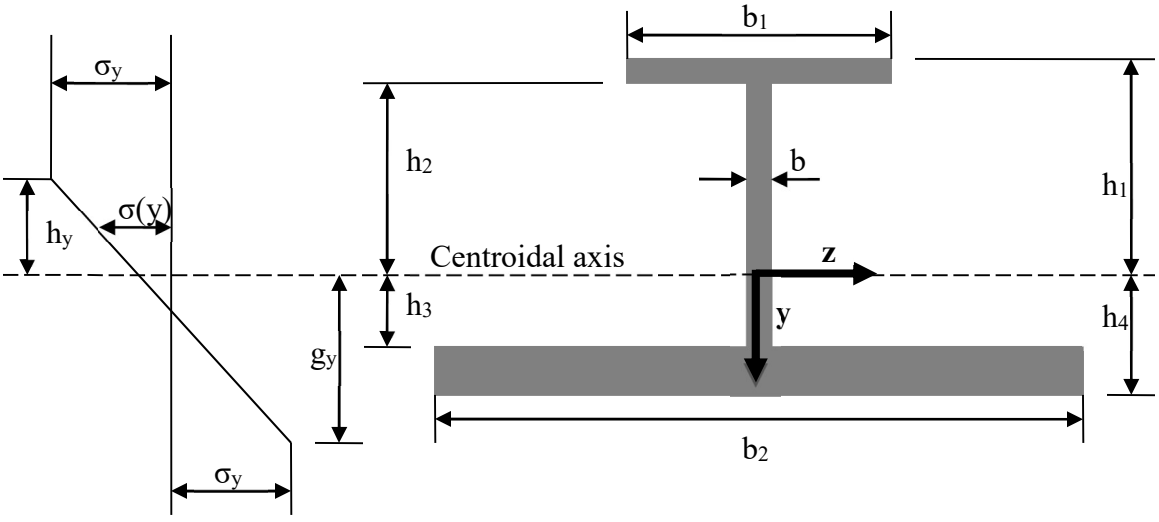

Figure 2-3. Strain diagram and cross-sectional geometry (asymmetric I).

In Figure 2-3, the geometry of beam-column cross-section is defined by parameters b, b_1, b_2, h_1, h_2, h_3 and h_4. Conventionally the cross-section of a T type stiffener with attached plating has been defined by plate width b_p, plate thickness t_p, web height h_w, web thickness t_w, flange width b_f and flange thickness t_f. The following relationships relate the two sets of parameters:

$$b_1 = b_f \,,\, b = t_w \,,\, b_2 = b_p \,,\, h_2 + h_3 = h_w \,,\, h_1 = h_2 + t_f \,,\, h_4 = h_3 + t_p \qquad (2.16)$$

The location of neutral axis can be easily determined by b_p, t_p, h_w, t_w, b_f and t_f in order to get h_1, h_2, h_3 and h_4.

κ_z is the curvature of the beam. If $\kappa_z < 0$, the deformed shape of beam-column is shown in Figure 2-4. The upper part of beam-column is in compression while the lower part may be in extension.

Figure 2-4. Deformed simply supported beam with $\phi < 0$.

In the strain diagram of I-shaped cross-section in Figure 2-3, h_y and g_y are the upper and lower boundaries of elastic zone respectively, i.e. where the elastic stress reaches yield stress. Elastic stress $\sigma(y)$ is calculated by Hooke's Law from elastic strain $\varepsilon(y)$, while in plastic zone the axial stress is always yield stress σ_y. γ_x is the strain at centroid/neutral axis. Therefore if $\kappa_z > 0$:

$$\sigma(y) = E\varepsilon(y),\ \varepsilon(y) = \gamma_x - \kappa_z y, \varepsilon_y = E\sigma_y, h_y = \frac{\gamma_x + \varepsilon_y}{\kappa_z},\ g_y = \frac{\varepsilon_y - \gamma_x}{\kappa_z} \qquad (2.17)$$

By comparing h_1, h_2, h_3 and h_4 with h_y and g_y at a cross section, it can be determined if there is yielding in the plating, web or flange of that cross section. More details of the stress-strain diagram can be found in Chen and Lui[14] and Chen[15].

If $\kappa_z < 0$, then the upper part of beam-column is in compression while the lower part may be in extension or less compression. Equation 2.17 remains valid except that the signs of κ_z and σ_y will change.

If $g_y > h_4$ and $h_y > h_1$ in $\kappa_z > 0$ case, the entire cross-section is in elastic range. Otherwise inside the cross-section there is yielding which could be in the stiffener flange, stiffener web or plate flange, which again depends on the values of h_y, g_y, h_1, h_2, h_3 and h_4. Totally there are 15

possible cases. Each case has different expressions of axial force P and internal moment M. For example, if $g_y > h_4$ and $h_y > h_1$:

$$P = \int_{-h_4}^{-h_3} E\varepsilon(y) b_2 dy + \int_{-h_3}^{h_2} E\varepsilon(y) b dy + \int_{h_2}^{h_1} E\varepsilon(y) b_1 dy \qquad (2.18)$$

$$M_z = \int_{-h_4}^{-h_3} E\varepsilon(y) b_2 y dy + \int_{-h_3}^{h_2} E\varepsilon(y) b y dy + \int_{h_2}^{h_1} E\varepsilon(y) b_1 y dy \qquad (2.19)$$

Expressions of P and M for all 15 cases can be found in the appendix.

By substituting $\varepsilon(y)$ of Equation 2.17 into Equation 2.18 and 2.19, functions $c_x(\gamma_x, \kappa_z)$ and $c_z(\gamma_x, \kappa_z)$ in Equation 2.14 and 2.15 can then be obtained. If $\kappa_z < 0$, the beam-column can be reversed vertically by 180 degrees. Then it is the same as $\kappa_z > 0$ case. That is, by exchanging the values of h_1 and h_4, h_2 and h_3, the functions $c_x(\gamma_x, \kappa_z)$ and $c_z(\gamma_x, \kappa_z)$ of $\kappa_z > 0$ case can still be used.

As an example, for the $\kappa_z > 0$ case if $g_y > h_4$ and $h_y > h_1$, we get the linear elastic law given by:

$$\begin{pmatrix} c_x(\gamma_x, \kappa_z) \\ c_z(\gamma_x, \kappa_z) \end{pmatrix} = \begin{pmatrix} C_{11} & C_{12} \\ C_{21} & C_{22} \end{pmatrix} \begin{pmatrix} \gamma_x \\ \kappa_z \end{pmatrix} \qquad (2.20)$$

where

$C_{11} = b_1 E(h_1 - h_2) + b\ E(h_2 + h_3) + b_2 E(h_4 - h_3)$,

$C_{12} = b_1 E(-h_1^{\,2} + h_2^{\,2})/2 + bE(-h_2^{\,2} + h_3^{\,2})/2 + b_2 E(-h_3^{\,2} + h_4^{\,2})/2$,

$C_{21} = b_1 E(h_1^{\,2} - h_2^{\,2})/2 + bE(h_2^{\,2} - h_3^{\,2})/2 + b_2 E(h_3^{\,2} - h_4^{\,2})/2$,

$C_{22} = b_1 E(-h_1^{\,3} + h_2^{\,3})/3 + bE(-h_2^{\,3} - h_3^{\,3})/3 + b_2 E(h_3^{\,3} - h_4^{\,3})/3$.

Similar expressions can be derived for all other possible cases.

Therefore, the last two governing equations 2.14 and 2.15 are obtained. The set of equations 2.10 to 2.15 has four differential equations and two nonlinear algebraic equations. There are also six unknown variables. With four boundary conditions, the equations can be solved by a proper nonlinear scheme. For half of a simply supported beam-column, the boundary conditions are:

Center: $F_y = 0$; $\theta_z = 0$.

Left end: $u_y = 0$; $M_z = 0$.

2.4.4 Numerical Method

Finite difference method is used to discretize the differential equations. Then the iterative Newton-Raphson scheme is used to solve the set of nonlinear equations.

The beam is discretized into N elements (of length ΔL) with $N+1$ nodes. The unknowns are the values of the variables at each node. (Total variables are $6\times(N+1)$.)

Figure 2-5 shows one discretized beam element and the nodal variables.

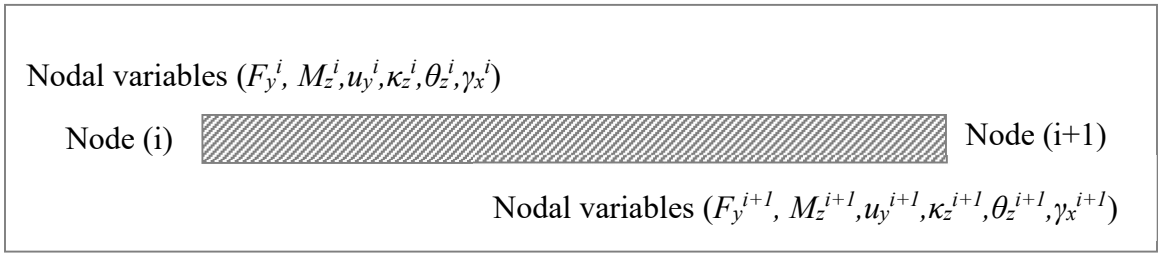

Figure 2-5. One beam element and nodal variables.

The differential equations are approximated for the element in terms of the nodal values using central differencing scheme ($4\times N$ equations). For example, equation 2.10 becomes

$$\frac{F_y^{i+1} - F_y^i}{\Delta L^i} - P\frac{\kappa_z^{i+1} - \kappa_z^i}{2} = k_z P \qquad (2.21)$$

The algebraic equations are satisfied directly at the nodes ($2 \times (N+1)$ equations). At the i[th] node, there is

$$c_x\left(\gamma_x^i, \kappa_z^i\right) = -P \qquad (2.22)$$

$$c_z(\gamma^i{}_x, \kappa^i{}_z) - M^i{}_z = 0 \qquad (2.23)$$

For half of a simply supported beam-column, the boundary conditions are satisfied at the ends. There are four equations:

Center: $F_y^{N+1} = 0$; $\theta^{N+1}{}_z = 0$.

Left end: $u^1{}_y = 0$; $M^1{}_z = 0$.

If there are more supports, elements have to be divided at each support and boundary conditions are added for each support. This will lead to more variables at each support, e.g. reaction force for pin joint, but also more equations.

A computer program ULTBEAM2 has been developed using this scheme to solve the set of Equations 2.10 to 2.15 for beam-columns with I-shaped cross-sections.

2.5 NUMERICAL EXAMPLES

The ultimate strength of two beam-columns calculated by ULTBEAM2 is compared with ABAQUS and ANSYS results. Results from the program ULTBEAM1 of Chen[15] is also listed, which uses the step-by-step integration method. Two different kinds of loading/boundary conditions are analyzed:

- Simply supported beam-column (single-span and three-span) under axial compression;
- Single span clamped beam-column under axial compression.

The ABAQUS model is fine meshed 2-D beam-column using 2 node Timoshenko beam element (B21). The ANSYS beam element model is created using Beam 188 element and the shell element model is created using Shell 181 element. Figure 2-6 shows ANSYS beam element model and shell element model for the half beam-columns. The cross sectional shape is the same as in Figure 2-3 and material property is similar to Figure 2-1. The beam element model is actually one dimensional but is plotted as 3-D to show the cross section and plate thickness. It's been verified that the results from beam element model and shell element model are nearly identical. All the results listed in following tables are from the beam element model.

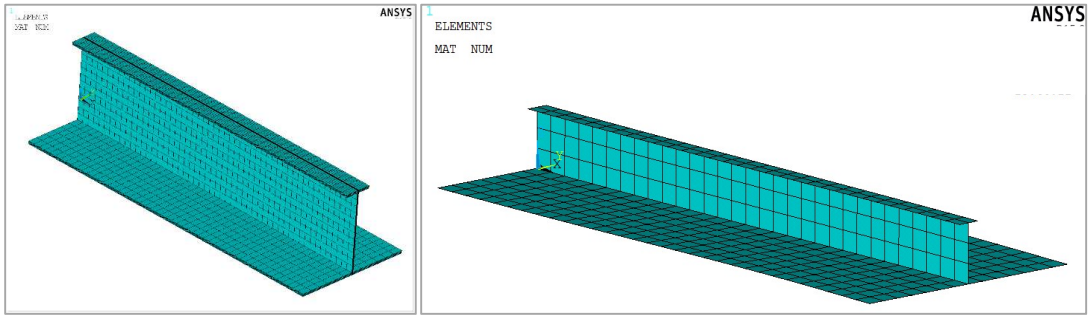

Figure 2-6. FEA model of beam-column B1 (beam element, left) and B2 (shell element, right).

2.5.1 Single Span Simply Supported Beam-Column Under Axial Compression

The initial deflected shape of the beam-columns is assumed to be sinusoidal as shown in Figure 2-4. Initial curvature at each node can be calculated from the maximum deflection. ULTBEAM2 is then used to trace the equilibrium path of beam-column under step-by-step increased axial compression. The maximum value of the axial force is the ultimate strength.

Two sample beam-columns (B1 and B2) with asymmetric I cross-section are studied. The scantlings are listed in Table 2-1. Parameter "a" is the beam length and "w_0" is the initial deflection

at the center of the beam. Other parameters have been explained earlier. These are the same beam-columns analyzed by Chen. Beam B1 has larger stiffener and beam B2 has smaller stiffener. Therefore, the two models represent two different categories of beam-columns.

Table 2-1. Geometric properties of one-span simply supported beam-column (mm).

	a	b_p	t_p	h_w	t_w	b_f	t_f	w_0
B1	5120	910	20	598.5	12	200	20	5.12
B2	1524	304.8	6.4	64.25	4.65	27.94	6.35	2.9

Material properties are:

B1: σ_y = 315.0 MPa, E = 208000 MPa, ν = 0.3

B2: σ_y = 247.3 MPa, E = 205800 MPa, ν = 0.3

Two cases with different initial deflections are studied. One is with the downward initial deflection (toward the plate side, which causes the stiffener-induced failure), and the other one is with the upward initial deflection (toward the stiffener side, which causes the plate-induced failure). The ultimate loads of both the stiffener-induced failure and the plate-induced failure from ULEBEAM1, ULTBEAM2 and ANSYS/ABAQUS are listed in Table 2-2.

Table 2-2. Ultimate strength (σ_{ult} (MPa)) of stiffener and plate induced failure).

	Stiffener-induced				Plate-induced			
	ULTBEAM		FEM		ULTBEAM		FEM	
	Ultbeam1	Ultbeam2	ANSYS	ABAQUS	Ultbeam1	Ultbeam2	ANSYS	ABAQUS
B1	304.1	301.5	304.0	303.6	310.8	309.9	311.3	310.8

B2	167.4	156.9	157.7	158.0	226.3	219.6	220.1	219.6

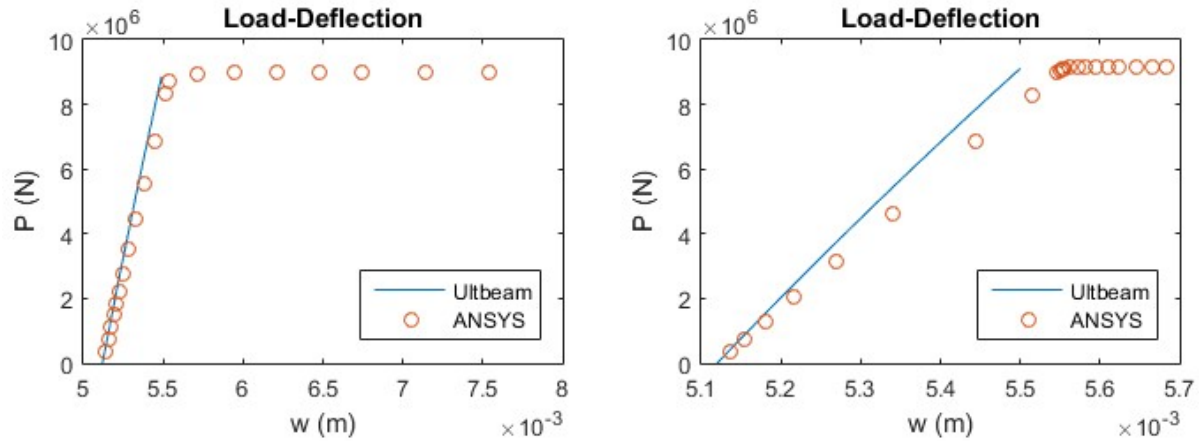

(a) Stiffener-induced failure (b) Plate-induced failure

Figure 2-7. Axial load (N) vs. max deflection (m) for B1.

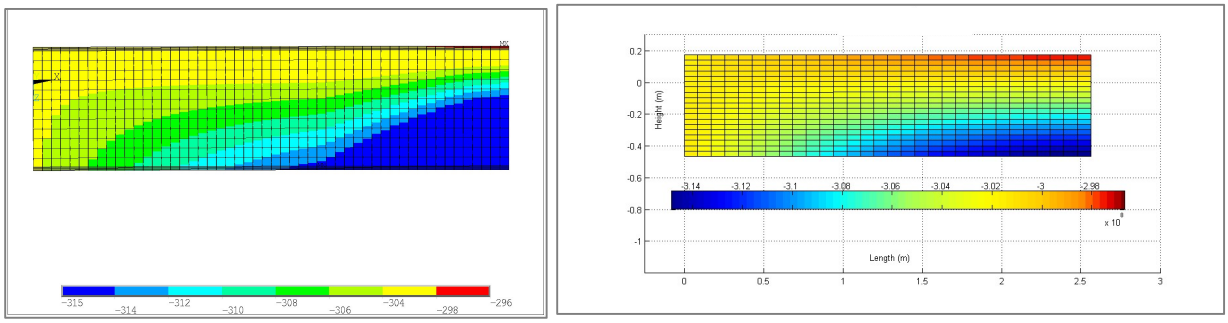

(a) ANSYS (MPa) (b) ULTBEAM2 (Pa)

Figure 2-8. Axial stress contour of B1 under ultimate load (stiffener-induced failure).

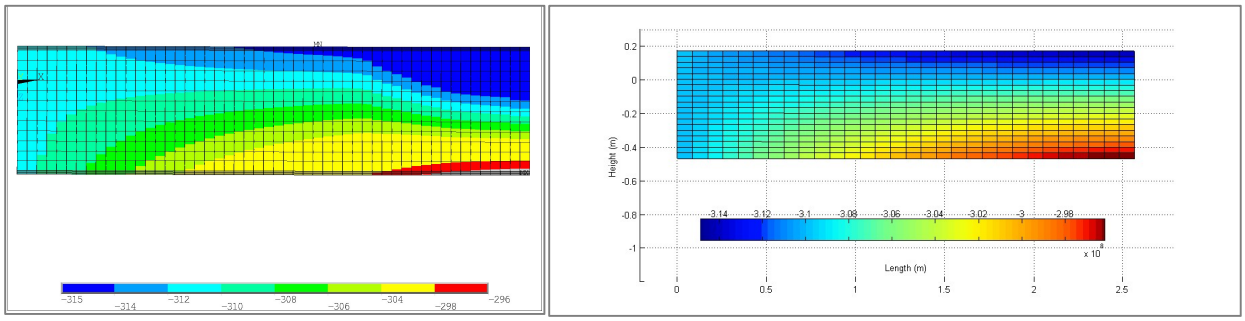

(a) ANSYS (MPa) (b) ULTBEAM2 (Pa)

Figure 2-9. Axial stress contour plot of B1 under ultimate load (plate-induced failure).

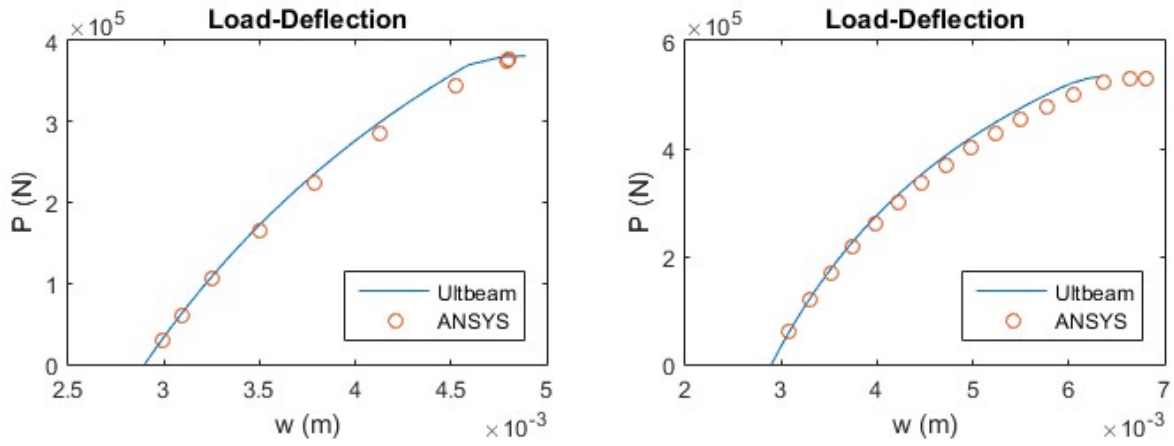

(a) Stiffener-induced failure (b) Plate-induced failure

Figure 2-10. Axial force (N) vs. max deflection (m) for B2.

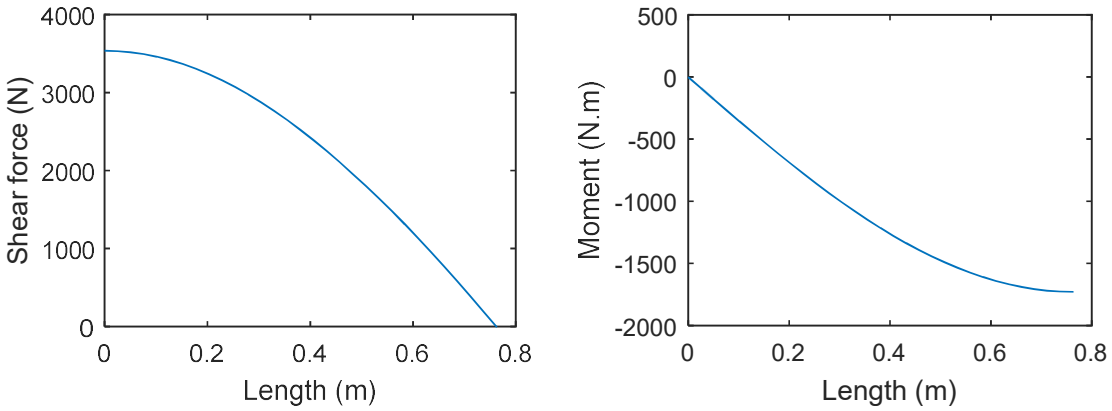

(a) Shear stress along half beam (b) Bending moment along half beam

Figure 2-11. Shear stress and bending moment along half beam of B2 under ultimate load (stiffener-induced failure).

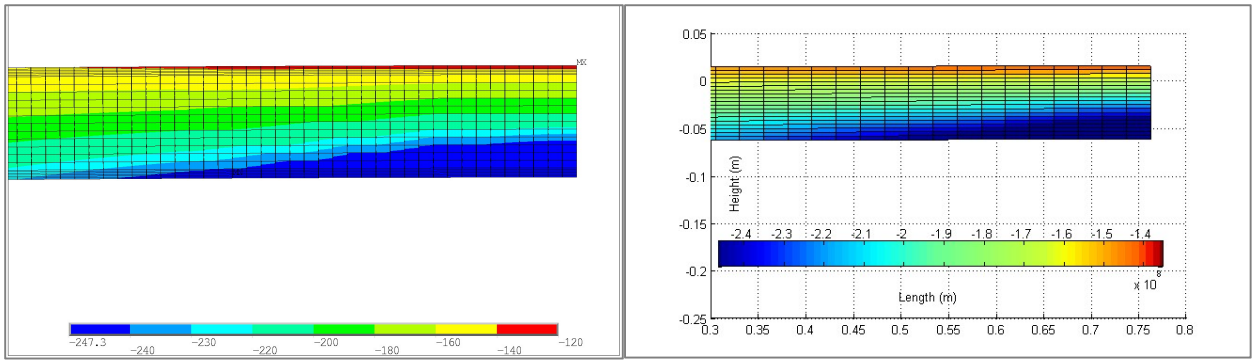

(a) ANSYS (MPa) (b) ULTBEAM2 (Pa)

Figure 2-12. Axial stress of B2 under ultimate load (stiffener-induced failure).

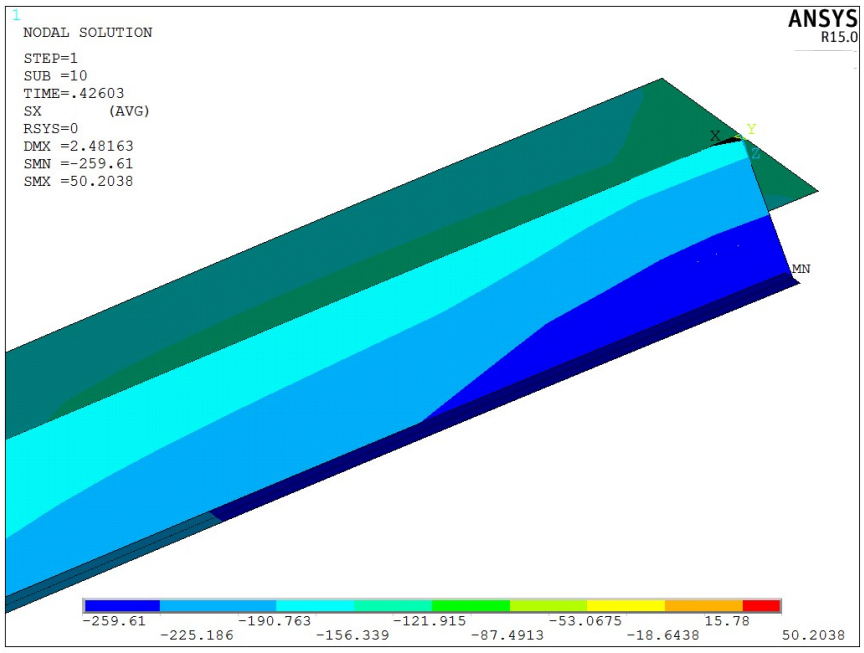

Figure 2-13. Axial stress (MPa) contour plot of B2 under ultimate load (stiffener-induced) by ANSYS shell element model.

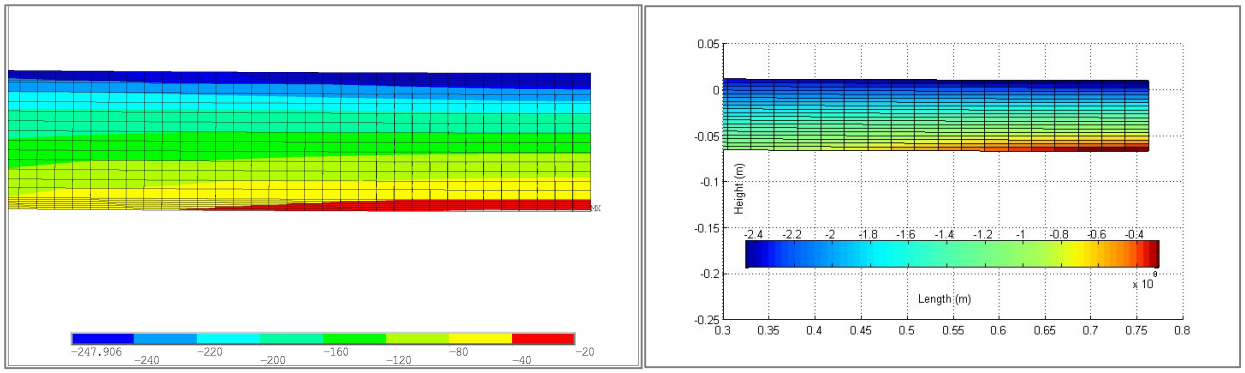

(a) ANSYS (MPa) (b) ULTBEAM2 (Pa)

Figure 2-14. Axial stress contour plot of B2 under ultimate load (plate-induced failure).

Table 2-2 shows that for single span simply supported beam-columns under axial compression the ultimate strength calculated by ULTBEAM2 is very close to ANSYS and ABAQUS results. For beam-column B2, ULTBEAM2 results are closer to FEM results than ULTBEAM1.

Figure 2-7 plots the applied axial force with beam-column maximum deflection (at center) of B1 (for stiffener-induced and plate-induced buckling respectively) from ULTBEAM2 calculation. The maximum value of force P is the ultimate load which is the product of the yield stress in Table 2-2 and the cross sectional area. These plots are similar to the load-deflection curve in Figure 2-1 except that the calculation is stopped at ultimate load. B1 is relatively strong so the ultimate strength is close to yield stress and the load path is close to a straight line in Figure 2-7. On the same figure ANSYS results are plotted. The final ultimate strength values are very close. Although there is difference of maximum deflection between ULTBEAM2 and ANSYS, the scale is minimal. Maximum difference is only about 0.05 mm which is negligible if compared with initial deflection 5.12 mm, plate thickness 21 mm and beam length 5120 mm. On the other hand, the ultimate load is of greater interest and it shows very good agreement.

The axial stress distributions under ultimate load from ULTBEAM2 calculation and ANSYS beam element model analysis are shown in Figure 2-8 for B1 stiffener induced case and Figure 2-9 for

B1 plate induced case. In these plots the plating is at the top and the stiffeners are downwards. The neutral axis is at height 0. The stress contour plots from ULTBEAM2 and ANSYS are very similar to each other.

Figure 2-10 plots the applied axial force with beam-column maximum deflection (at center) of B2 (for stiffener-induced and plate-induced buckling respectively) from ULTBEAM2 and ANSYS. The load-deflection curves in Figure 2-10 clearly show the plasticity of beam-column B2 under axial compression. The curves calculated by ULTBEAM2 are nearly identical with ANSYS results. Figure 2-11 plots the shear force and bending moment along the length of B2 under ultimate load (of stiffener-induced buckling) by ULTBEAM2.

The stiffener-induced inelastic buckling of beam B2 has also been verified by ANSYS shell element model using Arc Length method. The ultimate load calculated by ANSYS shell element model is 158 MPa which is the same as ANSYS beam element model and ABAQUS results in Table 2-2. Figure 2-12 plots the axial stress of B2 under compressive ultimate load calculated by ULTBEAM2 and ANSYS beam element model respectively. Figure 2-13 is the axial stress contour plots from ANSYS shell element model. The stress distributions are very similar in all three plots. Similarly, for plate-induced buckling, the stress distributions are compared in Figure 2-14.

2.5.2 Single Span Clamped Beam-Column Under Axial Compression

Beam-column scantlings are the same as in Table 2-1 for the case of clamped boundary condition. If both ends of the beam-column are clamped, the boundary condition becomes:

Center: $F_y^{N+1} = 0$; $\theta^{N+1}{}_z = 0$.

Left End: $u^1{}_y = 0$; $\theta^1{}_z = 0$.

There are only minor changes to the equation set 2.10 to 2.15 and the Jacobian of the discretized model. A scheme similar to the simply supported case has been used to calculate the beam-column ultimate strength.

Table 2-3 shows the comparison of ULTBEAM1, ULTBEAM2 and ABAQUS calculated ultimate strength. Due to the symmetry, there is no difference of ultimate strength from stiffener-induced and plate-induced failure. Results calculated by ULTBEAM2 are still very close to ABAQUS results with about only 1% difference.

Table 2-3. Ultimate strength (σ_{ult} (MPa)) of clamped beam-column.

	ULTBEAM1	ULTBEAM2	ABAQUS
B1	311.9	308.4	312.1
B2	228.3	230.2	229.0

Figure 2-15 plots the load-deflection curves of B1 and B2 under clamped boundary conditions from both ULTBEAM2 and ANSYS. The maximum deflection is measured at the center of the beam-column including the initial imperfection. Similar to simply supported load case, ULTBEAM results agree with FEM very well. Under ultimate load the maximum deflection of B2 is about 3.25 mm which is less than 1% of the beam length 1524 mm.

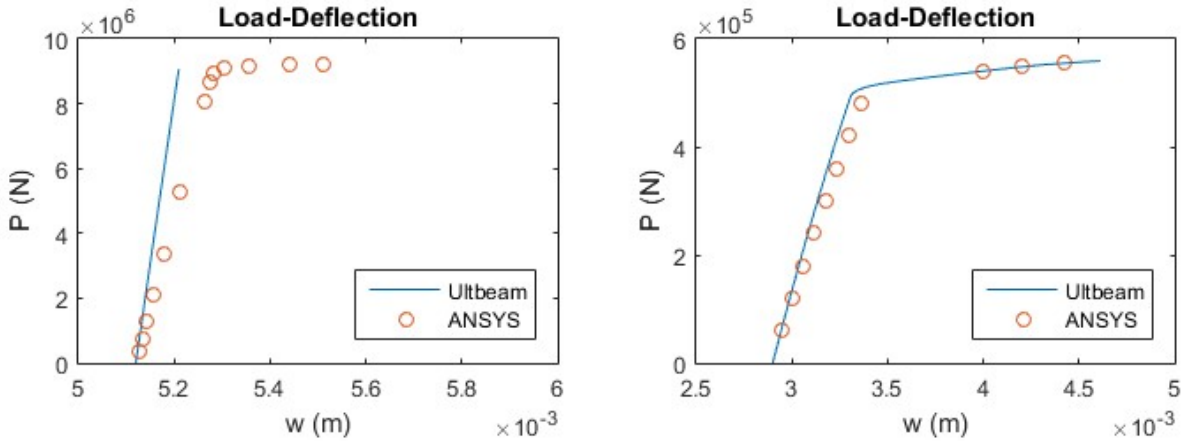

(a) Load-deflection curve of clamped B1 (b) Load-deflection curve of clamped B2

Figure 2-15. Axial force (N) vs. max deflection (m) for clamped beam-columns.

2.5.3 Three Span Simply Supported Beam-Column Under Axial Compression

In addition to the cases described above, 49 three span Beam-columns have been verified. The ultimate strength calculated by ULTBEAM2 and FEM have been compared in Table 4. The scantlings of the beam-columns are the same as from Chen (2003). Both ends of the beam-columns are simply supported and there are two additional restrains equally spaced between the two ends. The difference as indicated by the ratio in Table 2-4 is less than 10% for 45 of the 49 beam-columns. Only one of the 49 cases has large difference which is a beam-column of unusual size with large flange and small web. Correction to such beam-columns will be applied when the results are used for stiffened panel ultimate strength calculation.

Figure 2-16 compares ULTBEAM2 and ABAQUS ultimate strength in a non-dimensional format for all the 49 beam-columns. The ultimate strength has been divided by the yield stress 352.8 MPa. Each point has ULTBEAM2 result as abscissa and ABAQUS result as ordinate. It is visible that the difference is very small because all the data points are close to the diagonal line. Figure 2-17 shows that most of the ratio of ultimate strength from ULTBEAM2 and ABAQUS for the 49 beam-columns are very close to 1. The average of the ratio is 1.0363 and variance is 0.0006.

Table 2-4. Ultimate loads (σ_{ult} (MPa)) of three span simply supported beam-column.

	$\sigma_{ULTBEAM\,2}$	σ_{FEM}	$\sigma_{ULTBEAM\,2}/\sigma_{FEM}$
B1	112.01	102.99 *	1.088
B2	72.58	69.92 *	1.038
B3	82.12	78.20	1.050
B4	205.84	187.90	1.095

B5	145.92	140.20	1.041
B6	176.89	173.30	1.021
B7	321.48	318.40	1.010
B8	245.23	229.00	1.071
B9	235.80	228.60	1.032
B10	109.18	101.40	1.077
B11	68.83	64.30	1.070
B12	75.68	72.80	1.040
B13	160.75	154.30	1.042
B14	135.44	131.40	1.031
B15	116.81	113.20	1.032
B16	297.78	291.60	1.021
B17	270.45	264.10	1.024
B18	220.19	218.20	1.009
B19	86.48	83.10	1.041
B20	81.07	79.20	1.024
B21	48.70	47.43 *	1.027
B22	206.20	203.20	1.015

B23	189.07	187.10	1.011
B24	174.83	173.20	1.009
B25	37.36	36.20 *	1.032
B26	144.36	132.60	1.089
B27	95.13	88.20	1.079
B28	107.60	102.60	1.049
B29	246.05	226.10	1.088
B30	182.02	176.80	1.030
B31	213.19	210.30	1.014
B32	327.74	325.80	1.006
B33	283.34	275.80	1.027
B34	274.18	267.70	1.024
B35	140.01	132.90	1.054
B36	90.55	86.40	1.048
B37	99.30	95.10	1.044
B38	197.56	188.90	1.046
B39	170.35	166.80	1.021
B40	148.81	146.20	1.018

B41	315.44	311.80	1.012
B42	300.06	296.30	1.013
B43	256.05	251.50	1.018
B44	113.96	109.20	1.044
B45	107.04	103.80	1.031
B46	99.08	96.20	1.030
B47	248.28	239.60	1.036
B48	225.44	224.10	1.006
B49	210.71	209.50	1.006

*: ANSYS results.

All other FEM: ABAQUS results.

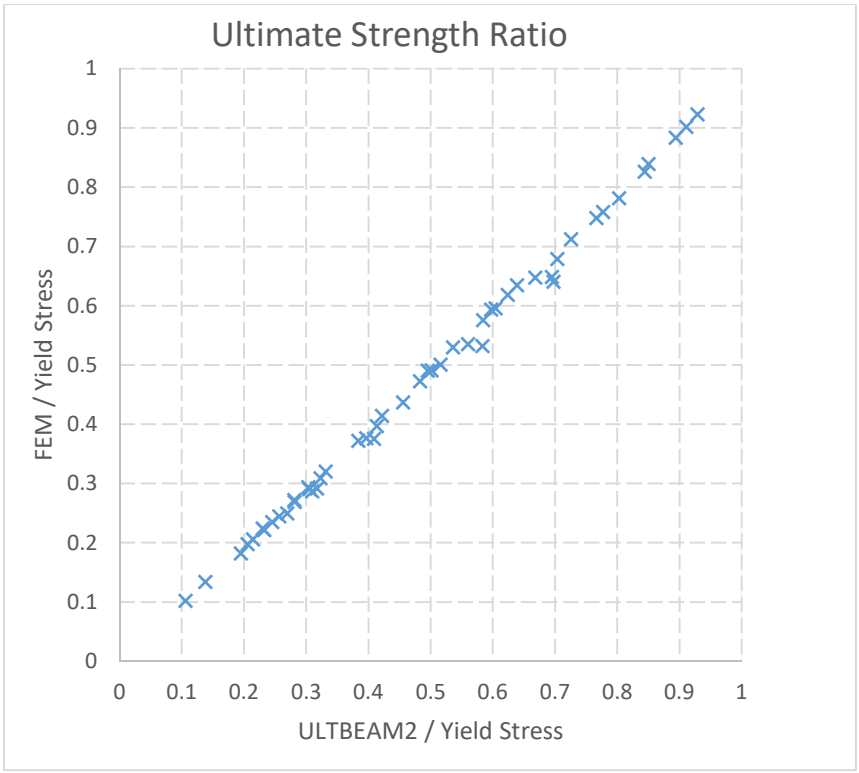

Figure 2-16. Ultimate strength comparison for 49 three-bay beam-columns.

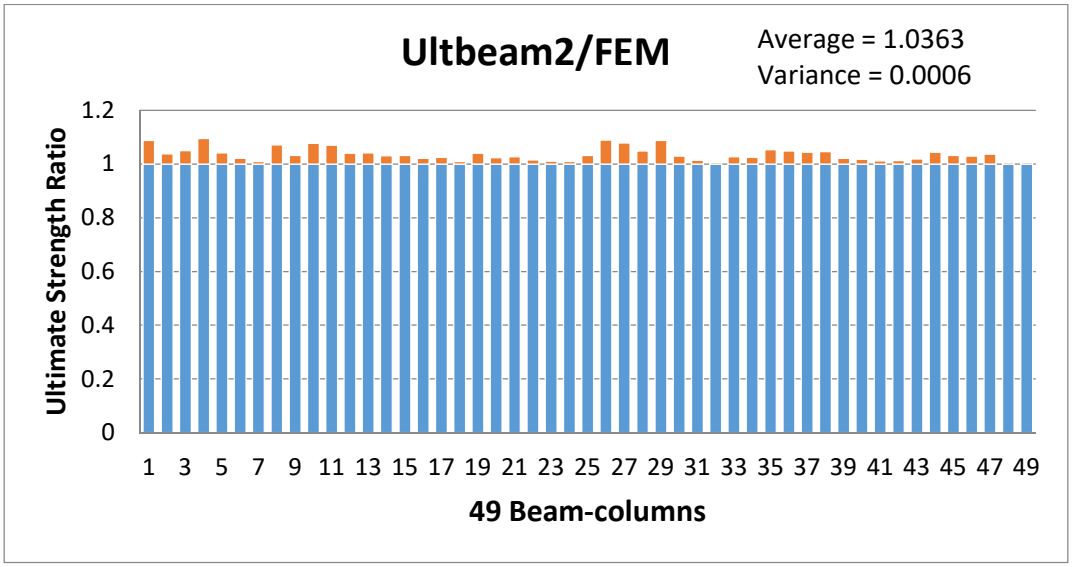

Figure 2-17. Ultimate strength comparison with FEM.

2.6 CONCLUSION

The method of beam-column ultimate strength calculation presented by this paper successfully calculated the axial compressive ultimate load of two single span, I-shaped cross-section, elasto-plastic beam-columns (with T bar stiffener and plate strip) for both simply supported and clamped boundary conditions. The results agree with nonlinear finite element analysis by ABAQUS and ANSYS. The method has also been used for 49 three-span, simply-supported beam-columns under axial compression. The calculated ultimate strength is very close to the results from nonlinear FEM.

This new method is more efficient than previously developed step-by-step integration method. Especially for multi span beam-columns this method only needs to add a few more equations and variables at additional supports without oversimplified assumptions or adding significant computing time.

As a semi-analytical approach, this new method can freely deal with different initial imperfections without simplifying assumptions. Therefore, as an efficient and accurate tool, it can be used for more extensive research regarding ultimate strength instead of using costly nonlinear FEM. The beam-column ultimate strength calculated by current method can be used effectively to predict stiffened panel ultimate strength by using the beam-column model.

Future research work includes improving the non-linear solver for beam-column model governing equations in order to get post buckling results by using Riks algorithm. More load combinations which include pressure will also be considered so that this ultimate strength calculation method can be extended to broader applications.

3 Chapter Three

Structural Optimization of Elasto-Plastic Beam-Columns under Uniaxial Compression

3.1 TITLE

Structural Optimization of Elasto-Plastic Beam-Columns under Uniaxial Compression

By: Zhongwei Li and Mayuresh Patil

3.2 ABSTRACT

This paper presents a procedure for structural optimization of inelastic beam-columns consisting of base plate and T-bar stiffener under uniaxial compression. The goal of the optimization is weight minimization under ultimate strength constraint. The ultimate compressive strength of such beam-columns is calculated using geometrically exact beam theory and the nonlinear constitutive law of elasto-plastic material. These equations are discretized using finite difference spatial discretization and solved using an iterative nonlinear solver, and has been shown to agree with nonlinear finite element analysis. The design variables are cross-section geometric properties including plate width, web height, flange width and member thicknesses. A gradient-based optimization algorithm is used to search for the optimal solution. The improved ultimate strength analysis method developed in this paper can also be used to calculate accurate analytical sensitivities. The analysis, sensitivity analysis and optimization are robust and efficient. Though the focus of the present work is on deterministic design, the optimization procedure can be combined with reliability analysis procedure to perform reliability-based structural optimization for such elasto-plastic beam-columns.

3.3 INTRODUCTION

Stiffened panels are widely used in aerospace, marine and land-based structures. Structural optimization is important in designing structures with lower weight (cost) and higher load carrying capacities.

Usually yield strength and buckling strength are the design criterion for these structures according to various commonly used design codes. Yield criteria does not take into account plastic deformation but in reality the plasticity of ductile material will allow the structure to carry additional load after yielding begins to occur. The true load-carrying limit is the ultimate strength. In addition, structures with initial imperfections will deform under small compressive load and as the load increases, the cross-section will transition from elasticity to progressive development of plasticity in contrast to the sudden collapse of perfect structures under the critical elastic buckling load. The ultimate strength is a more realistic load-carrying capacity of the structures if plastic deformation is allowed.

Structural optimization theories and techniques have been developed and applied to engineering designs. In the past decade, with the advance of the computer aided design tools, various optimization algorithms have been used in the design process. At the same time, ultimate strength design has also been gradually accepted as the design criteria for structures made of elasto-plastic materials like steel and aluminum. However, structural optimization based on ultimate limit state is still challenging due to the complexity of the nonlinear elasto-plastic analysis.

A beam consisting of a stiffener attached to a plate strip is the basic unit of a stiffened panel having multiple stiffeners. A large structural system like ship hulls has hundreds or thousands of such panels. Beam-column type buckling of stiffened panels is very common though it is often coupled with other buckling modes. The research of beam-column ultimate strength and optimization is important because it can be used to design the stiffened panels which in turn can be used in the design of the ship structural system.

Structural tests are the most trustworthy method of finding the ultimate strength. The results from tests may vary depending on the test condition and sample variation. It has been shown (Ghavamia, 2006; Shi, 2012; Xu, 2013) that ultimate strength calculated by nonlinear FEA is close to results of structural tests for beams, stiffened panels and ship hull models. Therefore, nonlinear FEA tools are generally regarded as benchmarks for other ultimate strength analysis approaches including semi-analytical method and simplified design formulas.

Hughes et al. (2004) used a beam-column model to predict the ultimate strength of stiffened panels under compression. The present authors have developed a more efficient method (Li, 2017) to calculate the beam-column ultimate strength and the results have been used to predict the ultimate strength of stiffened panels by applying a correction factor.

Paik et al. (2005) have developed a semi-analytical method for the ultimate strength of stiffened panels under combined loading conditions. This method is part of the panel ultimate strength analysis package ALPS/ULSAP and has been integrated into the ship structural design software MAESTRO.

There is also considerable research on inelastic beam design using various nonlinear buckling analysis methods and optimization algorithms. Palizzolo (2003) studied the minimum weight or maximum load multiplier design for elastic perfectly plastic beam under three limiting criterion.

Ba-abbad et al. (2003) developed a reliability-based optimization method for an elastic-plastic T beam. The gradient-based optimizer first found a deterministic optimum design based on nonlinear FEA. Then the first-order second-moment reliability analysis was used to reduce the structural weight or increase the reliability.

Bielski et al. (2008) optimized non-uniform I cross-section of elastic-plastic columns under axial compression. The nonlinear beam analysis used iterative step-by-step integration along beam segments to find the equilibrium path. The analysis omitted the progressive development of plastic zone. The optimizer used method of moving asymptotes to maximize the buckling load or stable buckling region for a given weight constraint.

Ohsaki et al. (2009) optimized cross-sectional shape of I beam under cyclic loads. The elasto-plastic beam's responses under the cyclic loads were calculated by nonlinear FEA and the optimizer used heuristic Simulated Annealing (SA) algorithm. The optimum design has maximum dissipated energy throughout the loading history which is better than the constant cross-section beams under cyclic loads.

Caseiro et al. (2010) studied sizing optimization of inelastic aluminum plate-stiffener combination under axial compression. The constrained ultimate strength was calculated by nonlinear FEA. Three optimization algorithms, gradient-based, simulated annealing and hybrid differential evolution particle swarm, were compared for minimum weight design. All three optimum inelastic beam designs reduced the weight but the design found by the gradient-based algorithm was not as good as the other two.

Cheng et al. (2010) optimized the stiffeners of moderately thick plates under uniaxial and biaxial compression. The minimum weight design is constrained to have a specified compressive ultimate strength calculated by orthotropic plate theory. The optimum designs obtained by math programming reduced weight from code designs.

Recently Ni et al. (2016) reviewed the progress of buckling and post-buckling optimization of isotropic and composite stiffened panels. It has shown that there hasn't been much research on structural optimization involving dynamic loading, ultimate strength (inelastic buckling) analysis and structures with initial imperfection.

There is some research applying the panel ultimate strength analysis for marine structural optimization. Rinsberg et al. (2013) used IACS ultimate strength design formulas and FEA for the structural optimization of corrugated shell plating on an offshore platform. The optimization of local corrugated shell plating parameters is based on parametric studies in order to reduce the number of analysis.

Hughes et al. (2014) applied vector evaluated genetic algorithm on multi objective ship hull structural design which included the ultimate limit failure modes. The integrated structural analysis

and optimization package is robust and efficient in finding designs of lower weight, cost and higher strength.

Ma et al. (2016) improved the ship structural optimization package based on semi-analytical ultimate strength analysis by decomposing the system level optimization and the multi objective optimization of detailed structures (stiffened panels) within the design software MAESTRO.

The purpose of this paper is to present the sizing optimization methodology of inelastic I beam-columns (T-bar stiffener and plate strip combination) by using gradient-based nonlinear search algorithm and beam ultimate strength analysis method developed by the present authors.

First, the sizing optimization problem is established. The objective function is the structural weight. Design variables are the cross-sectional geometric parameters. The constraint function is the required compressive ultimate strength (maximum load-carrying capacity). Next, the inelastic beam-column buckling analysis is explained including the calculation of design variable sensitivities. The original iterative numerical method is accurate in calculating the beam-column ultimate strength. The improved method presented here can solve for the exact beam ultimate strength directly and analytic sensitivity calculation method can be developed based on this new analysis method. The sequential quadratic programming (SQP) algorithm is used to solve the structural sizing optimization problem with ultimate strength constraint. Lastly, optimization of beam-columns with different design parameters are presented as numerical examples. The gradient-based optimization using the ultimate strength analysis shows robustness by converging at optimum designs efficiently. The convergence is much faster than non-gradient-based algorithm. The paper concludes with related future research topics including reliability-based ultimate strength optimization.

3.4 ULTIMATE STRENGTH ANALYSIS

3.4.1 Beam-Column Model

An I beam consists of a plate strip and attached T-bar stiffener as shown in Figure 3-1. There are six geometric parameters in the cross-section: plate width b, plate thickness t, web height h_w, web thickness t_w, flange width b_f and flange thickness t_f. Figure 3-2 shows the cross-section geometry of such beam-column.

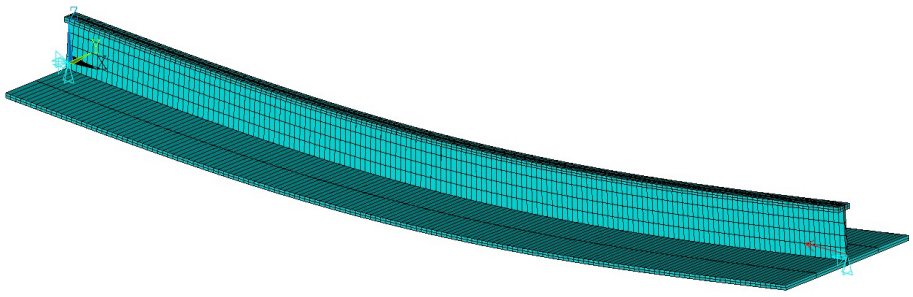

Figure 3-1. Simply supported I beam with initial deflection.

When an inelastic beam with initial imperfection is under compressive axial force, the beam will deflect as the load is applied. As the load is increased above the yield load, a plastic zone is formed at critical locations along the beam. The ultimate strength is the load at which the plastic zone progression leads to a plastic hinge and the beam can carry no more load. The ultimate strength is the maximum load carry capacity of the beam.

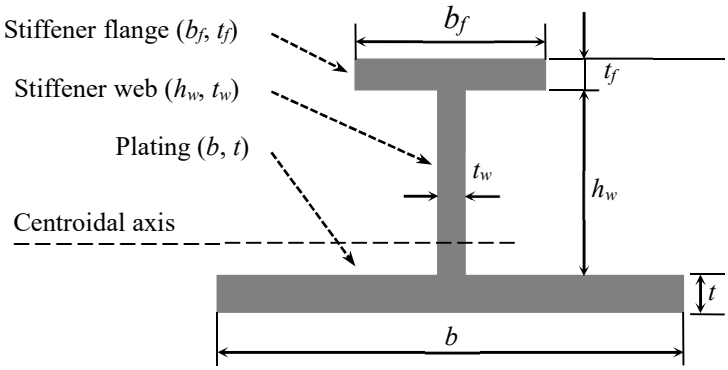

Figure 3-2. Cross-sectional parameters of I beam.

The equilibrium path of an Euler-Bernoulli beam can be calculated by solving following governing equations plus the boundary conditions:

$$F_y' - \kappa_z P - k_z P = 0 \qquad (3.1)$$

$$M_z' + F_y = 0 \qquad (3.2)$$

$$-\theta_z + u_y' = 0 \qquad (3.3)$$

$$\theta_z' - \kappa_z = 0 \qquad (3.4)$$

$$C_x(\gamma_x, \kappa_z) + P = 0 \qquad (3.5)$$

$$C_z(\gamma_x, \kappa_z) - M_z = 0 \qquad (3.6)$$

$$F_y = 0|_{at\ beam\ center} \qquad (3.7)$$

$$\theta_z = 0|_{at\ beam\ center} \qquad (3.8)$$

$$u_y = 0|_{at\ beam\ end} \qquad (3.9)$$

$$M_z = 0|_{at\ beam\ end} \qquad (3.10)$$

where P is the applied compressive load. F_y and M_z are the cross-sectional stress resultant force and moment. u_y and θ_z are the deflection and rotational angle. k_z and κ_z are the pre-twist/pre-curvature and deformed twist/curvature respectively. γ_x is the beam generalized axial strain. Equations 3.1 and 3.2 are the equations of equilibrium and Equations 3.3 and 3.4 are the strain-displacement relations. In Equations 3.5 and 3.6 the functions C_x and C_z represent the integrated cross-sectional axial force and moment respectively which take into account the development of plasticity. Equations 3.7 to 3.10 are the boundary conditions. By discretizing the beam into segments along the length, the equation set can be solved by spatial finite difference for a given axial load. Either by increasing the axial load or the strain, the equilibrium path can be obtained by Newton-Raphson scheme or Riks algorithm. The ultimate strength can be found as the peak load of the equilibrium path (load-deflection curve) (Li, 2017).

3.5 SIZE OPTIMIZATION OF I BEAM

3.5.1 Objective and Constraint Functions

The objective of present structural optimization problem is to minimize the structural weight. For a beam of fixed length and uniform density it is equivalent to minimizing the cross-sectional area. So the objective function is:

$$F(\bar{X}) = b \cdot t + h_w \cdot t_w + b_f \cdot t_f \qquad (3.11)$$

The design variable set $\bar{X}$ for the sizing optimization can be any one or several of the geometric parameters: $[b, t, h_w, t_w, b_f, t_f]$.

The design needs to ensure that the beam ultimate compressive strength (axial force P_u) is greater than a prescribed limit P_0. So the constraint function is:

$$G(\bar{X}) = P_0 - P_u(\bar{X}) \leq 0 \qquad (3.12)$$

The design variables are bounded by lower and upper limits chosen by manufacturing requirements and design experience. Thus:

$$\bar{X}_{min} \leq \bar{X} \leq \bar{X}_{max} \qquad (3.13)$$

The ultimate load in the analysis typically does not exceed the yield force for pure compressive or the beam Euler buckling force, thus are not considered here. Other constraints can be considered to avoid weak local buckling resistance or large deflection. In the beam analysis the initial imperfection includes only the vertical deflection. The stiffener web horizontal buckling load constraint is not included. Deflection constraint is easy to add but it's usually not important. It is necessary to cautiously check the optimum design for other non-dominant design constraints if they're not included in the optimization process.

3.5.2 Sensitivity Analysis

Sequential Quadratic Programming (SQP) algorithm is used for the optimization and the design variables sensitivities are calculated by finite difference. Like in other gradient-based algorithms the accuracy of sensitivity is crucial for the optimization. Often times when a nonlinear structural analysis package is used as a black box, the gradient-based algorithm may not work well due to inaccurate sensitivity. For these cases other non-gradient based algorithms like Simulated Annealing, Particle Swarm or Pattern Search may be used instead and so the computation time may increase significantly.

Due to the numerical analysis of the discrete beam, there are various ways to calculate the design variable sensitivity. Analytic sensitivity is the most reliable but it requires detailed study to find the terms in the linearized analytical form. Finite difference method is easy to use and often can give good approximation of the sensitivity. Sometimes the errors of finite difference from numerical approximation and small step size can cause problems in the optimization.

Figure 3-3 shows the load deflection curves of one original design (O-A-B) and a perturbed design (O-C-D) by adding a small perturbation to one design variable (web height). *P* is the axial force

applied on the beam end and u_c is the beam's central deflection. The peak load P_u is the ultimate load in the optimization constraint function. The equilibrium path (load deflection curve) of the original design is obtained by solving Equations 3.1 to 3.10 with Newton-Raphson scheme starting from the origin (point O in Figure 3-3). In each iteration the load is increased from previous iteration and the current solution is calculated using Newton-Raphson scheme and the solution of the previous iteration as the initial guess. The final maximum value of the load P_{max} (point A in Figure 3-3) will be close to the real peak value P_u (point B in Figure 3-3) within a defined limit. Riks algorithm or displacement-controlled Newton-Raphson scheme can extend the equilibrium path beyond the peak (point B) but the calculated ultimate strength P_{max} (point A) is still only an approximation of the real P_u. This iterative method is the approximate method.

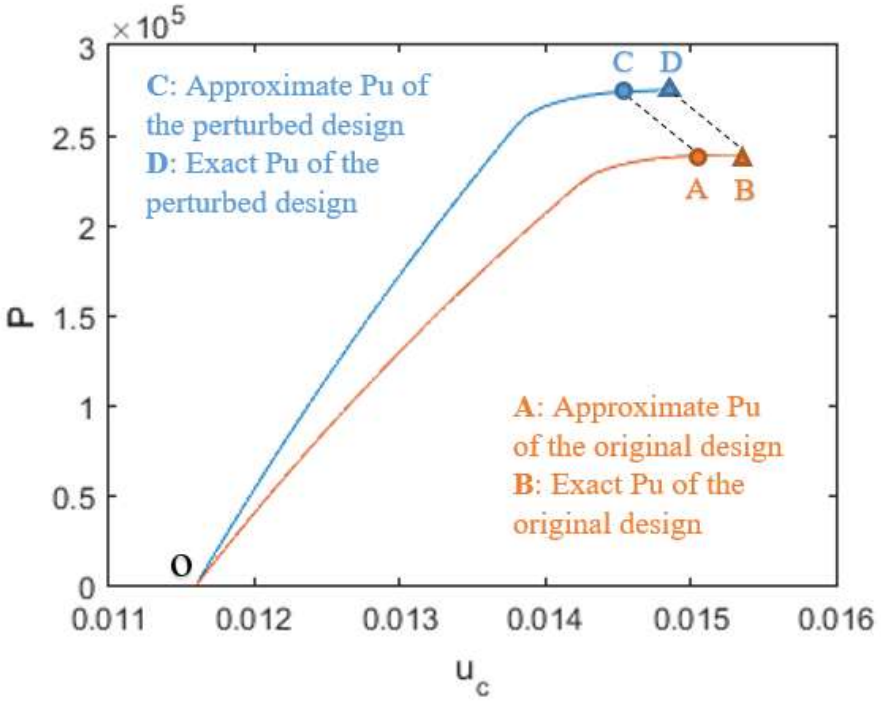

Figure 3-3. Equilibrium path of original and perturbed designs.

There are two major types of errors in the finite difference sensitivity calculated by the approximate method:

(1) Small finite difference step size: It is significant if the step size is too small relative to the error in the analysis solution. In the present analysis the error comes from
    a) Round-off error,
    b) Numerical error from Newton-Raphson iteration,
    c) Approximation error of P_u from P_{max} of the equilibrium path from load stepping.
(2) Large finite difference step size: It is significant if the step size is large compared to the second derivative of the performance /constraints.

The type (1)(b) error is controlled by the convergence criteria in the numerical iteration. The type (1)(a) error always exists in finite difference method but is typically negligible unless the step size is too small. It is important to monitor the type (1)(a) errors caused by finite difference step size. Error of type (2) can be minimized by taking a small step size but is possible only if error of type (1)(c) is avoided. The way to avoid type (1)(c) error is to use a modified method that can solve for P_u directly.

On the equilibrium path, P_u is characterized by the point where dP/du_c is zero. To solve for P_u, Equations 3.1-3.10 are differentiated with respect to u_c. P is treated as an unknown variable. Equations 3.14-3.19 are the differentiated form of Equations 3.1-3.6. The terms in the brackets can be expanded by using chain rule.

$$d\left(F_y' - \kappa_z P - k_z P\right)/du_c = 0 \qquad (3.14)$$

$$d\left(M_z' + F_y\right)/du_c = 0 \qquad (3.15)$$

$$d\left(-\theta_z + u_y'\right)/du_c = 0 \qquad (3.16)$$

$$d(\theta_z' - \kappa_z)/du_c = 0 \qquad (3.17)$$

$$d(C_x(\gamma_x, \kappa_z) + P)/du_c = 0 \qquad (3.18)$$

$$d(C_z(\gamma_x, \kappa_z) - M_z)/du_c = 0 \qquad (3.19)$$

The original set of equations and the differentiated set above (including the boundary conditions and their differentiation) can be solved by the addition of the following two equations.

$$dP_u/du_c = 0 \qquad (3.20)$$

$$du_c/du_c = 1 \qquad (3.21)$$

P_u can be directly solved if the Newton iteration starts from an estimate very close to the actual solution. The solution from the approximate method is a good estimate of the actual solution so it is suitable to be the initial guess. This method is called the exact method. The type (1)(c) error can be avoided with it and leads accurate gradients and convergence of the optimization algorithm.

By using the approximate method or the exact method, there are four ways to get the P_u of the perturbed design from the original design as shown on Figure 3-3:

(1) Solve for the approximated P_u of the perturbed system from the approximated P_u of the original system by the approximate method. (O to A to C on Figure 3-3). Compare to approximate P_u of original design.
(2) Solve for the approximated P_u of the perturbed system from the origin by the approximate method (full analysis). (O to A and O to C on Figure 3-3). Compare to approximate P_u of original design.
(3) Solve for the exact P_u of the perturbed system from the approximate P_u (full analysis) of the perturbed system by the exact method. (O to A to B and O to C to D on Figure 3-3). Compare to the exact P_u of original design.
(4) Solve for the exact P_u of the perturbed system from the exact P_u of the original system by the exact method. (O to A to B to D on Figure 3-3). Compare to the exact P_u of original design.

Figure 3-4 shows the comparison of sensitivity calculated by forward finite difference using the above four analysis methods for a range of finite difference step size.

In Figure 3-4, some calculated gradients have too large errors so the values are outside the range of the figure. The approximate methods 1 and 2 have large errors when the step size is moderately small (10^{-5} or 10^{-6}). The exact methods 3 and 4 only have large errors with very small step size (beyond 10^{-14}). Method 1 cannot calculate the correct P_u of the perturbed design with large step size (10^{-1} and 10^{-2}) because the new solution is not close to the original design so Newton-Raphson scheme didn't converge. It is obvious that method 3 and 4 are more reliable than method 1 and 2. Furthermore, method 4 is more efficient than method 3. That is because method 3 is based on a full analysis but method 4 is based on an abridged analysis. Therefore, method 4 as the most efficient way should be used to calculate the perturbed values for finite difference sensitivity. If method 4 doesn't work with large step size, method 3 can be used as an alternative. Correspondingly the best step size should be chosen from between 10^{-5} and 10^{-10}.

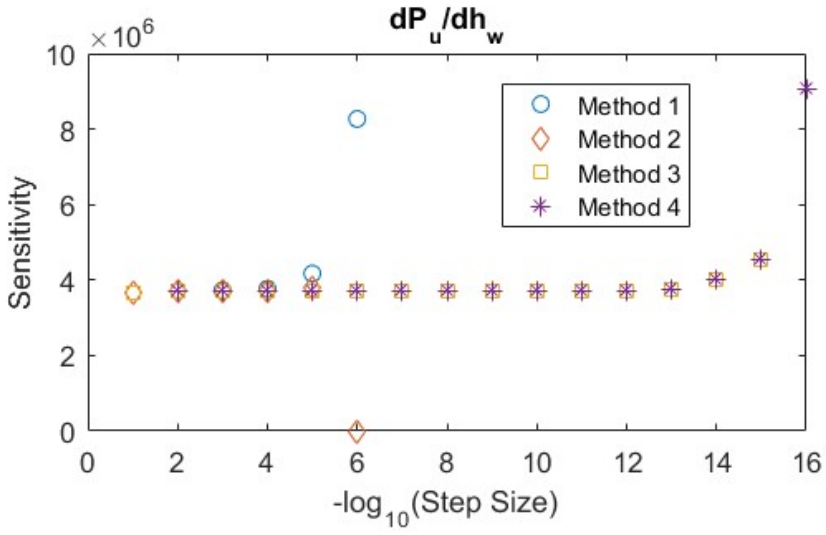

Figure 3-4. Comparison of finite difference sensitivity.

In order to avoid all the finite difference errors in the sensitivity, it is necessary to develop analytic sensitivity analysis. The gradient of the objective function (weight/area) is very simple but the ultimate strength calculation in the constraint function is computational. Based on the exact

method, the analytic sensitivity analysis of the constraint function (ultimate strength) with respect to each design variable can be developed. This is in follow-up research work of this paper.

3.5.3 Two Variable Design Space

A simply supported elastic-perfectly-plastic I beam has following properties:

$\sigma_y = 247.3$ MPa , $E = 205800$ MPa , $L = 1524$ mm , $b = 304.8$ mm , t $= 6.4$ mm , $t_w = 4.65$ mm, $t_f = 6.35$ mm.

The initial deflection is 11.6 mm, about 0.75% of the beam length. Design variables are $[h_w, b_f]$ with lower bound [50 mm, 50 mm] and upper bound [150 mm, 150 mm]. The required ultimate compressive load limit P_0 is 5.0×10^5 N.

The contour lines of the objective function (stiffener area) and the shaded feasible design space are shown in Figure 3-5. The optimization using sequential quadratic programming (SQP) algorithm and finite difference gradient found the optimum design as $[h_w = 135.7$ mm, $b_f = 50$ mm]. The objective function value is 948.68. This optimum design can be identified as the lower left vertex (red circle) of the shaded feasible region in Figure 3-5.

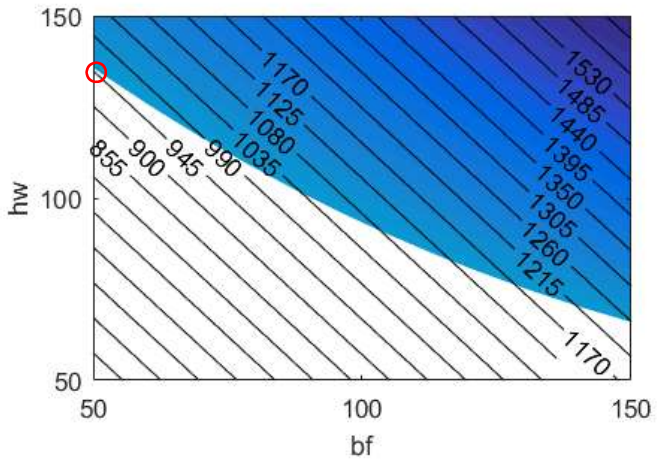

Figure 3-5. Design space of h_w and b_f (objective function contours and shaded feasible region).

3.5.4 Four Variable Optimization

The same beam now has the stiffener dimensions $[h_w, t_w, b_f, t_f]$ as the four design variables. The plate dimensions and other parameters are the same as the two variable problem. The lower and upper limits are [100, 5, 50, 5] mm and [250, 25, 250, 25] mm respectively. Table 3-1 lists a series of optimization problems with different ultimate load limit P_0 in each row.

Table 3-1. Four variables optimization results (case 1).

Optimum Design (mm)				Objective Function Value	Constraint Limit
t_w	b_f	t_f	h_w	Area (mm^4)	P_o (N)
5	50	5	142	960	5.00E+05
5	50	5	187.2	1186	6.00E+05
5	75.8	11.9	250	2152.02	9.00E+05
5	214.5	6	250	2537	1.00E+06
5	216.7	25	250	6667.5	2.00E+06
19.3	250	25	250	11075	3.00E+06

In Table 3-1, only the shaded cells have design variables not on the boundary. It is noticed that when the load limit is small, only h_w is not at the lower limit. Only after h_w reaches the upper limit under intermediate load constraint, b_f and t_f start to affect the design. Finally t_w becomes important only after the other three design variables are at the upper limit. This shows the influential level of each design variable for the beam design under different ultimate strength limit.

In Table 3-1 when P_0 is 9.0×10^5 N and 1.0×10^6 N, the optimum designs have both flange width and thickness values not on the boundary. Figure 3-6 and Figure 3-7 plot the objective function contour lines and shaded feasible region for these two optimization problems. It can be seen that the boundary of the feasible region is nearly a constant weight line. That means the optimizer may find any point on this boundary as the optimum design. In order to have a single optimum design, there can be additional objective functions for these special cases. Figure 3-6 and Figure 3-7 also show that the flange area will affect the design as a single variable instead of b_f and t_f separately.

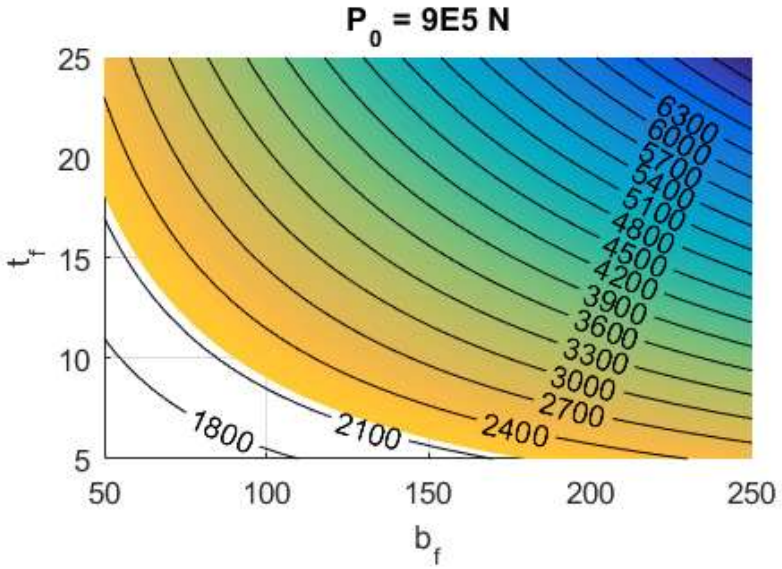

Figure 3-6. Design space of b_f and t_f (objective function contours and shaded feasible region).

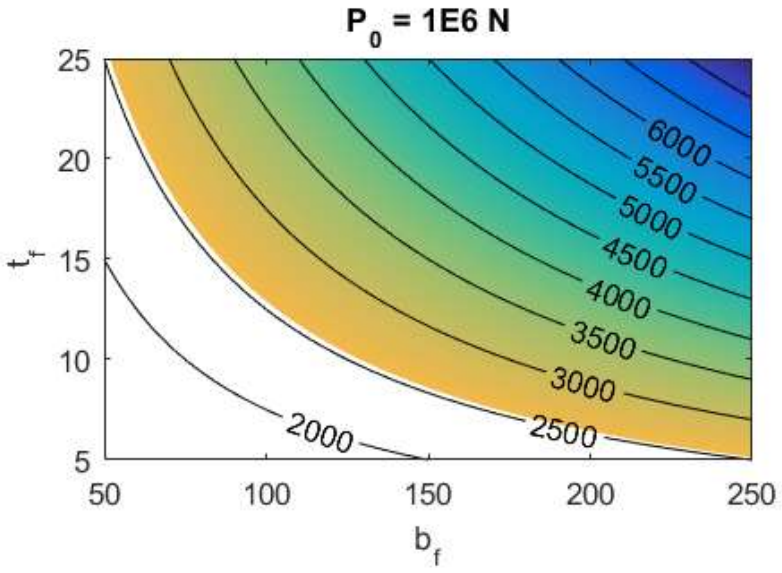

Figure 3-7. Design space of b_f and t_f (objective function contour and shaded feasible region).

Table 3-2 lists another series of optimization problems with a different set of four design variables: web height h_w and the thicknesses of plate, web and flange. It looks similar to Table 3-1 in the way that in each optimum design there is only one design variable not on the boundary.

Table 3-2. Four variables optimization results (case 2).

Optimum Design (mm)				Objective Function Value	Constraint Limit
t_w	t	t_f	h_w	Area (mm^4)	P_0 (N)
5	5	5	121.68	2382.38	4.00E+05
5	5	7.26	150	2636.73	5.00E+05
5	5	14.03	150	2975.27	6.00E+05
5	7.78	15	150	3440.57	7.00E+05

5	11	15	150	3924.57	8.00E+05
5	14.25	15	150	4410.95	9.00E+05
6.44	15	15	150	4964.12	1.00E+06

3.5.5 Six Variable Optimization

When all six cross-sectional geometric parameters: $[b, t, h_w, t_w, b_f, t_f]$ are design variables, the computation time is higher but the optimization is not more complex compared with less design variables. As long as the finite difference sensitivities are accurate enough, the optimizer will search along the direction corresponding to the local quadratic approximation and converge to the optimum design.

For the same I beam as the one described in previous section, six variable optimum designs found by SQP algorithm are shown in Table 3-3. When P_0 is equal to 2.0×10^6 N the optimization histories of SQP algorithm from four different initial points are shown in Figure 3-8. Figure 3-9 shows the optimization histories of non-gradient based Pattern Search algorithm from the same four initial points. SQP algorithm converges to the same optimal design from the four different initial points. Pattern Search algorithm doesn't converge well although points C and D are fairly close to the optimal design. The total number of function evaluation and CPU time of the two algorithms are compared in Table 3-4. SQP algorithm costs significantly less with less than 10% of the CPU time used by Pattern Search. It is obvious that SQP algorithm is more efficient and robust than the non-gradient based Pattern Search. Although there are other improved heuristic random search algorithms, they often require larger number of structural analysis as compared to the gradient-based search.

Table 3-3. Six variables optimization results (SQP).

Optimum Design (mm)						Objective Function Value	Constraint Limit
b	t	h_w	t_w	b_f	t_f	Area (mm4)	P_o (N)
250	10	250	5	58.45	15	4626.76	1.00E6
250	10	250	16.55	150	15	8887.88	2.00E6
250	25.78	250	20	150	15	13694.70	3.00E6
391.62	30	250	20	150	15	18998.69	4.00E6

Table 3-4. Comparison of SQP and Pattern Search (6 variable).

Initial Point	SQP			Pattern Search		
	Final Func. Value	Total Func. Count	CPU Time (S)	Final Func. Value	Total Func. Count	CPU Time (S)
A	8888	39	521	10733	626	9069
B	8888	33	451	10072	632	8797
C	8888	28	385	9035	261	3943
D	8888	21	296	8950	259	3797

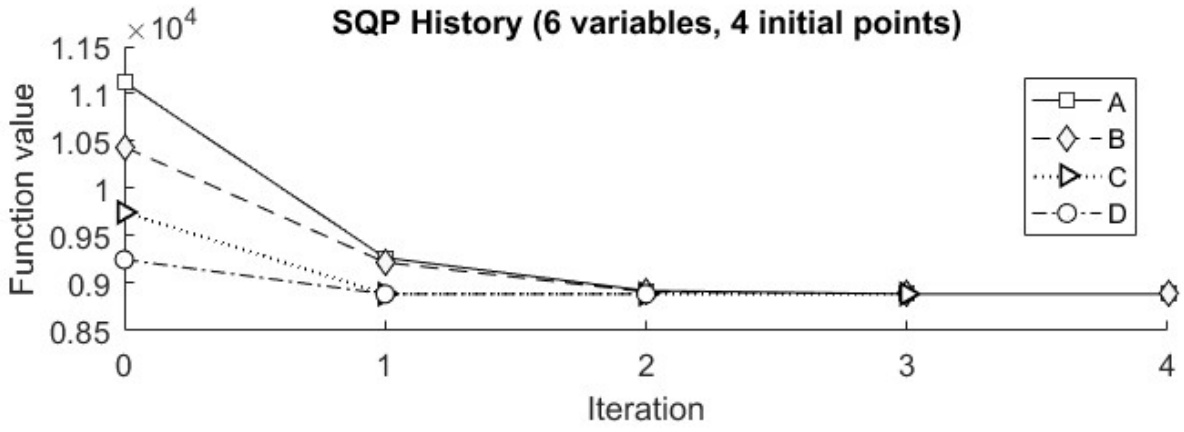

Figure 3-8. Six variable optimization (SQP) history.

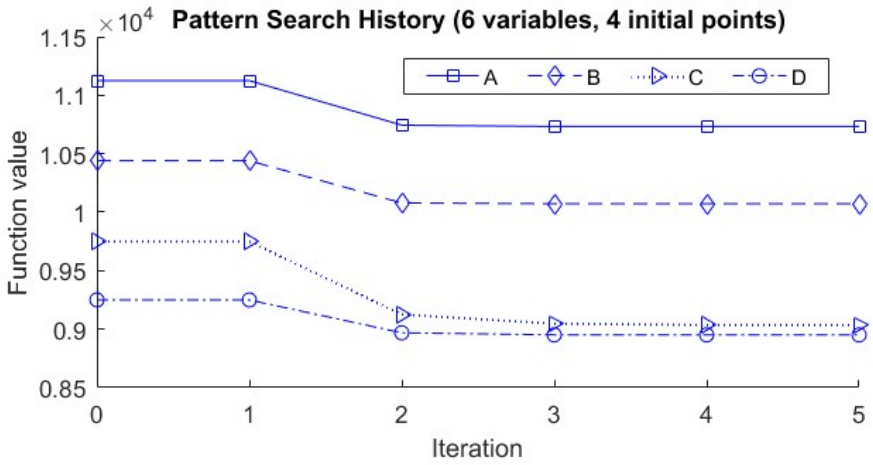

Figure 3-9. Six variable optimization (Pattern Search) history.

3.6 CONCLUSION

Structural optimization of elasto-plastic responses with nonlinear material constitutive law is complicated by the difficulties of calculating accurate design variable sensitivity.

The paper presents a methodology for structural optimization of inelastic I beam-columns using SQP algorithm with constraint on the maximum inelastic buckling strength (ultimate strength). The nonlinear buckling strength analysis has been improved to calculate robust and accurate ultimate strength and the corresponding design variable sensitivities. The optimization converges at optimum solutions much more efficiently than the non-gradient-based algorithm. The design space is explored thoroughly for various constraint limits and the importance of each design variables at different ultimate strength level is shown.

The key contribution of the work is the improved exact method of ultimate strength calculation which is essential to develop accurate analytic sensitivities. Finite difference sensitivity is easy to use but the accuracy is affected by the accuracy of the analysis and the finite difference step size.

The ultimate strength analysis and sensitivity analysis are shown to be fast and reliable for the deterministic optimization process. The ultimate strength analysis, sensitivity analysis and optimization method will be applied for the development of a reliability-based optimization methodology of the elasto-plastic beams in the future.

4 Chapter Four

Reliability Analysis of Ultimate Strength for Beam-Columns

4.1 TITLE

Reliability Analysis of Ultimate Strength for Beam-Columns

By: Zhongwei Li and Mayuresh Patil

4.2 ABSTRACT

The prediction of ultimate strength and reliability analysis are essential for structural safety and rational design. This paper presents a procedure to estimate the reliability of elasto-plastic beam-columns consisting of base plate and T-bar stiffener under axial compression. The ultimate compressive strength of such beam-columns is calculated by coupling geometrically exact beam theory and nonlinear constitutive law of the material. These equations are discretized using finite difference spatial discretization and solved using an iterative nonlinear solver. The random variables include structural scantlings (width, height and thickness), material properties and initial imperfection. The standard First Order Reliability Method (FORM) is used to calculate the reliability index and probability of failure. A gradient-based optimizer is used to solve the optimization problem of FORM. The sensitivity of the ultimate strength with respect to the random variables is calculated by finite difference and complex step method. Other than assessing the reliability of non-deterministic design, this reliability analysis procedure can also be used for reliability-based structural optimization of such elasto-plastic beam-columns.

4.3 INTRODUCTION

Ocean structures are designed and operated under large uncertainties. Besides the probabilistic structural loads, the material properties and structural member scantlings have to be represented by random variables. Human factors are also uncertain during the design and operation. Traditionally, ships are designed using deterministic analysis methods. The uncertainties that affect the performance and safety are accounted for by applying a safety factor to the structural strength. However, the deterministic designs often over/under estimate the effect of uncertainties on the ship structural response. On the other hand, probabilistic and non-probabilistic uncertainty analysis consider the scatter of design variables around their mean values. Reliability analysis predicts the probability that a system will perform its function under those uncertainties. It is an important part of the probabilistic design method since the reliability is used as a measurement of structural safety. Probabilistic design methods are gradually having broader applications partly due to the increasing computational power. For example, partial safety factor method has been commonly used in offshore structural design. The present research develops a method for the reliability analysis of the commonly used plate-stiffener combination structure including the progressive development of plasticity.

The ultimate strength is the true load-carrying capacity of structures made of elasto-plastic materials like steel and aluminum. The reliability analysis of such structures typically link the ultimate limit state function and the applied load. There are various ultimate strength analysis methods for beam-columns, stiffened panels and ship hull structures. Empirical design formulas based on structural tests and numerical data have been proposed in many forms (Zhang, 2016) but they are usually not accurate enough to be used for reliability assessment. Analytical solutions are difficult to obtain due to the complexity of nonlinear analysis. Numerical method like nonlinear finite element analysis (FEA) can calculate accurate ultimate strength results compared with structural tests. Paik et al (2007a, b) compared existing ultimate strength analysis methods for stiffened panels and hull structures. Hughes et al. (2004) used a beam-column model to predict the ultimate strength of stiffened panels under compression. The present authors (Li, 2017) have developed an efficient method to calculate the beam-column ultimate strength and the results can

be used to predict the stiffened panel's ultimate strength fairly well by applying a correction factor. It has shown that (Li, 2016) the initial deflection is an important variable for the ultimate strength of beam-columns.

Structural reliability analysis methods can be conducted using various methods including most probable point based method or simulation-based method. Both methods require accurate and efficient structural analysis. The former has fewer number of total analysis but needs accurate sensitivity with respect to random variables for finding the most probable failure point. The latter runs a large number of sample analysis to get approximate probability of failure and so the computation cost can become onerous if cost of a single analysis is high. Past research about structural ultimate limit state reliability analysis is based on nonlinear FEA (Ba-abbad, 2003), semi-analytical methods (Sharifi, 2011), simplified formulas (Zhao, 2016) and IACS incremental-iterative ultimate strength analysis (Xu, 2015).

Ba-abbad et al. (2003) developed a reliability-based optimization method for an elastic-plastic T beam. The gradient-based optimizer first found a deterministic optimum design based on nonlinear FEA. Then the first-order second-moment reliability analysis was used to reduce the structural weight or increase the reliability.

Sharifi and Paik (2011) used FORM and sampling analysis as the reliability analysis methods and an analytic ultimate strength formula to evaluate the risks of corroded steel-box girder bridges over its service time. Uncertainties due to time-dependent corrosion deterioration have been evaluated for the purpose of developing a reliability-based maintenance plan.

Xu et al. (2015) used model correction factor method on the reliability assessment of an oil tanker. The design by IACS ultimate strength rules was updated by a factor to match the nonlinear FEA of the same design after each iteration of the FORM reliability analysis. The process maintained the accuracy and reduced the computation effort at the same time by using the relatively simple incremental-iterative method for ultimate strength analysis and only a limited number of full nonlinear FEA to correct it.

Chojaczyk et al. (2015) combined Artificial Neural Network (ANN) models with Monte Carlo simulation for the reliability analysis of stiffened panels in ship structures. The structural analysis is based on nonlinear FEA. The uncertainties include probabilistic geometric variables, material properties, initial imperfection and applied bending moment. Reliability analysis method including FORM and Importance Sampling have been used to train the ANN. The limit state function evaluation by the ANN model was compared with reliability analysis without it.

Zhao et al. (2016) used FORM to evaluate the reliability of stiffened composite under ultimate compressive load. Other than using nonlinear FEA for ultimate strength analysis, a simplified method was developed by using an assumed function as a factor to link the critical elastic buckling load to inelastic ultimate load.

In the following sections, first the beam-column ultimate strength analysis method is introduced. The present authors have developed a method that solves for the ultimate strength directly so that analytic sensitivity of the random variables can be calculated based on it. The reliability analysis is based on First Order Reliability Method (FORM) where the most probable point is obtained by solving a constrained optimization problem using a gradient-based algorithm. The numerical examples present safety index and probabilities of failure of an elasto-plastic beam-column under various compressive forces. The results of FORM are compared with failure probabilities calculated by Monte Carlo simulation. In the conclusion, future research of developing reliability-based optimization method is introduced.

4.4 ULTIMATE STRENGTH ANALYSIS

4.4.1 Beam-Column Model

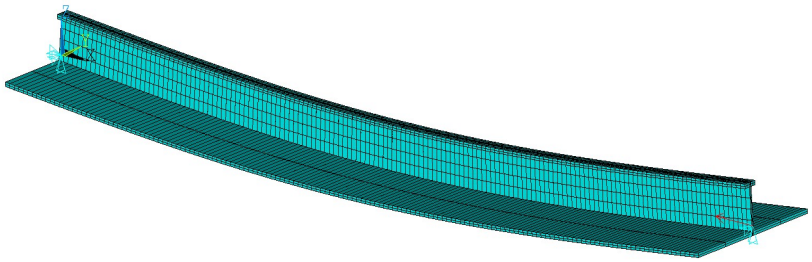

Figure 4-1. Simply supported I beam with initial deflection.

The beam-column consists of a plate strip and attached T-bar stiffener as shown in Figure 4-1. Figure 4-2 shows the cross-section geometry of the beam. There are six geometric parameters in the cross-section: plate width b, plate thickness t, web height h_w, web thickness t_w, flange width b_f and flange thickness t_f. Due to initial imperfection during manufacturing, the beam has initial vertical deflection.

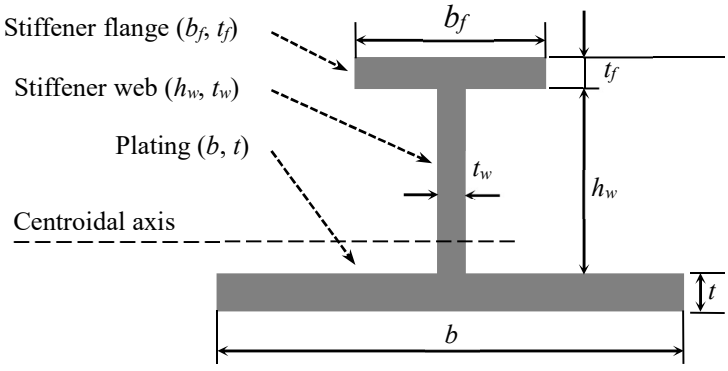

Figure 4-2. Cross-sectional parameters of I beam.

When an inelastic beam with initial imperfection is under compressive axial force, the beam will deflect as the load is applied. As the load is increased above the yield load, a plastic zone is formed at critical locations along the beam. The ultimate strength is the load at which the plastic zone progression leads to a plastic hinge and the beam can carry no more load. The ultimate strength is the maximum load carry capacity of the beam.

The load-deflection path of a nonlinear Euler-Bernoulli beam can be calculated by solving the following governing equations:

$$F_y' - \kappa_z P - k_z P = 0 \qquad (4.1)$$

$$M_z' + F_y = 0 \qquad (4.2)$$

$$-\theta_z + u_y' = 0 \qquad (4.3)$$

$$\theta_z' - \kappa_z = 0 \qquad (4.4)$$

$$C_x(\gamma_x, \kappa_z) + P = 0 \qquad (4.5)$$

$$C_z(\gamma_x, \kappa_z) - M_z = 0 \qquad (4.6)$$

$$F_y = 0|_{at\ beam\ center} \qquad (4.7)$$

$$\theta_z = 0|_{at\ beam\ center} \qquad (4.8)$$

$$u_y = 0|_{at\ beam\ end} \qquad (4.9)$$

$$M_z = 0|_{at\ beam\ end} \qquad (4.10)$$

where P is the applied compressive load. F_y and M_z are the cross-sectional stress resultant force and moment. u_y and θ_z are the deflection and rotational angle. k_z and κ_z are the pre-twist/pre-curvature and deformed twist/curvature respectively. γ_x is the beam generalized axial strain. Equations 3.1-3.2 are the equations of equilibrium and Equations 4.3-4.4 are the strain-

displacement relations. In Equations 4.5-4.6 the functions C_x and C_z represent the integrated cross-sectional axial force and moment respectively which take into account the development of plasticity. Equations 4.7-4.10 are the boundary conditions. By discretizing the beam into segments along the length, the equation set can be solved by spatial finite difference for a given axial load. Either by increasing the axial load or the strain, the equilibrium path can be obtained by Newton-Raphson scheme or Riks algorithm. The ultimate strength can be found as the peak load of the equilibrium path (load-deflection curve) (Li, 2017).

Figure 4-3 shows the load deflection curves of one original design (O-A-B) and a perturbed design (O-C-D) by adding a small perturbation to one beam variable. P is the axial force applied on the beam end and u_c is the beam's central deflection. The peak load P_u is the ultimate load in the limit state function. The equilibrium path (load-deflection curve) of the original design is obtained by solving Equations 4.1-4.6 with Newton-Raphson scheme starting from the origin (point O in Figure 4-3). In each iteration the load is increased from previous iteration and the current solution is calculated using the previous iteration's solution as the initial guess. The final maximum value of the load P_{max} (point A in Figure 4-3) will be close to the real peak value P_u (point B in Figure 4-3) within a defined limit. Riks algorithm or displacement-controlled Newton-Raphson scheme can extend the equilibrium path beyond the peak (point B) but the calculated ultimate strength P_{max} (point A) is still only an approximation of the real P_u. This method is the approximate method.

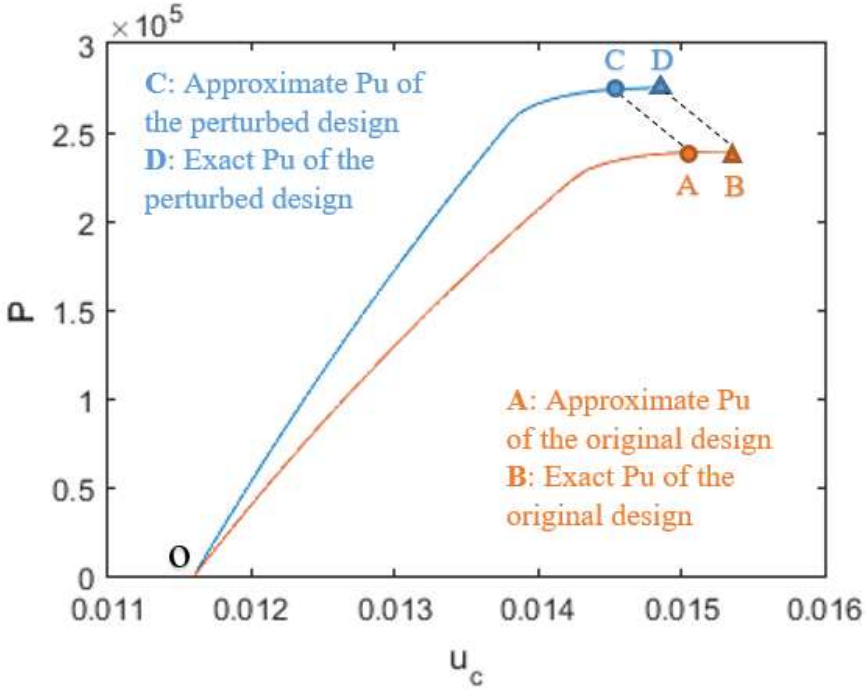

Figure 4-3. Equilibrium path of original and perturbed designs.

4.5 DIRECT METHOD

In order to calculate the analytical gradient of P_u with respect to beam variables, it is necessary to solve for P_u explicitly.

On the equilibrium path, P_u is characterized by the point where $\mathrm{d}P/du_c$ is zero. To solve for P_u, Equations 4.1-4.10 are differentiated with respect to u_c. P is treated as an unknown variable. Equations 4.11-4.16 are the differentiated form of Equations 4.1-4.6. The terms in the brackets can be expanded by using chain rule. Equations 4.15-4.16 have the most complicated form due to the complexity of functions C_x and C_z.

$$d\left(F_y' - \kappa_z P - k_z P\right)/du_c = 0 \qquad (4.11)$$

$$d\left(M_z' + F_y\right)/du_c = 0 \qquad (4.12)$$

$$d\left(-\theta_z + u_y'\right)/du_c = 0 \quad (4.13)$$

$$d(\theta_z' - \kappa_z)/du_c = 0 \quad (4.14)$$

$$d(C_x(\gamma_x, \kappa_z) + P)/du_c = 0 \quad (4.15)$$

$$d(C_z(\gamma_x, \kappa_z) - M_z)/du_c = 0 \quad (4.16)$$

The original set of equations and the differentiated set above (including the boundary conditions and their differentiation) can be solved by the addition of the following two equations.

$$dP_u/du_c = 0 \quad (4.17)$$

$$du_c/du_c = 1 \quad (4.18)$$

P_u can be directly solved if the Newton iteration starts from an estimate very close to the actual solution. The solution from the approximate method is a good estimate of the actual solution so it is suitable to be the initial guess. This method is called the exact method.

In Figure 4-3 the computation process first finds the path of O to A by using the approximate method. Then the solution of B is obtained by using the exact method and the solution of A as an initial guess.

4.6 SENSITIVITY ANALYSIS

First Order Reliability Method (FORM) uses an optimization procedure to find the Most Probable Point (MPP) of failure. The gradients of the limit state function are required during the optimization. Analytic sensitivity analysis is the most dependable and efficient method of calculating gradients but it requires development of analytic form of the derivatives of the analysis equations.

4.6.1 Finite Difference

Finite difference method is easy to use and usually gives good approximation of the sensitivity. Small step size is necessary to reduce the secant error but very small step size will lead to large subtractive cancelation error. It is important to monitor the errors related to finite difference step size.

In Figure 4-3, the derivative of the ultimate load P_u with respect to one design variable is calculated by adding a small perturbation on this variable in order to generate an adjacent design that has the equilibrium path O-C-D. The difference of P_u at B and D is divided by the design variable perturbation to calculate the sensitivity. It is not necessary to start from point O in order to get to point D. Instead, the solution at D can be calculated by Newton-Raphson iteration using the solution at B as an initial guess. Alternatively, the solution at C can be calculated from the solution at A by the approximate method first. Then the exact method is used to get to D from C.

4.6.2 Complex Step

Complex step method can be used to avoid the subtractive cancelation error. This method perturbs the function by adding a small imaginary value to the design variable. Then the imaginary part of the perturbed function output is divided by the variable perturbation to get the sensitivity without the subtractive cancelation error. To get the perturbed solution at D it is similar to finite difference method by taking the path B-D. Figure 4-4 shows the comparison of finite difference sensitivity and complex step sensitivity with various step size.

It can be seen from Figure 4-4 that the complex step sensitivity doesn't change with perturbation step size ($1x10^{-4}$ to $1x10^{-24}$) but the finite difference sensitivity starts to have very large errors with small step size (beyond $1x10^{-13}$). When analytic sensitivity is not available, complex step method can be used as an alternative. If finite difference method is used, it is always necessary to monitor and control the errors caused by small step size.

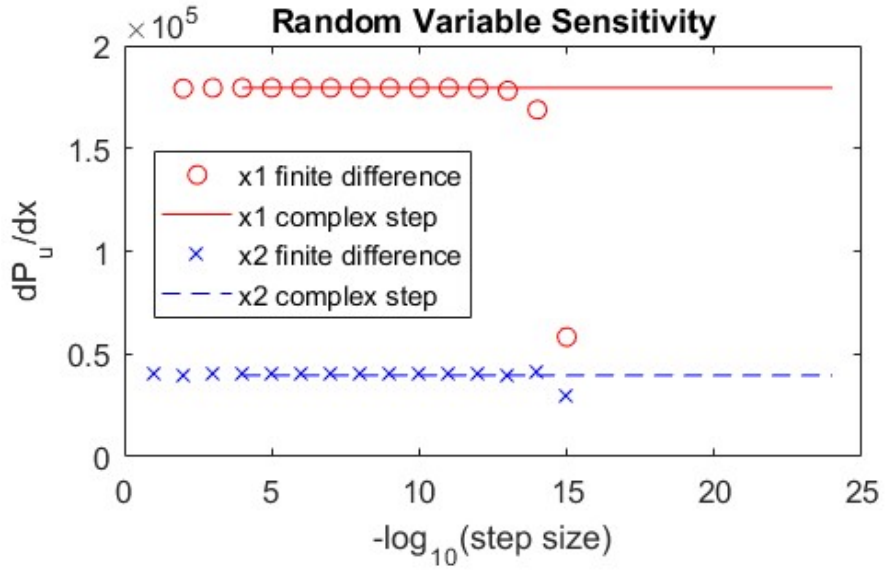

Figure 4-4. Comparison of sensitivity analysis.

4.7 RELIABILITY ANALYSIS

4.7.1 Limit State Function

The limit state function $G(\bar{X})$ of an inelastic I beam is defined as

$$G(\bar{X}) = P_u(\bar{X}) - P_0 \qquad (4.19)$$

where $\bar{X}$ is the vector of random variables, P_u is the ultimate strength calculated by solving Equations 4.1-4.18 and P_0 is the applied load. Random variables can include geometric parameters, material properties and initial imperfection. The applied load can also be treated as random variable. The failure surface is defined as $G(\bar{X}) = 0$. The Most Probable Point (MPP) is the point on the failure surface with the highest probability of failure.

4.7.2 FORM

First Order Reliability Method (FORM) first transforms the set of independent random variables $\bar{X}$ into a set of standard normal variables $\bar{U}$. The limit state function $G(\bar{X})$ is then expressed as $G(\bar{U})$. MPP is the point on the failure surface that has the shortest distance to the origin. In FORM, the limit state function is represented as the tangent hyperplane at the MPP. Reliability analysis thus focuses on finding the MPP and the corresponding shortest distance, i.e. the safety index β.

The distance of a point in the normalized space to the origin is $(\bar{U}^T\bar{U})^{\frac{1}{2}}$. So FORM involves solving the following constrained optimization problem:

$$\textit{Minimize:} \quad \beta(\bar{U}) = (\bar{U}^T\bar{U})^{\frac{1}{2}} \qquad (4.20)$$

$$\textit{Subject to:} \quad G(\bar{U}) = 0 \qquad (4.21)$$

Various optimization algorithms can solve the optimization problem, including Hasofer-Lind iteration method or other gradient-based optimization algorithms.

4.8 NUMERICAL EXAMPLES

4.8.1 Beam Reliability Analysis by FORM

An elasto-plastic beam-column as shown in Figure 4-1 and Figure 4-2 has following design values including the yield stress σ_y, Young's modulus E, beam-column length L, initial central deflection d and cross-sectional parameters.

$\sigma_y =$ 247.3 MPa , $E =$ 205800 MPa , $L = 1524$ mm , $b = 304.8$ mm , $t = 6.4$ mm , $h_w =$ 64.25 mm, $t_w = 4.65$ mm, $b_f = 27.94$ mm, $t_f = 6.35$ mm, $d = 3.81$ mm.

The ultimate compressive force calculated by Equations 4.1-4.10 is 351027 N. By solving Equations 4.1-4.18 the exact value of the ultimate compressive force is 351028 N. The difference

is controlled by the limit of load increment in the Newton-Raphson iteration which was set to be 1 N when solving Equations 4.1-4.10.

In reality all the above parameters are random. The random variables are typically described by a probabilistic distribution. The mean value is the design value and the coefficient of variance (COV) reflects the variation caused by the quality of fabrication. Table 4-1 lists the distributions of the random variables used in the present reliability analysis. The units are the same as in the above paragraph. Beam length L and plate width b are assumed to be deterministic.

Table 4-1. Random variables.

Variable	Distribution	Mean value	COV	Standard deviation
σ_y	Normal	247.3	0.1	24.73
E	Normal	2.058E5	0.1	2.058E4
t	Normal	6.4	0.02	0.128
h_w	Normal	64.25	0.01	0.6425
t_w	Normal	4.65	0.02	0.093
b_f	Normal	27.94	0.03	0.8382
t_f	Normal	6.35	0.02	0.127
d	Normal	3.81	0.5	1.905

In Table 4-1, all the random variables are assumed to be independent. The material is assumed to be elastic-perfectly-plastic. To simplify the process all variables are assumed to be normally

distributed. Sometimes lognormal distributions are used to avoid negative values. Non-Gaussian distributions have to be transformed into equivalent normal distribution before calculation of MPP.

In the FORM analysis, a gradient-based optimizer is used to solve the optimization problem as described by Equations 4.20-4.21. The sensitivity of σ_y, E and d are calculated by complex step method. Finite difference method is used to calculate the gradients of the other five variables.

Table 4-2 shows the reliability analysis results of the beam-column under various deterministic compressive force. The reliability index β is obtained from solving the optimization problem. The probability of failure is calculated from the reliability index by the standard normal cumulative distribution function.

Table 4-2. FORM reliability analysis results.

Load (N)	Reliability index β	Probability of failure
1.500E05	5.1809	1.1041E-07
1.750E05	4.3009	8.5053E-06
2.000E05	3.4725	2.5778E-04
2.100E05	3.1602	7.8836E-04
2.125E05	3.0834	0.0010
2.150E05	3.0082	0.0015
2.175E05	2.9330	0.0017
2.200E05	2.8582	0.0021
2.250E05	2.7126	0.0033

2.300E05	2.5694	0.0051
2.400E05	2.2923	0.0109
2.500E05	2.0277	0.0213

The applied load (axial force) can also be random. Assuming the load follows normal distribution, Table 4-3 lists the reliability analysis results of various mean load values and COV. By comparing Table 4-2 and Table 4-3, it can be seen that the probability of failure increases significantly if uncertainty of the applied load is included. Table 4-3 also shows that with larger COV or standard deviation the probability of failure is higher.

Table 4-3. FORM reliability analysis results for uncertain applied load in addition to the other random variables.

Mean of Load (N)	COV	Reliability index	Probability of failure
1.50E05	0.1	4.5873	2.2451E-06
1.75E05	0.1	3.7312	9.5296E-05
2.00E05	0.1	2.9751	0.0037
2.25E05	0.1	2.3116	0.0104
1.50E05	0.3	3.0072	0.0013
1.75E05	0.3	2.3712	0.0089
2.00E05	0.3	1.8508	0.0321
2.25E05	0.3	1.4163	0.0783

The ultimate compressive force of the deterministic design is 351028 N. By applying a safety factor of 2.0, the design load is about 1.75×10^{5} N. With this design load, it is shown in Table 4-2 that the probability of failure is 8.5053×10^{-6}. If this load is also probabilistic with a COV of 0.1 or 0.3, the probability of failure will increase to 9.5296×10^{-5} or 8.9×10^{-3}, respectively, as shown in Table 4-3. Therefore, the uncertainties of material properties, structural scantlings and environmental loads are all important factors that can affect the probability of structural failure. Use of safety factor in deterministic design will overlook all these uncertainties.

4.8.2 Monte Carlo Simulation

The Monte Carlo simulation (MCS) method generates a large sized sample of limit state evaluations. The failure rate is calculated by the number of infeasible designs in the sample. Large sample size is needed to approximate the failure rate accurately. Usually in structural design the allowable probability of failure is as small as 10^{-5}. The sample size has to be large enough to reflect the possibility of failure. If the ultimate strength analysis is not efficient, millions of such analyses are needed which will be extremely time-consuming. The beam-column ultimate strength analysis method presented in this paper is efficient and robust. To validate the FORM analysis, the sampling method is used with large sample size.

Table 4-4 compares the failure rates of MCS with the probabilities of failure calculated by FORM under four deterministic axial loads. The reliability results of MCS and FORM are very close.

Table 4-4. Reliability analysis by MCS compared with FORM.

Load (N)	MCS Sample size	MCS failure rate	FORM Probability of failure
2.00E05	2.5E05	2.68E-04	2.5778E-04
2.10E05	4.0E04	8.50E-04	7.8836E-04

2.15E05	1.0E04	0.00140	0.00150
2.40E05	2.99E04	0.013	0.01090

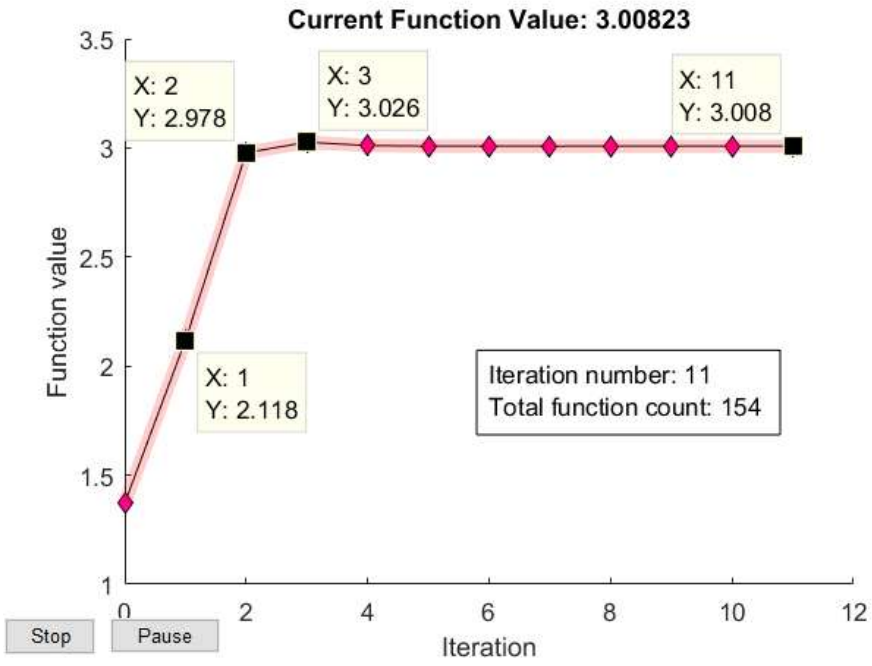

Figure 4-5. FORM optimization history ($P_0 = 2.15\times10^5$ N).

Figure 4-5 shows the iteration history of the optimization problem in FORM analysis. After three iterations, the reliability index is already very close to the final optimum value. The total number of analyses is only 154 which is only 1.54% of the sample size in MCS (1×10^4). The gradient-based FORM is much more efficient than the simulation method and is able to obtain similar probability of failure with much less computational effort.

4.9 CONCLUSION

This paper presented the reliability analysis of elasto-plastic beam-columns by using FORM analysis. The ultimate strength analysis includes the progression of plasticity. The ultimate strength is calculated directly by imposing a zero slope condition on the load-deflection equilibrium path. Analytic sensitivity of random variables can be calculated by this analysis method. A gradient-based optimizer is used to solve the constrained optimization problem for the safety index based on FORM. The FORM analysis using finite difference and complex step sensitivity is efficient and accurate compared with sampling method.

The reliability analysis method will be used for structural optimization in future research work. The reliability-based structural optimization will optimize the structural weight and maintain an acceptable level of safety by taking into account the uncertainty of design variables and other parameters.

5 Chapter Five

Reliability-Based Design Optimization of Elasto-Plastic Beam-Columns under Uniaxial Compression

5.1 TITLE

Reliability-Based Design Optimization of Elasto-plastic Beam-Columns under Uniaxial Compression

By: Zhongwei Li and Mayuresh Patil

5.2 ABSTRACT

This paper presents a procedure for reliability-based design optimization (RBDO) of nonlinear beam-columns consisting of base plate and T-bar stiffener under uniaxial compression. The optimization minimizes structural weight with reliability constraint on the ultimate compressive strength. The ultimate compressive strength of the beam-column is calculated using geometrically-exact beam theory and nonlinear constitutive law of elasto-plastic material. The governing equations are discretized using finite difference spatial discretization and solved using an iterative nonlinear solver. The design variables are cross-section geometric properties. Random variables include cross-sectional parameters, material properties, initial deflection and applied load. A direct solving method for ultimate strength analysis developed in an earlier paper is used to calculate accurate semi-analytic sensitivities. The direct solving method combines the original governing equation set and its derivatives w.r.t deflection to directly obtain the ultimate strength at the peak of load-deflection curve. The direct method avoids using load/displacement incremental method and allows calculation of analytic sensitivity. Here semi-analytic sensitivity is solved from a linear set of sensitivity equations using the Jacobian matrix of the original equations. Gradient-based

optimization algorithm is used to calculate reliability index and to search for the optimal design. The double loop RBDO based on the ultimate strength direct solving method and semi-analytic sensitivity analysis is robust and efficient. Numerical examples demonstrate the complete RBDO procedure for nondeterministic elasto-plastic beam-columns.

5.3 INTRODUCTION

Reliability-Based Design Optimization (RBDO) adds reliability constraint to optimization thus accounting for the uncertainties in the analysis and design parameters. RBDO considers the cost, performance and safety of the design under uncertainties at the same time. In structural design, RBDO is usually solved as a double loop optimization problem. In the outer loop, the objective of structural optimization is to minimize the weight and the main constraint is to limit the reliability index. The inner loop of RBDO calculates the reliability index at the current design point. First Order Reliability Method (FORM) is accurate in calculating the reliability index if the structure's failure surface is not highly nonlinear near the design point. The reliability index of FORM is the distance from the origin to the Most Probable Point (MPP) in the normalized random variable space. The search for MPP can be solved by an optimization procedure that finds the minimum distance from the origin to the failure surface. Thus RBDO using FORM is represented by a double loop optimization problem.

Wang et al. (1995) used nonlinear approximation of the design constraint to reduce the computational cost in safety index calculation and optimization for structural RBDO. Yu et al. (1997) mixed structural optimization and reliability-based design approach for probabilistic structural durability. Allen and Maute (2004) presented RBDO procedure for aeroelastic structures. Youn and Choi (2004) used Performance Measure Approach (PMA), response surface method and hybrid mean value method for RBDO. More recent works has been aimed on improving the efficiency and robustness of RBDO. For example, Motta and Afonso (2016) added reliability constraint to robust multi-objective optimization problem. PMA is used for reliability constraint assessment and approximation techniques like reduced-order modeling (ROM) are applied to the reliability-based robust design optimization. A number of researchers have focused on developing

semi or complete single-loop procedure for RBDO, e.g., Shan and Wang (2007), Liang et al. (2007), Nguyen et al. (2010), Lim and Lee (2016), Mansour and Olsson (2016), Jeong and Park (2017).

The ultimate strength is the true load-carrying capacity of structures made of elasto-plastic materials like steel and aluminum. Beam-column model has been used from early days to develop ultimate strength design formulas for stiffened panels. Hughes et al. (2004) used a beam-column model to predict the ultimate strength of stiffened panels under compression. A more efficient method based on nonlinear beam theory has been developed by the present authors ((Li et al., 2017) to calculate the beam-column ultimate strength and the results are used to predict the stiffened panel's ultimate strength by applying a correction factor. Structural optimization with ultimate strength constraint has been applied in many fields including civil engineering (Barros et al., 2012), ocean engineering (Ma et al., 2016), aerospace engineering (Ba-abbad and Kapania, 2003) and mechanical engineering (Bielski and Bochenek, 2008).

Ocean structures and aerospace structures are designed and operated under large uncertainties. Besides the probabilistic structural loads, the material properties and structural member scantlings have to be represented by random variables. Reliability analysis predicts the probability that a system will perform its function under those uncertainties. The reliability analysis of such structures typically link the ultimate limit state function and the applied load. FORM is commonly used for the reliability analysis of nonlinear structures with ultimate strength constraint. For example, Sharifi and Paik (2011) presented reliability analysis of corroded steel-box girder bridge by using ultimate strength formula and FORM. Zhao et al. (2016) did reliability analysis of stiffened composite panels with ultimate compressive strength calculated by nonlinear Finite Element Analysis (FEA).

Structural optimization and reliability analysis based on ultimate limit state is challenging due to the complexity of the nonlinear elasto-plastic analysis. One difficulty in RBDO for nonlinear structures is the calculation of the limit state function sensitivity and reliability index sensitivity. Usually the performance function of nonlinear structures cannot be represented by closed-form

equations. Nonlinear FEA uses a quasi-static approach to calculate ultimate strength of elasto-plastic structures by increasing load or displacement at each step. It is possible to develop analytic sensitivities for nonlinear structural analysis for a given load, but sensitivity of ultimate load is more involved. Finite difference method is often used for sensitivity analysis but it requires higher computation cost in analysis and extra caution to avoid precision errors from small step size. Complex step perturbation method is accurate but the computation cost is high because a full re-analysis with complex numbers is required for each design variable. Direct method also requires full re-analysis for each sensitivity calculation. Adjoint method can significantly reduce the computation cost. Approximation techniques are often used to avoid full re-analysis. When accurate sensitivities are available, many gradient-based optimization algorithms like Sequential Quadratic Programming (SQP) can be used for structural optimization and reliability analysis. Without accurate sensitivity, non-gradient based optimization algorithms have to be used.

Vaz and Hinton (1995) used optimization algorithm to solve the elastoplastic constitutive law in finite element shape sensitivity calculation. Haukaas and Scott (2006) used direct differentiation method to develop the finite element shape sensitivity of nonlinear structures. The same method has been used for sensitivity analysis of path-dependent inelastic structures (Haukaas, 2006), second-order response sensitivity (Bebamzadeh and Haukaas, 2008) and response sensitivity of nonlinear Timoshenko frame elements (Scott and Azad, 2017).

If FORM is used in the inner loop of RBDO, the reliability index sensitivity in the outer loop can be calculated from the limit state function sensitivity at the MPP as shown by early sensitivity studies (Hohenbichler and Rackwitz, 1986, Bjerager and Krenk, 1987, Kwak and Lee, 1987). This method has been widely used in structural RBDO (Wang et al. 1995, Yu et al. 1997, Allen and Maute, 2004, Youn and Choi, 2004).

The nonlinear beam-column analysis method presented in this paper solves for the ultimate strength directly from a set of discretized nonlinear equations. The direct solving method combines the original governing equation set and its derivatives w.r.t deflection to directly obtain the ultimate strength at the peak of load-deflection curve. Semi-analytic sensitivity analysis method is

developed from this ultimate strength direct solving method. First the sensitivity of the structural residual equations is calculated using complex step. Then the semi-analytic sensitivity is solved from a linear set of sensitivity equations using the Jacobian matrix of the original equations. The RBDO of nonlinear beam-columns uses semi-analytic sensitivity and gradient-based algorithm for the double loop optimization.

In the following sections, first the double-loop RBDO problem of nonlinear beam-column is established. The inner loop reliability analysis is based on FORM and the outer loop structural optimization uses SQP algorithm. Next the load-incremental ultimate strength analysis and direct solving method are introduced, followed by the semi-analytic sensitivity analysis of the limit state function (ultimate strength). The sensitivity of the safety index needed in the outer loop is calculated based on the results of the inner loop MPP. Last, the numerical examples present ultimate strength analysis, sensitivity analysis, structural optimization, reliability analysis and RBDO. The design variables are the cross-sectional dimensions and the random variables include axial load, material properties, initial deflection and cross-sectional dimensions.

5.4 RELIABILITY-BASED DEISIGN OPTIMIZATION FORMULATION

The double loop RBDO has a structural optimization problem as the outer loop which is defined as:

$$\textit{Minimize:} \quad F(\bar{X}) \tag{5.1}$$

$$\textit{subject to:} \quad \beta_0 - \beta(\bar{X}) \leq 0 \tag{5.2}$$

$$\bar{X}_{min} \leq \bar{X} \leq \bar{X}_{max} \tag{5.3}$$

where $\bar{X}$ is a vector of design variables, β is the safety index, and β_0 is the defined limit of β.

The calculation of the safety index β is the inner loop of RBDO. FORM is applied on a set of independent standard normal variables $\bar{U}$. Any non-Gaussian or non-standard normal distribution and correlated random variables have to be transformed before using FORM. MPP is the point on

the failure surface that has the shortest distance to the origin in the normalized space. In FORM, the limit state function is represented by the tangent hyperplane at the MPP. Reliability analysis thus focuses on finding the MPP and the corresponding shortest distance, i.e. the safety index β. The inner loop reliability analysis is formulated as an optimization problem:

$$\textit{Minimize:} \quad \beta(\bar{U}) = (\bar{U}^T \bar{U})^{\frac{1}{2}} \qquad (5.4)$$

$$\textit{subject to:} \quad G(\bar{U}) = 0 \qquad (5.5)$$

where $\bar{U} = T(\bar{Y})$ which is the vector of standard normal variables transformed from the original random variables $\bar{Y}$. T is the transform function. $G(\bar{U})$ is the limit state function of the structural system in terms of the normal variables.

The design variables can be random or deterministic, which means the variables in $\bar{X}$ may or may not be in $\bar{Y}$ depending on whether it is random or deterministic.

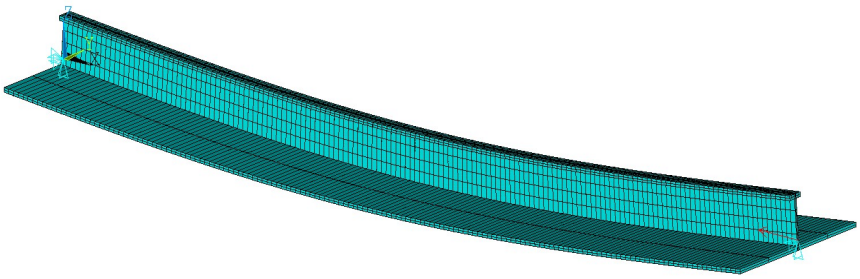

Figure 5-1. Simply supported I beam with initial deflection.

An I beam consists of a plate strip and attached T-bar stiffener as shown in Figure 5-1. There are six geometric parameters in the cross-section: plate width *b*, plate thickness *t*, web height h_w, web thickness t_w, flange width bf and flange thickness t_f. Figure 5-2 shows the cross-section geometry of such a beam-column.

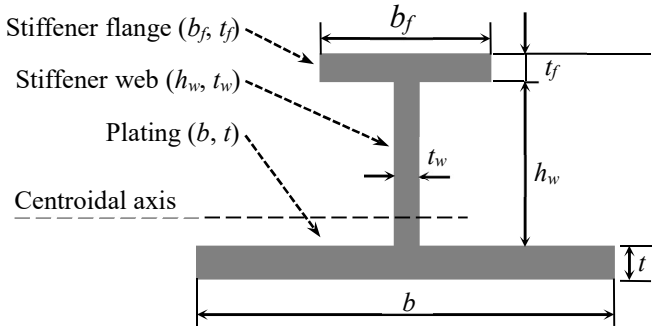

Figure 5-2. Cross-sectional parameters of I beam.

When an elasto-plastic beam-column with initial deflection d is under axial compression, the beam will deflect as the load is applied. As the load is increased, the stress in the beam increases. When the stress at any point goes above the yield stress, a plastic zone is formed at critical locations along the beam. The ultimate strength is the load at which the plastic zone progression leads to a state that the beam can carry no more load. The ultimate strength is the maximum load carrying capacity of the beam. This maximum compressive force P_u is the ultimate load. Figure 5-3 shows the equilibrium path (load-deflection curve) of an inelastic beam-column under axial compression. The beam is made of elastic-perfectly-plastic material and has geometry shown in Figure 5-1 and Figure 5-2.

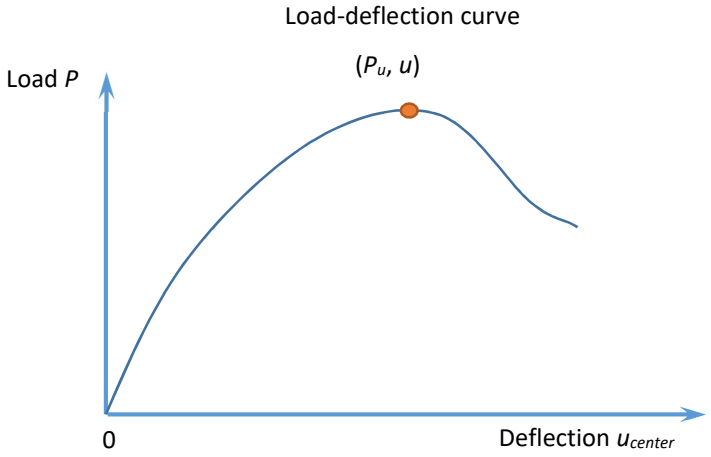

Figure 5-3. Load-deflection curve of I beam under uniaxial compression.

The six cross sectional variables are the design variables in $\bar{X}$. The objective function Equation 5.1 in the outer loop of RBDO for the beam-column is:

$$F(\bar{X}) = b \cdot t + h_w \cdot t_w + b_f \cdot t_f \quad (5.6)$$

The inner loop reliability analysis of RBDO is based on the ultimate strength analysis of the beam-column. The limit state function in Equation 5.5 is:

$$G(\bar{U}) = P_u(\bar{U}) - P_0 \quad (5.7)$$

where P_0 is the applied load which is also the limit of the ultimate load P_u.

The initial deflection d, material properties (yield stress σ_y and Young's modulus E) and cross-sectional variables $\bar{X}$ are chosen as the original random variables of $\bar{Y}$.

5.5 ULTIMATE STRENGTH ANALYSIS OF NONLINEAR BEAM-COLUMNS

5.5.1 Beam-Column Model

The equilibrium path (Figure 5-3) of a simply-supported nonlinear Euler-Bernoulli beam (Figure 5-1 and Figure 5-2) can be calculated by solving following governing equations (Equation 5.8-5.13) and boundary conditions (Equation 5.14-5.17):

$$F_y' - \kappa_z P - k_z P = 0 \quad (5.8)$$

$$M_z' + F_y = 0 \quad (5.9)$$

$$-\theta_z + u_y' = 0 \quad (5.10)$$

$$\theta_z' - \kappa_z = 0 \quad (5.11)$$

$$C_x(\gamma_x, \kappa_z) + P = 0 \quad (5.12)$$

$$C_z(\gamma_x, \kappa_z) - M_z = 0 \quad (5.13)$$

$$F_y = 0|_{at\ beam\ center} \quad (5.14)$$

$$\theta_z = 0|_{at\ beam\ center} \quad (5.15)$$

$$u_y = 0|_{at\ beam\ end} \quad (5.16)$$

$$M_z = 0|_{at\ beam\ end} \quad (5.17)$$

where P is the applied compressive load. F_y and M_z are the cross-sectional stress resultant force and moment. u_y and θ_z are the deflection and rotational angle. k_z and κ_z are the pre-twist/pre-curvature and deformed twist/curvature respectively. γ_x is the beam generalized axial strain. Equations 5.8-5.9 are the equilibrium equations and Equations 5.10-5.11 are the strain-displacement relations. In Equations 5.12-5.13 the functions C_x and C_z represent the integrated cross-sectional axial force and moment respectively which take into account the development of plasticity. Equations 5.14-5.17 are the simply-supported boundary conditions for half beam. By discretizing the beam into segments along the length, the equation set can be solved by spatial finite difference for a given axial load. Either by increasing the axial load or the displacement, the equilibrium path can be obtained by Newton-Raphson scheme or Riks algorithm. The ultimate strength is the peak load of the equilibrium path (load-deflection curve) (Li, 2017).

5.5.2 Numerical Scheme

Equations 5.8-5.11 are differential equations with respect to (w.r.t) beam axial coordinate. If the beam in Figure 5-1 is discretized into 2×N equal length elements, only half of the beam (N elements) need to be considered because of the symmetry at the center. Equations 5.1-5.4 can be represented by the nodal values using spatial finite difference. There are six unknown variables at each node which are $[F_y, M_z, u_y, \kappa_z, \theta_z, \gamma_x]$. The total number of unknown variables are 6×(N+1).

Discretized Equations 8-11 are satisfied at N elements. Equations 5.12-5.13 are satisfied at (N+1) nodes. Including four boundary Equations 5.14-5.17, there are total 6×(N+1) equations which is equal to the number of unknown variables. The discretized system of the nonlinear equations is:

$$f_i(\bar{x}|P) = 0\,,\ \ i = 1, 2 \ldots 6 \times (N+1) \qquad (5.18)$$

Newton-Raphson scheme is used to solve the nonlinear equation set. At load step (j), the load is increased by a step size dP from previous load P_{j-1}. The change of solution $\{d\bar{x}_j^k\}$ from previous solution $\{\bar{x}_j^k\}$ is solved iteratively by:

$$-\left[J\left(\bar{x}_j^k\right)\right]\{d\bar{x}_j^k\} = \left\{f\left(\bar{x}_j^k|P_j\right)\right\},\ \ k = 0, 1, 2, \ldots \qquad (5.19)$$

where $[J]$ is the Jacobian matrix of Equation 5.19 and $\bar{x}_j^{k+1} = \bar{x}_j^k + d\bar{x}_j^k$. k is the iteration number at current load step (j). The above iterations stop when a convergence criteria $\left\|\mathrm{f}\left(\bar{x}_j^{k+1}|\mathrm{P_j}\right)\right\| < \varepsilon$ is met where ε is a given limit. The converged $\{\bar{x}_j^{k+1}\}$ is the solution $\{\bar{x}_j\}$ at load step (j). The Jacobian matrix is written as:

$$[J] = \begin{bmatrix} \partial f_1/\partial x_1 & \cdots & \partial f_1/\partial x_n \\ \vdots & \vdots & \vdots \\ \partial f_n/\partial x_1 & \cdots & \partial f_n/\partial x_n \end{bmatrix},\ n = 6 \times (N+1) \qquad (5.20)$$

At load step $(j+1)$, $\{\bar{x}_{j+1}^0\}$ is the initial guess of the solution which is the solution of previous load step $\{\bar{x}_j\}$. If $\{\bar{x}_j\}$ is close to $\{\bar{x}_{j+1}\}$, the solution of Equation 5.18 converges after a few iterations. If the load step from $\mathrm{P_j}$ to $\mathrm{P_{j+1}}$ is too large, the numerical scheme may not converge and load step has to be reduced. Then the solution under reduced load $\mathrm{P_{j+1}}$ is searched for by Equation 5.18 using the solution under load $\mathrm{P_j}$ as an initial guess.

Figure 5-3 shows a typical load-deflection curve of the beam-column in Figure 5-1 under uniaxial compression. The peak load P_u is the ultimate compressive strength of the beam-column. Load-incremental Newton-Raphson scheme simulates the quasi-static loading sequence from zero load to the peak load P_u. Displacement-controlled Newton-Raphson scheme or Riks algorithm can

get the solution beyond the peak of the curve. However, these methods can only find the approximation of peak load P_u. Furthermore, these methods cannot be used to calculate sensitivity accurately. The derivative of load w.r.t the displacement at the peak is zero. Small change of load corresponds to very large change of displacement. The load step when approaching the peak must be small enough in order to converge to a solution close to the exact peak value. The step size will determine the difference between the approximate P_u and the exact P_u.

For analysis purpose, the approximate P_u is accurate enough. For ultimate strength based design optimization and reliability analysis, however, using finite difference method to calculate the sensitivity of P_u is inefficient and inaccurate for large or small step size. In order to calculate more robust analytic sensitivity, it is necessary to solve for P_u directly instead of using the load-incremental method.

5.5.3 Direct Solving Method

On the equilibrium path of the beam-column (load-deflection curve in Figure 5-3), P_u is characterized by the point where $\mathrm{d}P/du_c$ is zero. u_c is any deflection. Here we choose the the central deflection u_{center}. To solve for P_u , Equations 5.8-5.17 are differentiated w.r.t u_c. P is treated as an unknown variable P_u. Equations 5.21-5.30 are the differentiated form of Equations 5.8-5.17. The terms in the brackets can be expanded by using chain rule.

$$d\left(F_y^{'} - \kappa_z P_u - k_z P_u\right)/du_c = 0 \qquad (5.21)$$

$$d\left(M_z' + F_y\right)/du_c = 0 \qquad (5.22)$$

$$d\left(-\theta_z + u_y'\right)/du_c = 0 \qquad (5.23)$$

$$d(\theta_z' - \kappa_z)/du_c = 0 \qquad (5.24)$$

$$d(C_x(\gamma_x, \kappa_z) + P_u)/du_c = 0 \qquad (5.25)$$

$$d(C_z(\gamma_x, \kappa_z) - M_z)/du_c = 0 \qquad (5.26)$$

$$dF_y/du_c = 0|_{at\ beam\ center} \quad (5.27)$$

$$d\theta_z/du_c = 0|_{at\ beam\ center} \quad (5.28)$$

$$du_y/du_c = 0|_{at\ beam\ end} \quad (5.29)$$

$$dM_z/\partial u_c = 0|_{at\ beam\ end} \quad (5.30)$$

The original set of equations (Equations 5.8-5.17) and the differentiated set (Equations 5.21-5.30) can be solved together by the addition of following two equations.

$$dP_u/d\,u_c = 0 \quad (5.31)$$

$$du_c/d\,u_c = 1 \quad (5.32)$$

In the original discretized system of equation set (Equation 5.18), load P is replaced by the unknown variable P_u. It becomes:

$$f_i(\bar{x}, P_u) = 0\,,\ \ i = 1, 2 \ldots 6 \times (N+1) \quad (5.33)$$

where $\{\bar{x}\}$ is the original $6 \times (N+1)$ nodal variables. The differentiated equation set is discretized as:

$$\dot{f}_i\left(\bar{x}, \bar{\dot{x}}, P_u, \dot{P_u}\right) = 0\,,\ \ i = 1, 2 \ldots 6 \times (N+1) \quad (5.34)$$

where the overdot notation represent partial derivative w.r.t u_c. u_c is one unknown variable in $\{\bar{x}\}$. $\{\bar{\dot{x}}\}$ is the derivative of $\{\bar{x}\}$ w.r.t u_c. $\dot{P_u}$ is $\partial P_u/\partial\, u_c$. The total number of unknown variables is $(6 \times (N+1) \times 2 + 2)$. Combine Equations 5.31-5.34 and there are $(6 \times (N+1) \times 2 + 2)$ equations. The analysis method which solves the combined equation set is the direct solving method.

P_u can be directly solved from the combined equation set by Newton-Raphson scheme. The Newton iteration must start from an estimate very close to the actual solution. The solution from

the load-incremental method is a good estimate of the actual solution so it is suitable as the initial guess. The solution of P_u from direct solving method is called exact P_u which is to be distinguished from the approximate P_u of load-incremental method. The Jacobian matrix $[\,JA\,]$ of the combined equation set contains the Jacobian matrix $[\,J\,]$ of the original equation set.

$$[\,JA\,] = \begin{bmatrix} [\,J\,] & \partial f/\partial \bar{y} \\ \partial \dot{f}/\partial \bar{x} & \partial \dot{f}/\partial \bar{y} \end{bmatrix} \qquad (5.35)$$

where $\{\bar{y}\} = \{\,\bar{\dot{x}}; P_u; \dot{P}_u\}$. Similar to the Newton-Raphson scheme expressed by Equation 5.19 in the load-incremental method, the iterative scheme for the direct solving method is:

$$-[JA(\bar{z}_k)]\{d\bar{z}_{k+1}\} = \{f(\bar{z}_k)\}\,,\ k = 0, 1, 2, \ldots \qquad (5.36)$$

where $\{\overline{z_k}\} = \{\bar{x}\,;\ \bar{y}\} = \{\bar{x}\,;\ \bar{\dot{x}}\,; P_u\,; \dot{P}_u\}$ at the kth iteration.

Although the difference between the exact P_u and the approximate P_u is very small, the direct solving method solves for the ultimate load P_u by explicit equations. Thus, it is possible to develop analytic or semi-analytic sensitivities of P_u which is important for RBDO of nonlinear beam-columns with ultimate load constraint.

5.6 SENSITIVITY ANALYSIS

5.6.1 Finite Difference Sensitivity Analysis

The inner loop reliability analysis Equation 5.4-5.5 uses gradient-base optimization algorithm to search for the MPP. The sensitivity of the limit state function is required by the algorithm. From Equation 5.7, the sensitivity of the limit state function is equal to the derivative of the ultimate load P_u w.r.t random variables in $\overline{U}$.

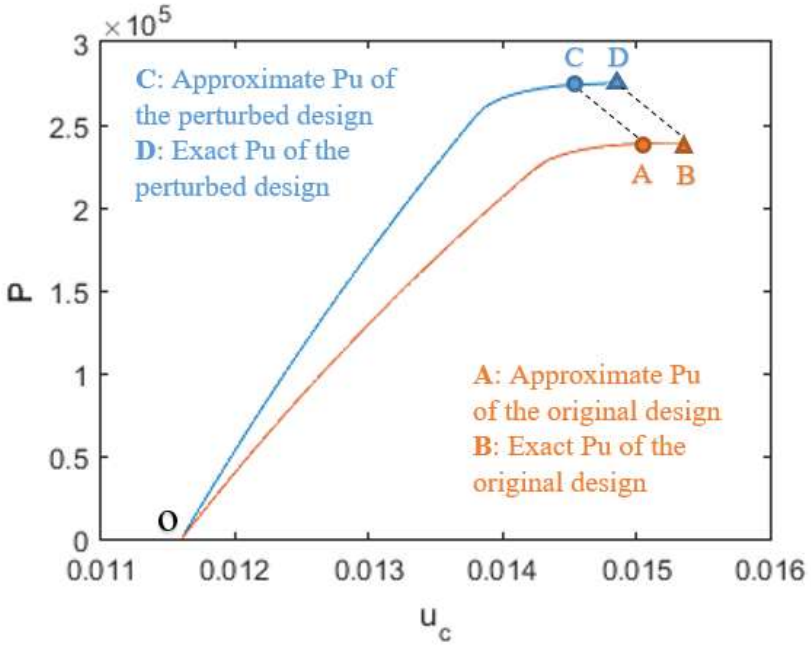

Figure 5-4. Equilibrium path of original and perturbed designs.

Figure 5-4 shows the load deflection curves of one original design (O-A-B) and a perturbed design (O-C-D) by adding a small perturbation to one design variable. P is the axial force applied on the beam end and u_c is the beam's central deflection. The peak load P_u is the ultimate load in the optimization constraint function. The equilibrium path (load deflection curve) of the original design is obtained by solving Equations 5.8-5.17 with Newton-Raphson scheme starting from the zero load (point O in Figure 5-4). In each iteration the load is increased from previous iteration and the current solution is calculated using Newton-Raphson scheme and the solution of the previous iteration as the initial guess. The final maximum value of the load P_{max} (point A and C in Figure 5-4) can be calculated by the load-incremental method. P_{max} will be close to the real peak value P_u (point B and D in Figure 5-4) within a defined limit. The difference of P_u of A and C is divided by the perturbation step size to get the finite difference sensitivity if load-incremental method is used.

There are two major types of errors in the finite difference sensitivity calculated by the load-incremental method:

(1) Small finite difference step size: It is significant if the step size is too small relative to the error in the analysis solution. In the present analysis the error comes from
    a. Numerical errors from spatial discretization and Newton-Raphson iteration,
    b. Approximation error of P_u from P_{max} of the equilibrium path from load stepping.
    c. Round-off error,
(2) Large finite difference step size: It is significant if the step size is large compared to the second derivative of the performance /constraints.

The type (1)(a) error is controlled by the convergence criteria in the numerical iteration. Type (2) error can be minimized by taking a small step size but is possible only if error of type (1)(b) is avoided. The way to avoid type (1)(b) error is to use the direct solving method which uses the difference of P_u of B and D to calculate the finite difference sensitivity.

Full analysis by the direct solving method can be used to solve for the exact P_u of the perturbed design, which is by the path from O to C to D. However, the more efficient way is to solve for the exact P_u at D (perturbed design) by using the solution at B (original design) as the initial guess for the direct solving method provided that the perturbation is small. The exact P_u at B and D are compared. The difference of P_u divided by the perturbation step size is the sensitivity of the limit state function at current design point. Thus the type (1)(b) error is eliminated by using the direct solving method to calculate finite difference sensitivity.

The type (1)(c) error always exists in finite difference method but is typically negligible unless the step size is too small. Small finite difference step size is necessary to avoid type (2) error. However, if the step size is too small, type (1)(c) error becomes significant because of the subtractive cancellation. It is important to monitor type (1)(c) errors caused by finite difference step size.

5.6.2 Analytic Sensitivity of Limit State Function

Sensitivity of the limit state function (ultimate load P_u) can be solved directly by differentiating Equations 5.8-5.17 and 5.21-5.32 w.r.t a design variable X_i. Denote the combined equation set as

$$F(\bar{Z};\bar{X}) = 0 \qquad (5.37)$$

where $\bar{Z}$ is the unknown variable vector and $\bar{X}$ is the design variable vector. Differentiate Equation 5.37 w.r.t X_i, it becomes

$$\frac{\partial F(\bar{Z};\bar{X})}{\partial X_i} + \frac{\partial F(\bar{Z};\bar{X})}{\partial \bar{Z}} \frac{\partial \bar{Z}}{\partial X_i} = 0 \qquad (5.38)$$

Rearrange Equation 5.38 as

$$\frac{\partial F(\bar{Z};\bar{X})}{\partial \bar{Z}} \frac{\partial \bar{Z}}{\partial X_i} = -\frac{\partial F(\bar{Z};\bar{X})}{\partial X_i} \qquad (5.39)$$

After spatial discretization, Equation 5.39 becomes

$$[JA] \frac{\partial \bar{z}}{\partial X_i} = -\frac{\partial f(\bar{z};\bar{X})}{\partial X_i} \qquad (5.40)$$

where $[JA]$ is the same Jacobian matrix in Equation 5.35-5.36. The analytic form of the right hand side of Equation 5.40 is required to solve for the derivatives of all unknown variables w.r.t to X_i. The needed sensitivity $\frac{\partial P_u}{\partial X_i}$ is one element of the full solution $\frac{\partial \bar{Z}}{\partial X_i}$.

For each design variable, analytic sensitivity is solved from Equation 5.40 after having the analytic form of the right hand side.

Take Equation 5.12 and 5.25 as examples. By removing the subscripts, Equation 5.12 becomes

$$C(\gamma, \kappa) + P = 0 \qquad (5.41)$$

The simplified expansion of Equation 5.25 is

$$C_\gamma \dot{\gamma} + C_\kappa \dot{\kappa} + \dot{P} = 0 \qquad (5.42)$$

where the subscript is the notation of partial derivative. The overdot notation is the derivative w.r.t u_c. $\dot{\gamma}$, $\dot{\kappa}$ and $\dot{P}$ are unknown variables.

Differentiate Equation 5.41 w.r.t a design variable X_i to obtain the sensitivity equation.

$$C_\gamma \gamma^* + C_\kappa \kappa^* + P^* = -\frac{\partial\left(C(\gamma,\kappa,\bar{X})\right)}{\partial X_i} \qquad (5.43)$$

where the asterisk notation is the derivative w.r.t X_i. $P^* = \frac{\partial P_u}{\partial X_i}$, which is the needed sensitivity for RBDO.

Similarly, the differentiated Equation 5.42 is

$$C_\gamma \dot{\gamma}^* + \dot{\gamma} C_{\gamma,\gamma} \gamma^* + \dot{\gamma} C_{\gamma,\kappa} \kappa^* + C_\kappa \dot{\kappa}^* + \dot{\kappa} C_{\gamma,\kappa} \gamma^* + \dot{\kappa} C_{\kappa,\kappa} \kappa^* + \dot{P}^*$$
$$= -\dot{\gamma} \frac{\partial\left(C_\gamma(\gamma,\kappa,\bar{X})\right)}{\partial X_i} - \dot{\kappa} \frac{\partial\left(C_\kappa(\gamma,\kappa,\bar{X})\right)}{\partial X_i} \qquad (5.44)$$

In Equation 5.43-5.44, all the coefficients of sensitivity terms on the left hand side have been developed for the Jacobian matrix in Equation 5.35. On the right hand side, $\dot{\gamma}$ and $\dot{\kappa}$ are solved at the design point. $C(\gamma, \kappa)$, $C_\gamma(\gamma, \kappa)$ and $C_\kappa(\gamma, \kappa)$ are functions of γ, κ and these functions contain the design variable X_i. The analytic form of the derivatives on the right hand side of Equation 5.43-5.44 needs to be developed in order to solve the linear sensitivity equation set for P^* which is the sensitivity of the ultimate load P_u.

5.6.3 Semi-Analytic Sensitivity of Limit State Function

Alternatively, another way to avoid the subtractive cancelation error is to use complex step method for sensitivity analysis. This method perturbs a random variable by adding a small imaginary value. Then the imaginary part of the complex P_u solved for the perturbed design is divided by the variable perturbation to calculate the sensitivity. Complex step sensitivity requires a full re-

analysis which uses the complex Jacobian matrix to solve the complex equation set iteratively. The cost of computation is high but the perturbation step size will not affect the sensitivity.

A more efficient approach is to use complex step method to calculate the derivatives on the right hand side of Equation 5.40.

$$\frac{\partial f(\bar{z};\bar{X})}{\partial X_i} = \frac{Im(f(\bar{z};\bar{X}|_{X_i=X_i+Ih}))}{h} \qquad (5.45)$$

where X_i is the design variable that is perturbed by the imaginary perturbation Ih. h should be a very small real number, for example, 10^{-30}.

The derivatives calculated by Equation 5.45 has no subtractive cancellation error. The calculation is simple and the results are accurate. Then by using Equation 5.40 the sensitivities can be solved by using the analytic Jacobian matrix. The semi-analytic sensitivity is more robust than finite difference sensitivity without the subtractive cancelation error caused by small step size. The semi-analytic sensitivity is also more efficient than full complex step sensitivity analysis.

When analytic sensitivity is not available, semi-analytic sensitivity can be used as an alternative because of the accuracy and robustness. The inner loop reliability analysis of RBDO can be solved efficiently by providing the semi-analytic sensitivity to a gradient-based optimizer like SQP.

5.6.4 Sensitivity of Reliability Index

In the outer loop optimization of RBDO, Equation 5.1-5.3, the sensitivity of reliability index β is needed for gradient-based optimization algorithm. Finite difference sensitivity can be used but it is not robust, especially when there is nonlinearity in both the ultimate strength analysis and the reliability analysis.

If FORM is used in the inner loop of RBDO, the sensitivity of reliability index β has following form:

$$\frac{\partial \beta}{\partial X_i} = \frac{1}{|\nabla G(U_{mp}, X_i)|} \frac{\partial G(U_{mp}, X_i)}{\partial X_i} \quad (5.46)$$

where U_{mp} is the MPP of the inner loop reliability analysis, $\nabla G(U_{mp},\ X_i)$ is the gradient of the limit state function at MPP, i.e.

$$\nabla G(U_{mp},\ X_i) = \frac{\partial G(U_{mp}, X_i)}{\partial U} \quad (5.47)$$

If the design variable X_i is a deterministic variable, the first term of Equation 5.46 is the result of the inner loop reliability analysis, and the second term has to be calculated separately. It is shown from Equation 5.7 that the derivative of limit state function is equal to the derivative of the ultimate load P_u. The same semi-analytic sensitivity analysis method for the inner loop reliability analysis can be used. By adding a very small imaginary perturbation to the design variable X_i, Equation 5.40 and 5.45 can be used to calculate the second term on the right hand side of Equation 5.46.

If the design variable X_i is also a random variable, the sensitivity of reliability index β in Equation 5.46 can be simplified as:

$$\frac{\partial \beta}{\partial X_i} = \frac{1}{\beta} U_{mp} \frac{\partial T(Y_{mp})}{\partial X_i} \quad (5.48)$$

where $T(.)$ is the function that transforms original random variables $\overline{Y}$ into the standard normal random variables $\overline{U}$, Y_{mp} is the MPP in the original random variable space corresponding to U_{mp}.

Usually the transform function $T(.)$ is in explicit form of the nondeterministic variables including Y_i. The sensitivity of reliability index in Equation 5.48 can be easily calculated from the RBDO inner loop results β and U_{mp}.

For example, if all the random variables are independent normal variables, Y_i has a mean μ_i and standard deviation σ_i, the corresponding standard normal U_i is obtained by

$$U_i = T(Y_i) = \frac{Y_i - \mu_i}{\sigma_i} \quad (5.49)$$

If the design variable X_i is the mean μ_i, the last term of the right hand side of Equation 5.48 is

$$\frac{\partial T(Y_i)}{\partial \mu_i}|_{Y_i=Y_{i,mp}} = -\frac{1}{\sigma_i} \qquad (5.50)$$

In some cases, the coefficient of variation (COV) is a constant c, which means $\sigma_i = c\mu_i$. Equation 5.49 becomes

$$U_i = T(Y_i) = \frac{Y_i-\mu_i}{c\mu_i} = \frac{Y_i}{c\mu_i} - \frac{1}{c} \qquad (5.51)$$

Equation 5.50 becomes

$$\frac{\partial T(Y_i)}{\partial \mu_i}|_{Y_i=Y_{i,mp}} = -\frac{Y_i}{c}\frac{1}{{\mu_i}^2}|_{Y_i=Y_{i,mp}} \qquad (5.52)$$

The reliability index sensitivity is accurate and robust by using the semi-analytic sensitivity of the limit state function. By providing the reliability index sensitivity to a gradient-based algorithm like SQP, the RBDO outer loop optimization can be solved efficiently.

5.7 NUMERICAL EXAMPLES

Figure 5-5 shows the process of ultimate strength analysis based RBDO for nonlinear beam-columns. Both the inner loop reliability analysis and outer loop structural optimization use SQP algorithm as optimizer. The solution of load-incremental ultimate strength analysis is used as initial guess for direct solving method. Semi-analytic sensitivity based on the ultimate strength direct solving method is supplied to the SQP optimizer for reliability analysis and structural optimization.

The simply supported nonlinear beam-column as shown in Figure 5-1 with the cross-section shown in Figure 5-2 has initial deflection d at the center. The initial unloaded shape is half sinusoidal wave. Uniaxial compressive force P is applied at both ends. The material is elastic-perfectly-plastic. When the compressive force increases, the load-deflection curve is shown as in Figure 5-3. The RBDO problem of the nonlinear beam-column is formulated as Equation 5.1-5.7. The ultimate

load in the limit state function Equation 5.7 is calculated by the direct solving method. Semi-analytic sensitivity of the limit state function and the reliability index are used for the inner loop and outer loop optimization of RBDO, respectively.

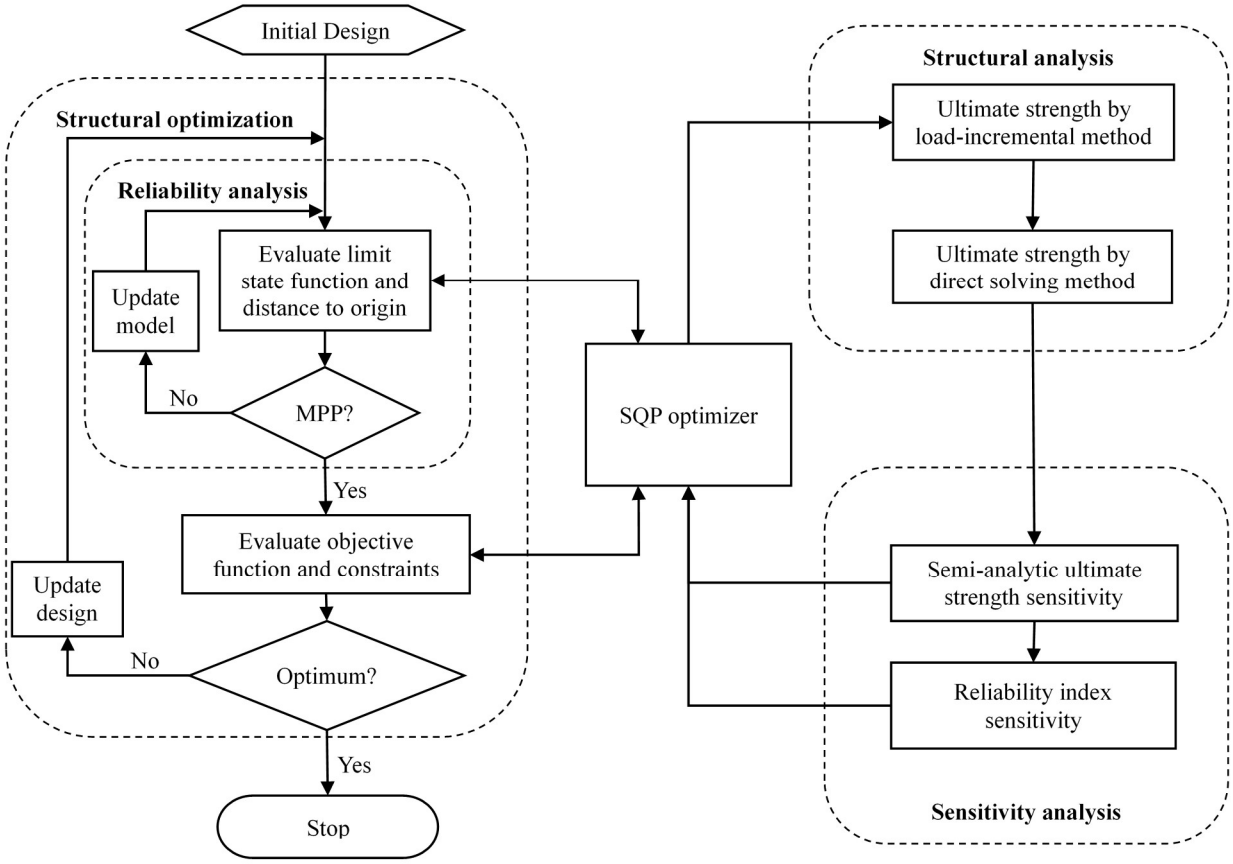

Figure 5-5. Double-loop RBDO flow chart.

5.7.1 Ultimate Strength Analysis

A beam-column has following design values including the yield stress σ_y, Young's modulus E, beam-column length L, initial central deflection d and cross-sectional parameters:

$\sigma_y = 247.3$ MPa , $E = 205800$ MPa , $L = 1524$ mm , $b = 304.8$ mm , $t = 6.4$ mm , $h_w = 64.25$ mm, $t_w = 4.65$ mm, $b_f = 27.94$ mm, $t_f = 6.35$ mm, $d = 2.9$ mm.

The ultimate strength of the beam-column calculated by a MATLAB program ULTBEAM which solves the discretized original governing equation set (Equations 5.8-5.17) by load-incremental method is compared with ABAQUS and ANSYS nonlinear FEA results. For clamped boundary conditions Equations 5.15-5.17 are replaced accordingly. The ABAQUS model is fine meshed 2-D beam-column using 2 node Timoshenko beam element (B21). The ANSYS beam-column model uses Beam188 element.

Figure 5-6. Beam-column cross-section diagram.

Figure 5-7. Half of initially curved beam-column (deflection towards the plate side).

The initial unloaded shape of simply-supported beam-column is assumed to be sinusoidal as shown in Figure 5-1. Clamped beam-column has cosine wave as the initial unloaded shape. The initial maximum deflection d at the beam center is 2.9 mm. Simply-supported beam-column under axial compression will have either stiffener-induced failure (stiffener side under greater compression) or plate-induced failure (plating side under greater compression) depending on the direction of initial deflection (towards the plate side, which causes the stiffener-induced failure or towards the stiffener side, which causes the plate-induced failure). For clamped beam-column, there is no such difference because of the symmetry of deformed shape.

As shown by the comparison in Table 5-1, ultimate strength calculated by ULTBEAM using the presented method is very close to nonlinear FEA for all three cases. The load-deflection curves of the three cases from the start of load step to the ultimate strength are compared in Figure 5-8 to Figure 5-10. The load path from ULTBEAM is very close to nonlinear FEA.

Table 5-1. Ultimate strength (MPa) compared with nonlinear FEA.

Boundary Condition	Simply-supported		Clamped
Failure mode	Stiffener-induced	Plate-induced	
ULTBEAM	156.9	219.6	230.2
ANSYS	157.7	220.1	229.5
ABAQUS	158	219.6	229.0

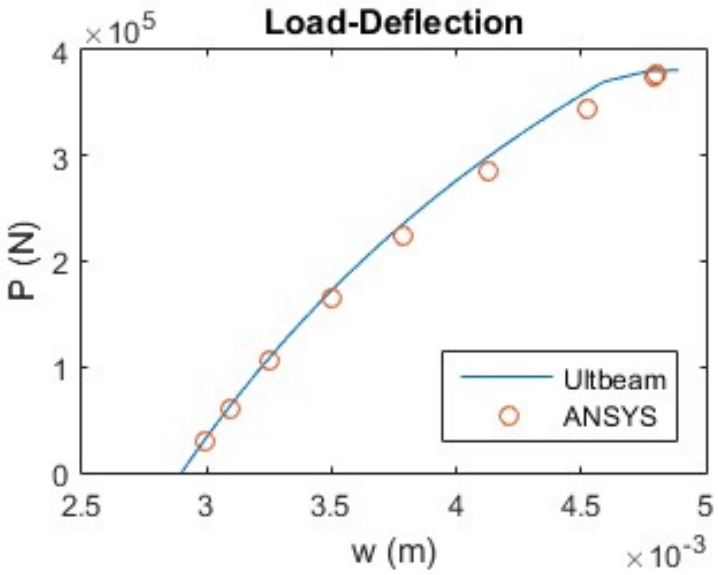

Figure 5-8. Load-deflection curve of simply-supported beam-column (stiffener-induced failure).

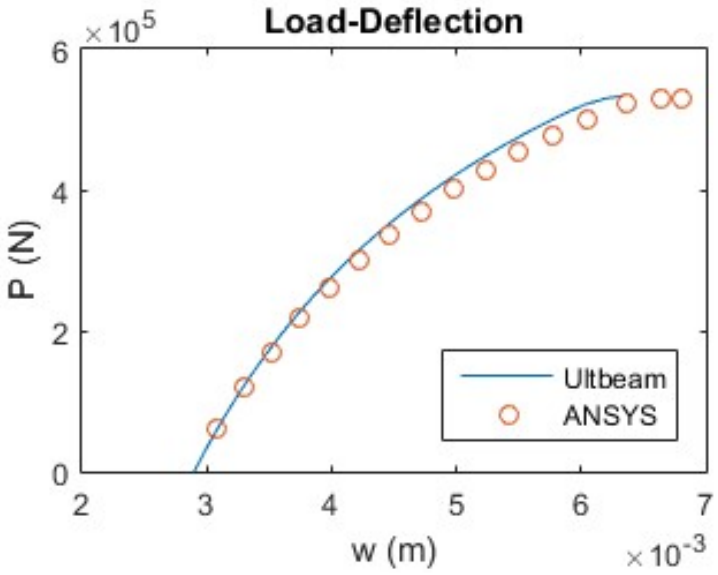

Figure 5-9. Load-deflection curve of simply-supported beam-column (plate-induced failure).

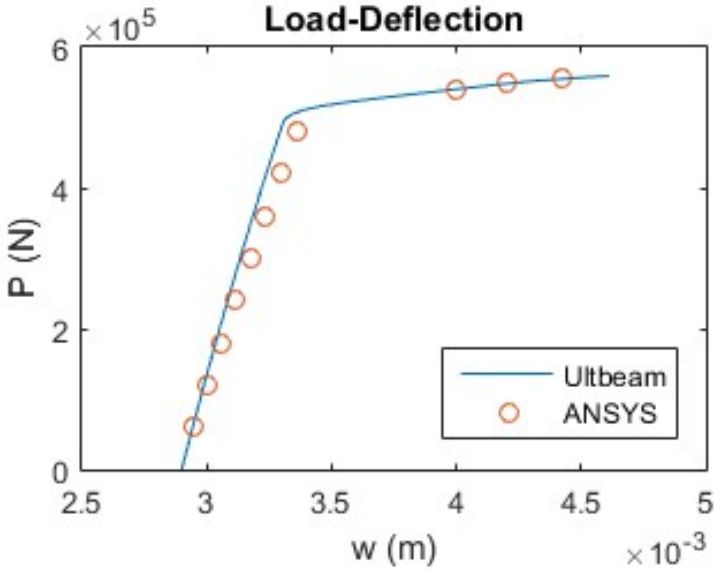

Figure 5-10. Load-deflection curve of clamped beam-column.

5.7.2 Sensitivity Analysis

Figure 5-11 shows the sensitivity of ultimate strength with respect to h_w for the simply-supported beam-column in 5.7.1 on a semi-log plot. Sensitivity calculated under different step size by three methods are compared. Forward finite difference sensitivity uses two analysis methods, load-incremental method and direct solving method, respectively. Semi-analytic sensitivity is based on the direct solving method. Finite difference sensitivity calculated by load-incremental method starts to have large errors from step size smaller than 10^{-5}. By using the direct solving method, errors of finite difference sensitivity only become significant for step size smaller than 10^{-15}. The semi-analytic sensitivity is constant at different perturbation step size (10^{-1} to 10^{-30}). Thus the semi-analytic sensitivity is more robust and efficient as compared to the finite difference sensitivity.

Figure 5-12 shows the sensitivity of reliability index with respect to one random design variable which is the mean of h_w by using two methods, finite difference and Equation 5.46. The inner loop reliability analysis uses semi-analytic sensitivity so the main errors are from the reliability index sensitivity analysis alone. As shown in the semi-log plot, the errors of finite difference sensitivity become significant at step size smaller than 10^{-13}. By using Equation 5.46, there is no step size in the calculation so the sensitivity has constant value from the same MPP solution of the reliability analysis. Figure 5-13 shows similar comparison for the sensitivity of reliability index with respect to one deterministic design variable which is the mean of b. The outer loop of RBDO using Equation 5.46 to calculate the reliability index sensitivity is robust and efficient.

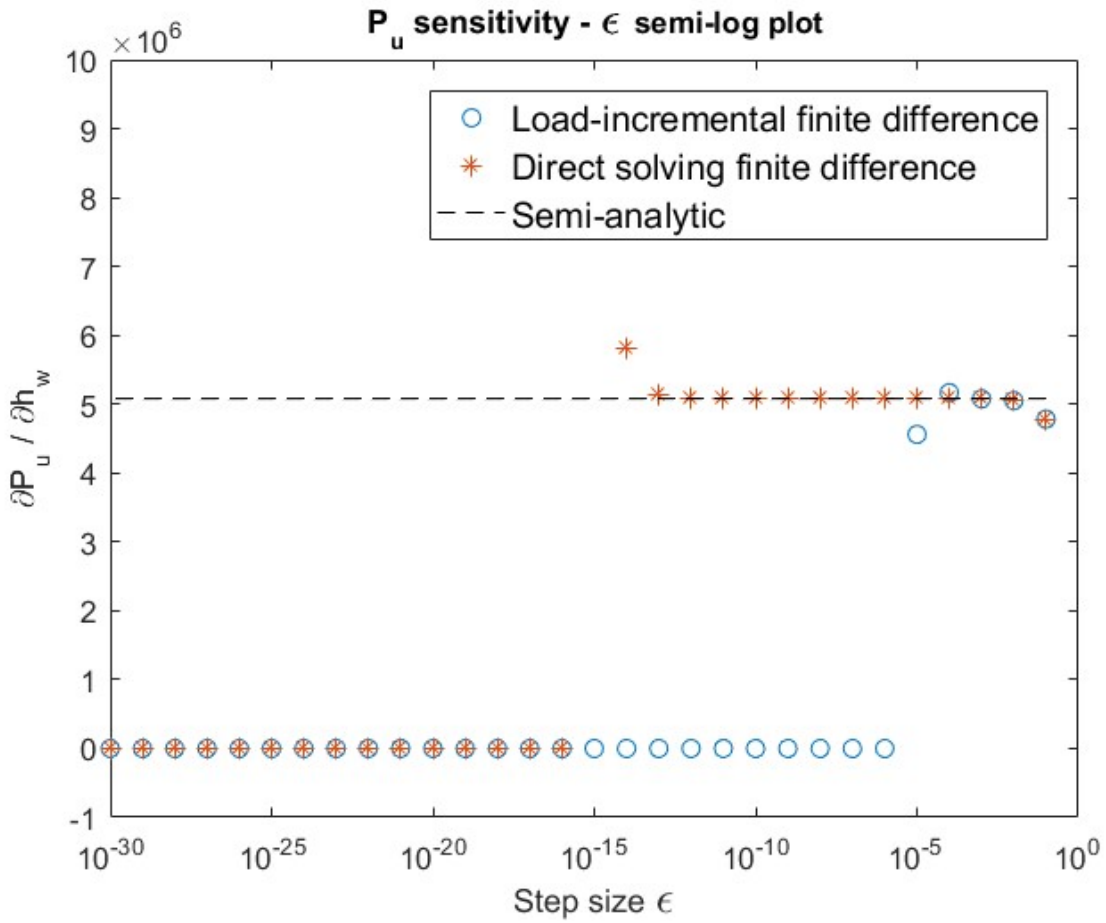

Figure 5-11. Comparison of ultimate strength finite difference sensitivity by two analysis methods and semi-analytic sensitivity.

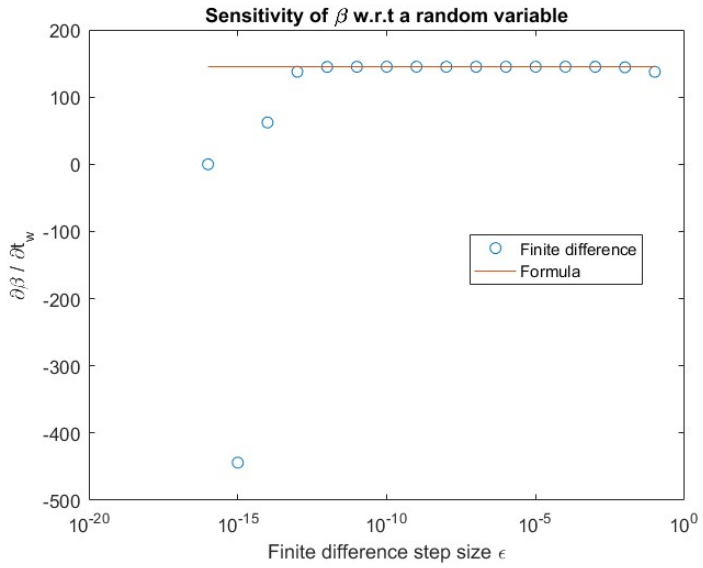

Figure 5-12. Comparison of reliability index sensitivity w.r.t a random variable by finite difference and Equation 5.46.

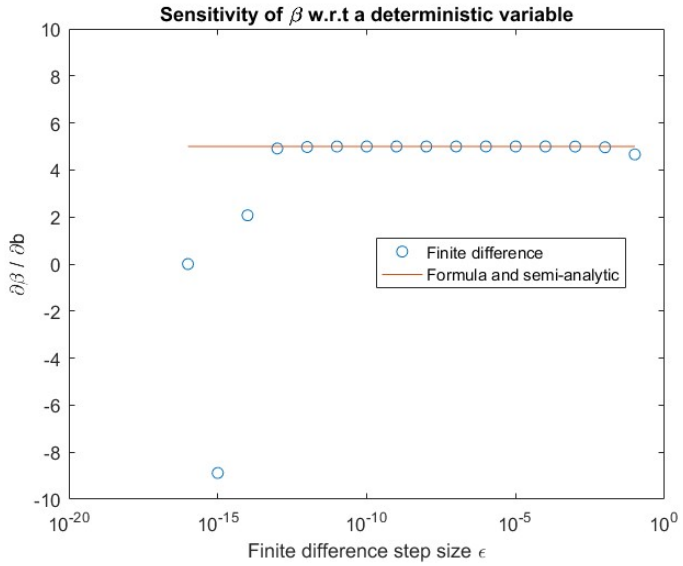

Figure 5-13. Comparison of reliability index sensitivity w.r.t a deterministic variable by finite difference and Equation 5.46.

5.7.3 Sensitivities for Change in Failure Pattern

When an initially curved asymmetrical beam-column is under axial compression and reaches ultimate strength, both the plating and flange could be under compression at the center where maximum stress is at. If the initial deflection is towards the plating side, under axial compression the flange side will have larger compressive stress because the area is smaller than the plating so the distance to neutral axis is larger. In this case the increment of cross-sectional dimensions will in general increase the ultimate strength. However, if the initial deflection is towards the flange side, under axial compression the plating side will have compressive stress but the flange side would have either compressive or tensile stress depending on the geometry. The yield will first occur either in the plating side in compression or in the flange side in extension. As the yield zone progresses from the surface towards the center, the beam-column will reach the ultimate strength with both compressive and tensile failure in the cross-section. In some cases, by increasing the cross-sectional dimension the shifting of neutral axis will cause different failure patterns to happen and result in decrease of ultimate strength.

Figure 5-14 plots the ultimate strength of a beam-column with different plate width while all other geometric and material parameters are fixed with following properties:

$\sigma_y = 247.3$ MPa, $E = 205800$ MPa, $L = 1524$ mm, $t = 10.0$ mm, $h_w = 100.0$ mm, $t_w = 10.0$ mm, $b_f = 300.0$ mm, $t_f = 10.0$ mm, $d = 50.0$ mm.

The plate width b changes in the range of 1.0 m to 2.0 m. The initial deflection is towards the stiffener flange side. The ultimate strength increases with the plate width from 1.0 m and reaches a peak when at about 1.4 m. Between 1.4 m to 2.0 m plate width, the ultimate strength actually decreases with increasing plate width. Figure 5-15 plots the ultimate strength sensitivity, i.e. derivative w.r.t the plate width. The sensitivity is positive and near constant from 1.0 m to 1.2 m where it starts to drop and reaches to zero at 1.4 m beyond which point it is negative. Figure 5-14shows the change of failure pattern in the beam-column cross-section due to nonlinearity and asymmetry will affect the ultimate strength and sensitivity. The increment of axial compression

will cause stress re-distribution not only in the cross-section but also along the length. Since the beam-column has constant cross-sectional geometry, the change of failure pattern still results in smooth change of ultimate strength which is reflected by the continuous sensitivity shown in Figure 5-15.

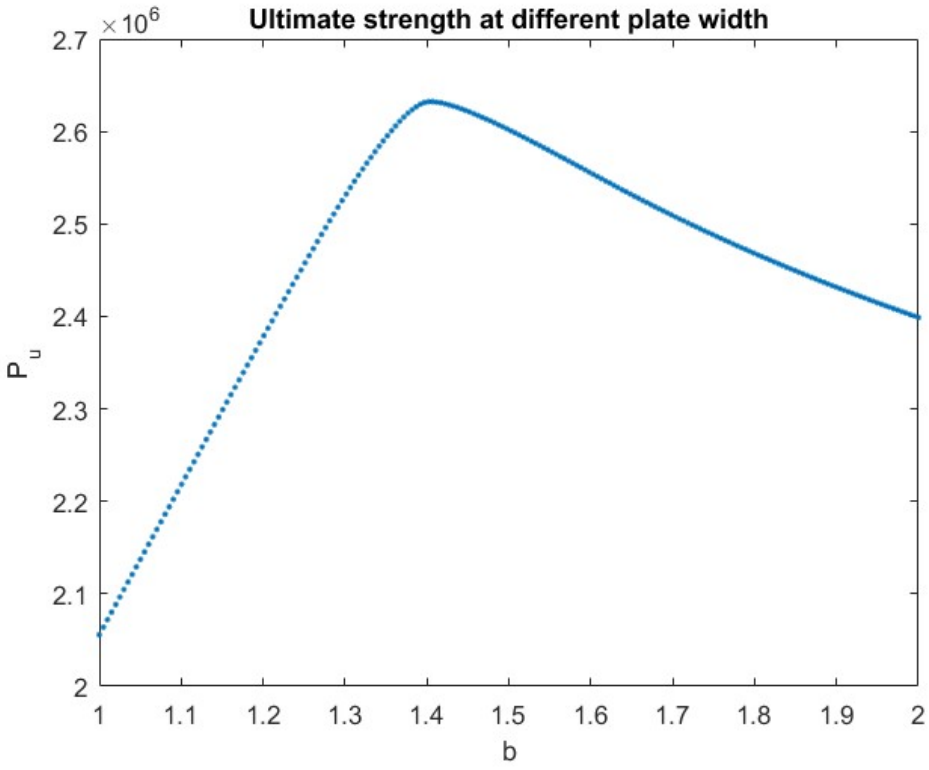

Figure 5-14. Validation of P_u with b around change in failure pattern.

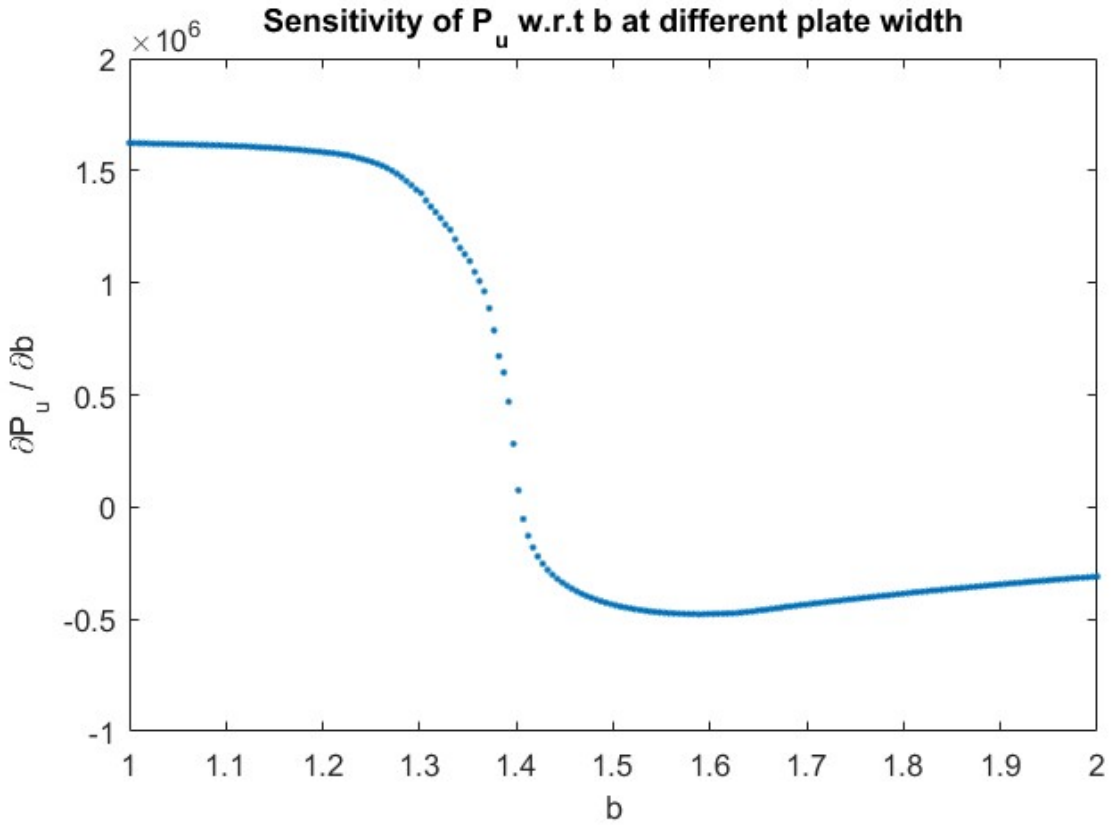

Figure 5-15. Change in the sensitivity of P_u w.r.t b with change in failure pattern.

5.7.4 Deterministic Structural Optimization

Structural optimization of elasto-plastic beam-column is defined as

$$\textit{Minimize:} \quad F(\bar{X}) \tag{5.53}$$

$$\textit{subject to:} \quad P_0 - P(\bar{X}) \leq 0 \tag{5.54}$$

$$\bar{X}_{min} \leq \bar{X} \leq \bar{X}_{max} \tag{5.55}$$

where $F(\bar{X})$ is the cross-sectional area, $\bar{X}$ is a vector of design variables, P is the ultimate strength calculated by the direct solving method, and P_0 is the defined limit of P.

The semi-analytic sensitivity of the constraint function is calculated by Equation 5.45 and SQP algorithm is used to solve for the optimum design.

First, two design variables $[h_w,\ b_f]$ of a simply supported beam-column are optimized. The beam-column has following properties:

$\sigma_y =$ 247.3 MPa , $E =$ 205800 MPa , $L = 1524$ mm , $b = 304.8$ mm , $t = 6.4$ mm , $t_w =$ 4.65 mm, $t_f = 6.35$ mm, $d = 2.9$ mm.

The initial deflection d is 11.6 mm, about 0.75% of the beam length, towards plating side. The required ultimate compressive load limit P_0 is 5.0×10^5 N. The two design variables $[h_w,\ b_f]$ have lower bound $\bar{X}_{min} =$ [50 mm, 50 mm] and upper bound $\bar{X}_{max} =$ [150 mm, 150 mm]. Figure 5-16 shows the contour lines of the objective function (cross-sectional area) and the shaded feasible design space. The optimum design is found as $[h_w = 135.7 \text{ mm},\ b_f = 50 \text{ mm}]$. The objective function value is 948.68 mm^4. This optimum design can be identified as the lower left vertex (red circle) of the shaded feasible region in Figure 5-16.

Next, four design variables $[t_w, t, t_f, h_w]$ are optimized with a series of ultimate load limit P_0. The lower and upper bounds are [5, 5, 5, 100] mm and [15, 15, 15, 150] mm, respectively. Table 5-2 lists the optimum design for different ultimate load limit P_0 in each row.

In Table 5-2, only the shaded cells have design values not on the boundary. It is noticed that when the load limit is small, only h_w is not at the lower limit. Only after h_w reaches the upper limit under intermediate load constraint, t_f starts to affect the design. Then comes t and finally t_w becomes important only after the other three design variables are at the upper limit. This shows the influence of each design variable under different ultimate strength limit.

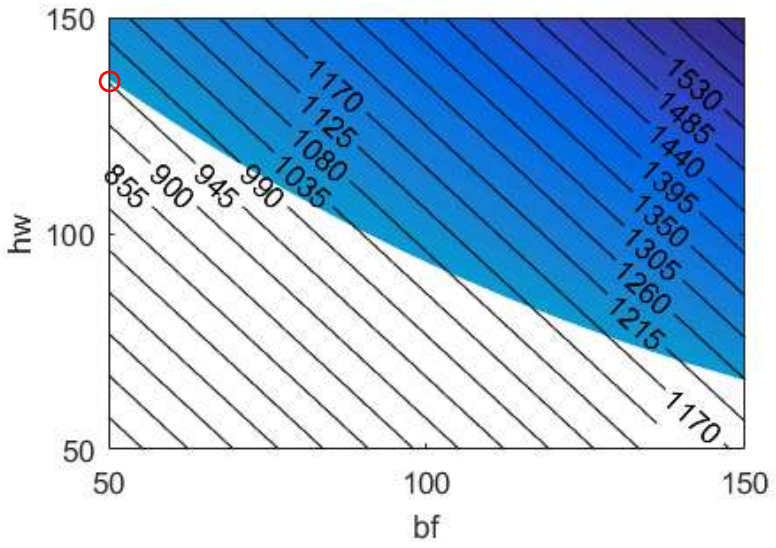

Figure 5-16. Design space of h_w and b_f (objective function contours and shaded feasible region).

Table 5-2. Four variables optimization results.

Optimum Design (mm)				Objective Function Value	Constraint Limit
t_w	t	t_f	h_w	Area (mm^4)	P_o (N)
5	5	5	121.68	2382.38	4.00E+05
5	5	14.03	150	2975.27	6.00E+05
5	11	15	150	3924.57	8.00E+05
6.44	15	15	150	4964.12	1.00E+06

5.7.5 Structural Reliability Analysis

The Structural reliability problem of the elasto-plastic beam-column is defined by Equations 5.4-5.5. The limit state function is Equation 5.7. Original random variables are transformed by

Equation 5.51. The semi-analytic sensitivity of the limit state function is calculated by Equation 5.44 and SQP algorithm is used to solve for safety index.

Except length L and plate width b, all other geometric and material parameters are normally distributed random variables. The initial design values are the mean values of the random variables. The Coefficient of Variation (COV) and Standard Deviation of all the random variables are listed in Table 5-3. All the random variables are assumed to be independent.

Table 5-3. Random variables.

Variable	Distribution	Mean value	COV	Standard deviation
σ_y	Normal	247.3	0.1	24.73
E	Normal	2.058E5	0.1	2.058E4
t	Normal	6.4	0.02	0.128
h_w	Normal	64.25	0.01	0.6425
t_w	Normal	4.65	0.02	0.093
b_f	Normal	27.94	0.03	0.8382
t_f	Normal	6.35	0.02	0.127
d	Normal	3.81	0.5	1.905

The ultimate compressive load of the initial deterministic design is 351028 N. With a safety factor of 2.0, the design load is about 1.75×10^5 N. With a safety factor of 3.0, the design load is about 1.15×10^5 N. Table 5-4 lists the reliability analysis results of the initial design under different design load by FORM. The design load is deterministic in first section and nondeterministic with two values of COV for comparison. The probability of failure P_f is calculated from reliability index β by:

$$P_f = \emptyset(-\beta) \qquad (5.56)$$

where $\emptyset(.)$ is the cumulative distribution function (CDF) of standard normal distribution.

Table 5-4. FORM reliability analysis results.

Load (N)	Deterministic load		Normally distributed load COV = 0.1		Normally distributed load COV = 0.2	
	β	P_f	β	P_f	β	P_f
1.15E5	6.45	5.5E-11	5.95	1.33E-9	4.99	2.94E-7
1.25E5	6.09	5.7E-10	5.55	1.47E-8	4.59	2.26E-6
1.50E5	5.18	1.10E-7	4.59	2.25E-6	3.69	1.13e-04
1.75E5	4.30	8.51E-6	3.73	9.53E-5	2.94	0.0016
2.00E5	3.47	2.58E-4	2.97	0.0037	2.32	0.0102

Monte Carlo simulation (MCS) method uses large sample of limit state evaluations to estimate the failure rate. When the probability of failure is small, the sample size has to be large enough to reflect the occurrence of failure event. For example, structural design could allow probability of failure to be as small as 10^{-5}. So the sample size of MCS should be about 10^7 to have an accurate estimate. Even if the ultimate strength analysis is efficient, millions of such analyses will be extremely time-consuming. Each simulation will have different result due to the variance so multiple tests are necessary to get better estimate. By contrary, FORM will give an accurate and consistent estimation of small probability of failure if the failure surface near the MPP does not have large curvature, i.e. it can be approximated by the linearized limit state function and.

MCS is used to validate FORM analysis. Table 5-5 compares the failure rates by MCS with the probabilities of failure calculated by FORM for deterministic design load. The sample size of MCS is 2.5×10^5. For four cases of different deterministic axial loads, the reliability results of MCS and FORM are fairly close but FORM requires three orders of magnitude less ultimate strength evaluation than MCS sample size.

Table 5-5. Reliability analysis by FORM compared with MCS (2.5×10^5 sample size).

Load (N)	MCS failure count	MCS failure rate	FORM probability of failure	FORM function count
2.00E05	67	2.68E-04	2.5778E-04	137
2.10E05	179	7.16E-04	7.8836E-04	190
2.15E05	314	0.001256	0.00150	154
2.40E05	2793	0.011172	0.01090	235

5.7.6 Reliability-Based Design Optimization

Table 5-6 lists the RBDO results for a beam-column under a normally distributed axial compressive load of 2.0E5 N with a COV of 0.1. The initial deflection d has a mean of 11.6 mm and a COV of 0.5. Mean and standard deviation for all other random variables are the same values as listed in Table 5-3. Six design variables are the cross-sectional geometric parameters which are the deterministic plate width b and the mean values of other five variables. The standard deviation of the nondeterministic design variables remain constant as the values listed in Table 5-3.

In Table 5-6 the baseline design point is the average of the upper and lower limit. The deterministic optimum design has the same safety factor of the baseline design, i.e. the ultimate strength is the same. The RBDO design uses the baseline design's reliability index as constraint limit. Both the deterministic optimum design and RBDO design reduced the weight from the baseline design with the RBDO design having slightly lower weight. Additional RBDO designs use various levels of reliability index as constraint limits. All optimum designs have only one design variable value not on the boundary (in shaded cells). Designs of higher reliability have higher structural weight.

Table 5-6. RBDO results. (The mean of d is 11.6 mm and COV is 0.5. Other random variables' distribution and standard deviation are the same as listed in Table 5-3.)

Load = 2.0E5 N COV = 0.1	Design variable (mm)						Ultimate load (N)	Objective function	Reliability index	Probability of failure
	b	t	h_w	t_w	b_f	t_f	P_u	Area (mm^2)	β_0	P_f
Lower limit $\bar{X}_{min}$	200.0	10.0	80.0	5.0	30.0	5.0	2.7616E5	2550.00	1.2977	0.0972
Upper limit $\bar{X}_{max}$	400.0	15.0	120.0	10.0	50.0	10.0	1.1077E6	7700.00	7.6941	7.1247E-15
Baseline $\bar{X}_0$	300.0	12.5	100.0	7.5	40.0	7.5	6.1657E5	4800.00	5.3111	5.4471E-8
Deterministic optimum design	200.0	10.0	120.0	7.7	50.0	10.0	6.1657E5	3425.95	5.9266	1.5460E-9
RBDO design	200.0	10.0	120.0	5.0	48.87	10.0	5.4401E5	3088.73	5.3111	5.4471E-8
RBDO with different reliability limit	200.0	10.0	91.8	5.0	30.0	5.0	3.1763E5	2608.85	2.0	0.0228
	200.0	10.0	110.3	5.0	30.0	5.0	3.7776E5	2701.71	3.0	0.0013
	200.0	10.0	120.0	5.0	30.0	7.37	4.4067E5	2821.05	4.0	3.1671E-5
	200.0	10.0	120.0	5.0	40.83	10.0	5.1592E5	3008.30	5.0	2.8665E-7
	200.0	10.0	120.0	8.0	50.0	10.0	6.2368E5	3459.98	6.0	9.8659E-10
	200.0	11.1	120.0	10.0	50.0	10.0	7.0443E5	3922.10	6.5	4.0160E-11
	209.7	15.0	120.0	10.0	50.0	10.0	8.2677E5	4845.66	7.0	1.2798E-12
	321.6	15.0	120.0	10.0	50.0	10.0	1.0040E6	6523.30	7.5	3.1909E-14

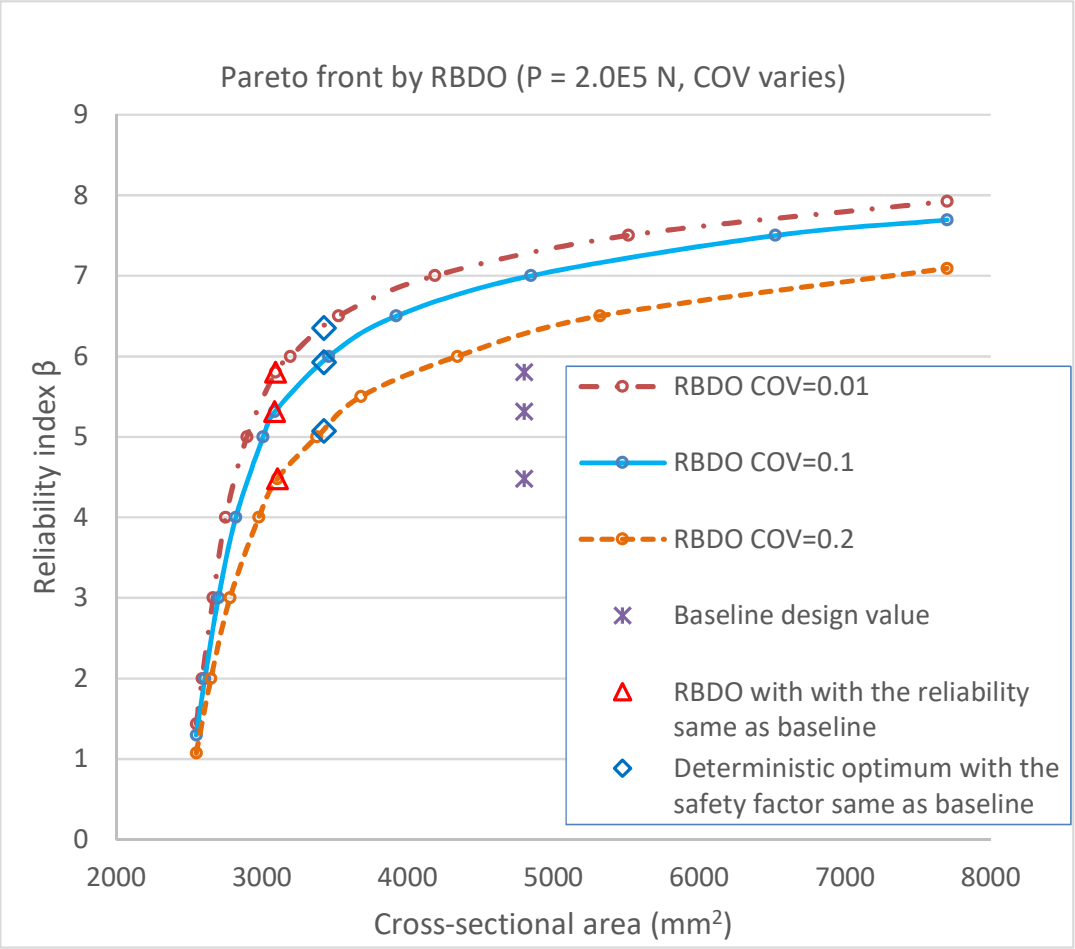

Figure 5-17. Pareto front of RBDO for three load conditions.

The weight (area) and reliability index results of Table 5-6 are plotted in Figure 5-17 to show the Pareto front along with results of two additional loading conditions with axial loads having the same mean but different COV (0.01 and 0.2). It is shown that at low reliability levels the optimum designs of three load cases are close. At the same reliability level, optimum designs under load of larger COV have higher weight. The reliability index of the deterministic optimum design (with the same safety factor as the baseline design) are calculated under all three load cases and plotted as diamonds. The RBDO designs with the same reliability index as the baseline design are plotted as triangles. Among these design cases, the deterministic optimums are very close to the Pareto front calculated by RBDO.

A series of deterministic optimum designs are obtained under different levels of safety factor. The reliability index of each design is calculated under the three load conditions. The results are plotted with the Pareto front by RBDO in Figure 5-18.

In Figure 5-19 and Figure 5-20, the Pareto front calculated from the same series of deterministic designs are plotted as lines. In Figure 5-19, the three cases have applied load of different mean but same COV (0.1). In Figure 5-20, the two cases have the same random load applied but the COV of initial deflection is different. All other random variables have a COV of 0.1. A few RBDO designs under the same loading conditions are plotted as triangle, square and diamond in Figure 5-19 and Figure 5-20 for comparison.

From Figure 5-18 to Figure 5-20 it can be seen that the Pareto fFront by RBDO and deterministic design approach are very close.

In Figure 5-21, the Pareto front line is plotted in segments. The random variables are the same as in Table 5-6. Each segment is bounded by the designs at vertices where all design variables are at upper or lower boundary. Within each segment, only one design variable has values not on the boundary and it is regarded as the dominant variable. As the reliability index increases, the slope of the segments decreases. One reason is that the standard deviation of each design variable is a constant value in these designs. Thus it is the mean value of design variables that affects the reliability the most. As the required reliability increases, more influential design variables will take effect first and reach its upper limit before other design variables start to increase from the lower limit. There is no difference between the results from deterministic design and RBDO for this type of Pareto front. However, if the variances of different design variables have large gaps, the sequence of design variables taking effect in RBDO may be different from the sequence in deterministic optimization. For example, in the lower first two segments in Figure 5-21, h_w in increased before t_f in both deterministic optimization and RBDO. Under some circumstances, if h_w has very large COV compared to t_f, increasing h_w will actually be less effective than increasing t_f in terms of improving the reliability. In extreme cases, the reliability will actually decrease when the mean value of one design variable increases if the COV of it is large. This will

be reflected in the Pareto front line of deterministic designs with the lower segment having lower slope as compared to the higher segment, which is different from the lines shown in Figure 5-21. In these cases, RBDO will consider both the objectives, weight and reliability, in one design process and consequently have a different sequence of effective (dominant) design variables. Thus the Pareto front line from RBDO will still look similar to the one in Figure 5-21, and it will have advantage over the deterministic optimization which does not account for the influence of design variable's large variance on reliability.

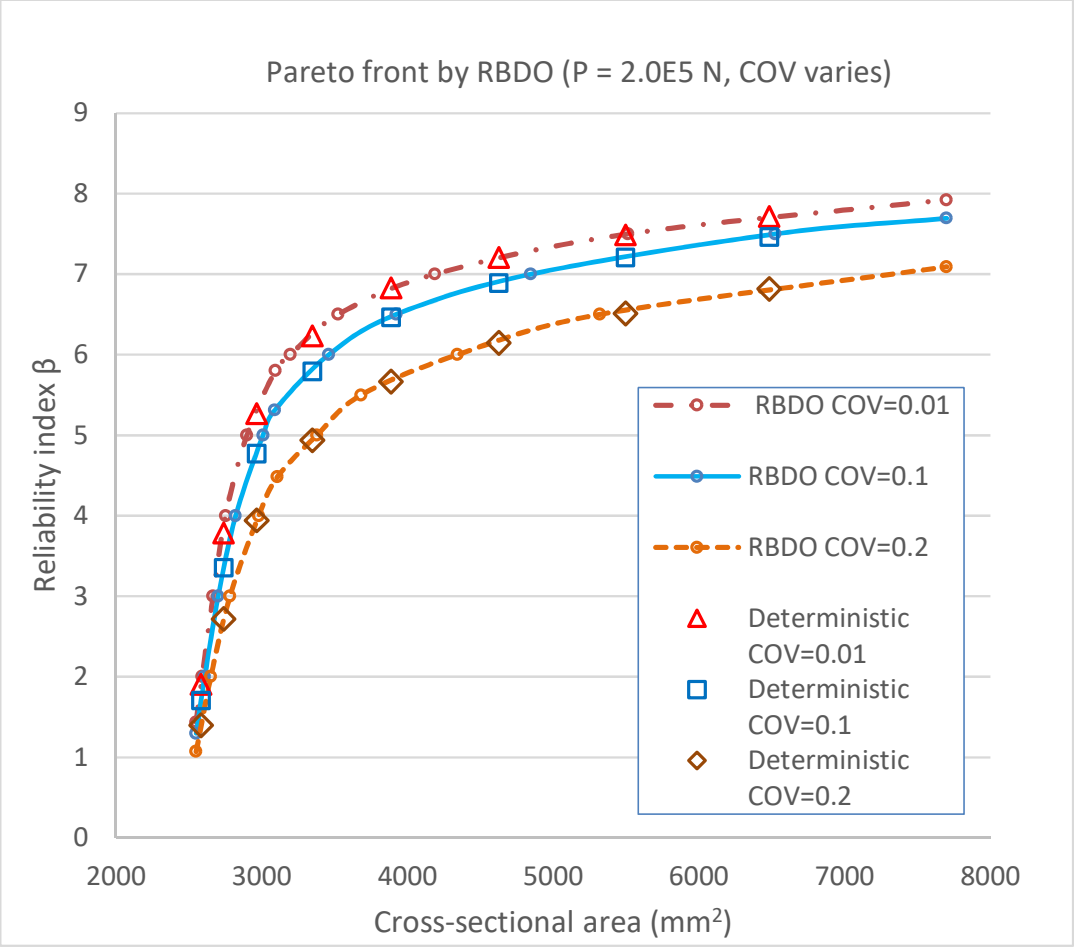

Figure 5-18. Pareto front by RBDO for three load conditions of different COV compared with deterministic design.

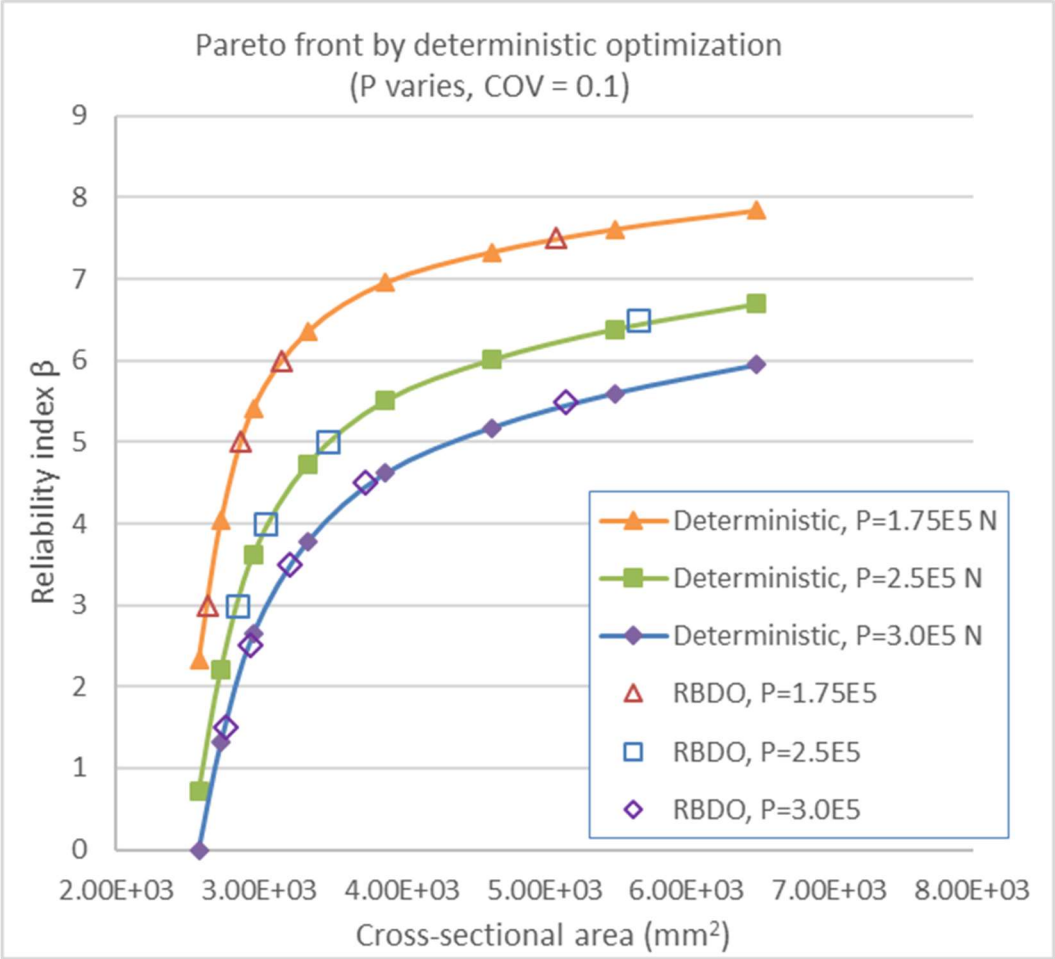

Figure 5-19. Pareto front by deterministic design for three load conditions of different mean compared with RBDO design.

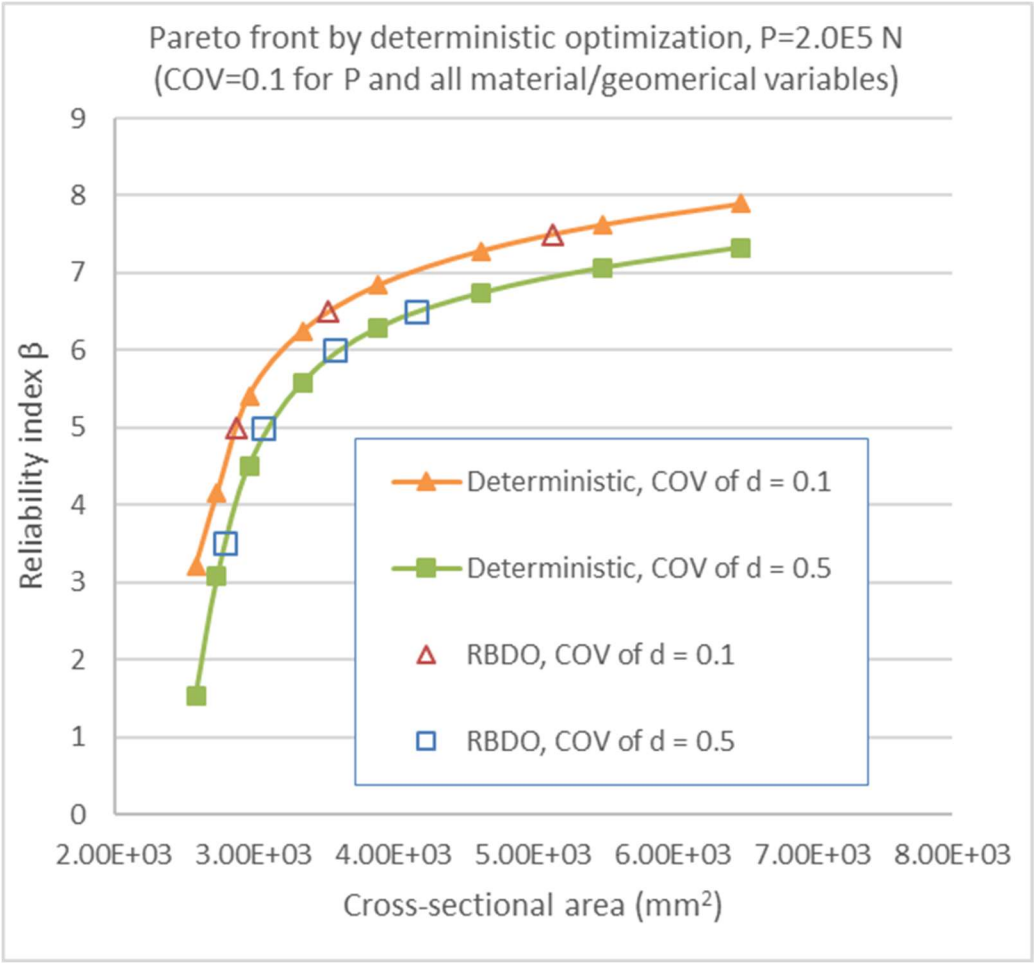

Figure 5-20. Pareto front by deterministic design for design series of different COV for d compared with RBDO design.

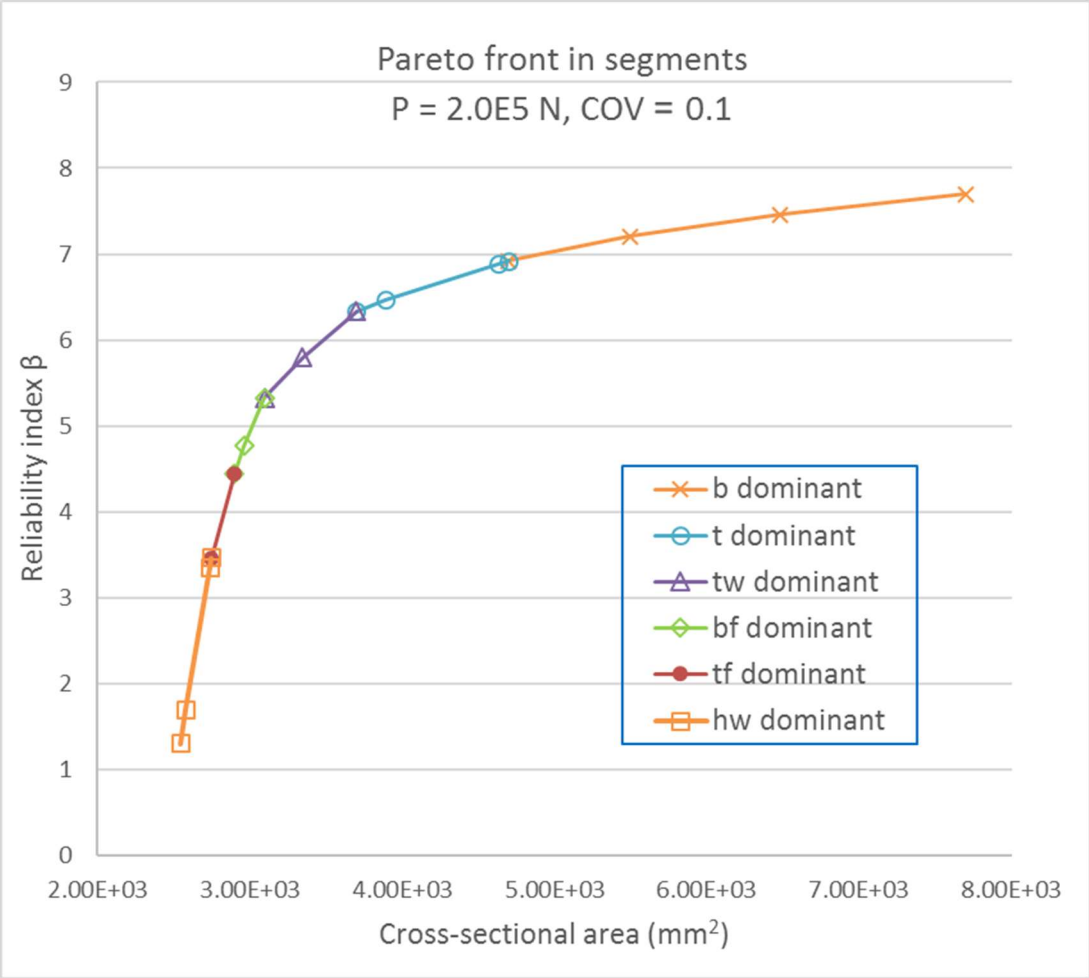

Figure 5-21. Pareto front by deterministic design plotted in segments bounded by vertices.

5.8 CONCLUSION

A RBDO procedure for nonlinear beam-columns of inelastic material and asymmetric I cross-section is introduced in this paper. The ultimate strength analysis based-on nonlinear beam theory and nonlinear constitutive law is accurate and efficient. The direct solving method combines the governing equations and their derivatives with respect to a deformation parameter, and solves for the ultimate strength directly. Semi-analytic sensitivity of the ultimate load is calculated by solving a linear set of sensitivity equations based on the ultimate strength direct solving method. This approach is found to be robust and efficient as compared to finite difference sensitivity analysis. Structural reliability analysis and optimization use gradient-based SQP algorithm by providing the semi-analytic sensitivity to the optimizer. Double-loop RBDO minimizes the weight of nonlinear beam-column with nondeterministic applied load, geometric parameters and material properties under reliability constraints. Sensitivity of reliability index is calculated from the gradient of limit state function at the MPP of inner loop reliability analysis. The RBDO procedure presented in this paper is robust and efficient. The ultimate strength analysis, semi-analytic sensitivity analysis, reliability analysis, optimization and RBDO methods can be applied for combined load cases, beam-columns of non-constant cross-sections, frame system consisting of multiple beam-columns and other large engineering structures including stiffened panels and aerospace/ocean structures.

6 Chapter Six

Conclusions

This dissertation presents a Reliability-Based Design Optimization (RBDO) procedure for beam-columns of inelastic material and asymmetric I cross-section. The RBDO procedure is robust and efficient and uses the ultimate strength direct solving method, semi-analytic sensitivity of the ultimate strength and gradient-based optimization algorithm for structural optimization and reliability analysis.

In Chapter 2, the ultimate strength load-incremental analysis method is based on nonlinear beam theory with material and geometric nonlinearities. Nonlinear constitutive law is developed for elastic-perfectly-plastic beam cross-section consisting of base plate and T-bar stiffener. The results of load-incremental ultimate strength analysis are validated using commercial nonlinear finite element analysis for single-span simply-supported/clamped beam-columns and multi-span simply-supported beam-columns.

In Chapter 3, a new ultimate strength direct solving method is introduced, which combines the original governing equations with their derivatives with respect to a deformation parameter and solves for the ultimate strength directly. The direct solving method is more robust than load-incremental method in calculating finite difference sensitivity of the ultimate strength. Deterministic beam-column structural optimization results are presented using the ultimate strength direct solving method and a gradient-based optimization algorithm. The convergence is faster and more robust than non-gradient-based algorithm.

In Chapter 4, structural reliability analysis is presented for nonlinear beam-columns with ultimate strength constraint by using First Order Reliability Method. The sensitivity of the limit state function is calculated by using complex step method and ultimate strength direct solving method. The complex step sensitivity is more robust than finite difference sensitivity as it eliminates the

subtractive cancellation error at small step size. Structural failure probabilities calculated by FORM are validated by Monte Carlo Simulation.

In Chapter 5, the Reliability-Based Design Optimization procedure for nonlinear beam-columns is introduced by using the ultimate strength direct solving method, semi-analytic sensitivity and gradient-based optimization algorithm. Semi-analytic sensitivity of the ultimate strength is solved from a linear set of sensitivity equations using the Jacobian matrix of the direct solving method. The derivatives of the structural residual equations in the sensitivity equation set are calculated using the complex step method. The semi-analytic sensitivity is more robust and efficient as compared to finite difference sensitivity. The semi-analytic sensitivity is more efficient than complex step sensitivity which requires full re-analysis by solving complex equation set. The sensitivity of reliability index with respect to design variables is calculated from the gradient of limit state function at the MPP of reliability analysis. Double-loop RBDO minimizes structural weight with reliability index constraint. By using the ultimate strength direct solving method, semi-analytic sensitivity and gradient-based optimization algorithm, the RBDO method developed in this dissertation is found to be robust and efficient. Pareto front with structural cost and reliability objectives is calculated for the nonlinear beam-columns under different nondeterministic loads and is compared with deterministic optimization.

The RBDO procedure for nonlinear beam-columns of inelastic material and asymmetric I cross-section presented in this dissertation is robust and efficient as it uses the semi-analytic sensitivity. The ultimate strength direct solving method, semi-analytic sensitivity analysis, reliability analysis, optimization and RBDO methods can be applied for combined load cases, nonlinear beam-columns of non-constant cross-sections, frame system consisting of multiple beam-columns, and large/complicated engineering structures including stiffened panels, aerospace/ocean structures.

References

American Bureau of Shipping. (2017). *Steel vessel rules*. Houston: American Bureau of Shipping.

Allen, M., & Maute, K. (2004). Reliability based optimization of aeroelastic structures. *Structural and Multidisciplinary Optimization*, 27, 228-242.

ANSYS. (2013). ANSYS: User's Manual (Version 15.0) [Software].

Ba-abbad, M. A., Nikolaidis, E., & Kapania, R. K. (2006). New approach for system reliability-based design optimization." *AIAA Journal*, 44, 1087-1096.

Ba-abbad, M. A., & Kapania, R. K., et al. (2003). Reliability-based structural optimization of an elastic-plastic beam. *AIAA Journal*, 41(8), 1573-1582.

Badran, S. F., Saddek, A. B., & Leheta, H. W. (2013). Ultimate strength of Y and T stiffeners subjected to lateral loads with three different levels of initial imperfection. *Ocean Engineering*, 61, 12-25.

Barros A. F. M., Barros M. H. F. M., & Ferreira C.C. (2012). Optimal design of rectangular RC sections for ultimate bending strength. *Structural and Multidisciplinary Optimization*, 45(6), 845–860.

Bebamzadeh, A., & Haukaas, T. (2008). Second-order sensitivities of inelastic finite element response by direct differentiation. *ASCE Journal of Engineering Mechanics*, 134(10), 867-880.

Bielski, J., & Bochenek, B. (2008). On a compressed elastic-plastic column optimized for post-buckling behavior. *Engineering Optimization*, 40(12), 1101-1114.

Bjerager, P., & Krenk, S. (1987). Sensitivity measures in structural reliability analysis. P. Thoft-Christensen (Ed.), *Proc. 1st IFIP Working Conf. on Reliability and Optimization of Structural Systems* (pp. 459-70). Berlin: Springer.

Brubak, L., Andersen H., & Hellesland, J. (2013). Ultimate strength prediction by semi-analytical analysis of stiffened plates with various boundary conditions. *Thin-Walled Structures*, 89, 1574-1585.

Caseiro, J. F., Valente, R. A. F., Andrade-Campos, A., & Yoon, J. W. (2011). Elasto-plastic buckling of integrally stiffened panels (ISP): an optimization approach for the design of cross-section profiles. *Thin-Walled Structures*, 49, 864-873.

Chen, W. F., & Atsuta, T. (1976). *Theory of beam-columns* (Vol. 1). New York: McGraw-Hill.

Chen, W. F., & Lui, E. M. (1987). *Structural stability, theory and implementation*. New York: Elsevier.

Chen, Y. (2003). *Ultimate strength analysis of stiffened panels using a beam-column method. PhD dissertation*. Virginia Tech, Blacksburg, Virginia.

Cheng, B., Xiao, R., Zhao, J., & Cheng, J. (2010). Optimal stiffener design of moderately thick plates under uniaxial and biaxial compression. *Journal of Constructional Research*, 66, 1218-1231.

Cho, S. R., Kim, H. S., Doh, H. M., & Chon, Y. K. (2013). Ultimate strength formulation for stiffened plates subjected to combined axial compression, transverse compression, shear force and lateral pressure loadings. *Ships and Offshore Structures*, 8, 628-637.

Choi, S. K., Grandhi, R. V., & Canfield, R. A. (2007). *Reliability-based structural design*. London: Springer.

Chojaczyk, A. A., Teixeira, A. P., Neves, L. C., Cardoso, J. B., & Guedes Soares, C. (2015). Review and application of artificial neural networks models in reliability analysis of steel structures. *Structural Safety*, 52, 78-89.

Dassault Systems. (2016). ABAQUS: User's Manual [Software].

Det Norsk Veritas. (2014). *Design of offshore steel structures, general (LRFD method).* Oslo: Det Norsk Veritas.

Ghavamia, K., & Khedmatib, M. R. (2006). Numerical and experimental investigations on the compression behavior of stiffened plates. *Journal of Constructional Research*, 62, 1087-1100.

Haftka, R. T., & Gurdal, Z. (1992). *Elements of Structural Optimization*. The Netherlands: Kluwer Academic Publishers.

Hale, L. E. (2016). *Aerodynamic uncertainty quantification and estimation of uncertainty quantified performance of unmanned aircraft using non-deterministic simulations*. *PhD dissertation*. Virginia Tech, Blacksburg, Virginia.

Haukaas, T. (2006). Efficient computation of response sensitivities for inelastic structures. *ASCE Journal of Structural Engineering*, 132(2), 260-266.

Haukaas, T., & Scott, M. H. (2006). Shape sensitivities in the reliability analysis of nonlinear frame structures. *Computers & Structures*, 84(15), 964-977.

Hodges D. H. (2003). Geometrically-exact, intrinsic theory for dynamics of curved and twisted anisotropic beams. *AIAA Journal*, 41, 1131-1137.

Hodges D. H. (2006). *Nonlinear composite beam theory for engineers*. Virginia: AIAA.

Hohenbichler, M. & Rackwitz, R. (1986). Sensitivity and importance measures in structural reliability. *Civil Engineering Systems*, 3(4), 203–209.

Hughes, O. F. & Paik, J. K. (2010). *Ship structural analysis and design*. New Jersey: SNAME.

Hughes, O. F., Ma, M. & Paik, J. K. (2014). Applications of vector evaluated genetic algorithms (VEGA) in ultimate limit state based ship structural design. *Proceedings of the ASME 2014 33rd International Conference on Ocean, Offshore and Arctic Engineering* (Vol. 7).

Hughes, O. F., Ghosh, B. & Chen, Y. (2004). Improved prediction of simultaneous local and overall buckling of stiffened panels. *Thin-Walled Structures*, 42, 827-856.

International Association of Classification Societies. (2005). *Common Structural Rules*. London: IACS.

Jeong, S. B., & Park, G. J. (2017). Single loop single vector approach using the conjugate gradient in reliability based design optimization. *Structural and Multidisciplinary Optimization*. 55(4), 1329-1344.,

Kwak, B. M., & Lee, T. W. (1987). Sensitivity analysis for reliability-based optimization using an AFOSM method. *Computers & Structures*, 27, 399–406.

Lamberti, L., Venkataraman, S., Haftka, R. T., & Johnson, T. F. (2003). Preliminary design optimization of stiffened panels using approximate analysis models. *International Journal for Numerical Methods in Engineering*, 57, 1351-1380.

Li, Z., Patil, M., & Yu, X. (2017). Ultimate strength of steel beam-columns under axial compression. *Proceedings of the Institution of Mechanical Engineers, Part M: Journal of Engineering for the Maritime Environment*, 231(4), 828-843.

Li, Z., & Yu, X. (2016). A semi-analytical analysis on beam-column ultimate strength with different initial deflections. *World Journal of Engineering*, 13, 487-493.

Liang, J. H., Mourelatos, Z. P., & Nikolaidis, E. (2007). A single-loop approach for system reliability-based design optimization. *Journal of Mechanical Design*. 129, 1215-91224.

Lim J., & Lee B. C. (2015). A semi-single-loop method using approximation of most probable point for reliability-based design optimization. *Structural and Multidisciplinary Optimization*. 53(4), 745–757.

Ma, M., Paik, J. K., & McNatt, T. (2016). Hierarchically decomposed multi-level optimization of ship structural design. *Proceedings of the ASME 2016 35th International Conference on Ocean, Offshore and Arctic Engineering* (Vol. 9).

Ma, M., Hughes O. F., & Paik J. K. (2013). Ultimate strength based stiffened panel design using multi-objective optimization methods and its application to ship structures. *Proceedings of the 12th international symposium on practical design of ships and other floating structures* (PRADS). Changwon, South Korea.

MAESTRO Marine. (2017). MAESTRO: User's Manual (Version 11.5) [Software].

Mansour, R., & Olsson, M. (2016). Response surface single loop reliability-based design optimization with higher-order reliability assessment. *Structural and Multidisciplinary Optimization*, 54, 63–79.

Motta, R. S., & Afonso, S. M. B. (2016). An efficient procedure for structural reliability-based robust design optimization. *Structural and Multidisciplinary Optimization*, 54, 511–530.

Mukherjee, K. S., & Yao, T. (2006). Buckling/elastoplastic collapse behavior and strength of continuous Tee-bar stiffened plates. *Journal of OMAE*, 128, 145-155.

Nguyen, T. H., Song, J., & Paulino, G. H. (2010). Single-loop system reliability-based design optimization using matrix-based system reliability method: theory and applications. *Journal of Mechanical Design, Transactions of the ASME*, 132(1), 011005-011005-11.

Ni, X. Y., Prusty, G., & Hellier, A. K. (2016). Buckling and post-buckling of isotropic and composite stiffened panels: a review on optimization (2000-2015). *Trans RINA*, 158, 251-268.

Ohsaki, M. B. & Pan, P. (2009). Shape optimization of reduced beam section under cyclic loads. *Journal of Constructional Steel Research*, 65, 1511-1519.

Paik, J. K., & Thayamballi, A. K. (2003). *Ultimate limit state design*. England: Wiley.

Paik, J. K., & Lee, S. M. (2005). A semi-analytical method for the elastic–plastic large deflection analysis of stiffened panels under combined biaxial compression/tension, biaxial in-plane bending, edge shear, and lateral pressure loads. *Thin-Walled Structures*, 43(3), 375-410.

Paik, K. M., & Kumar, Y. V. S. (2006). Ultimate strength of stiffened panels with cracking damage under axial compression or tension. *Journal of Ship Research*, 50, 231-238.

Paik, J. K. (2007). The effective use of experimental and numerical data for validating simplified expressions of stiffened steel panel ultimate compressive strength. *Marine Technology*, 44, 93-105.

Paik, J. K., Bong, J. K., & Jung, K. S. (2008a). Methods for ultimate limit state assessment of ships and ship-shaped offshore structures: part I unstiffened panels. *Ocean Engineering*, 35, 261-270.

Paik, J. K., Bong, J. K., & Jung, K. S. (2008b). Methods for ultimate limit state assessment of ships and ship-shaped offshore structures: part II stiffened panels. *Ocean Engineering*, 35, 271-280.

Paik, J. K., Bong, J. K., & Jung, K. S. (2008c). Methods for ultimate limit state assessment of ships and ship-shaped offshore structures: part III hull girders. *Ocean Engineering*, 35, 281-286.

Paik, J. K. (2008d). Ultimate strength of perforated steel plates under combined biaxial compression and edge shear loads. *Thin-Walled Structures*, 46, 207-213.

Palizzolo, L. (2004). Optimization of continuous elastic perfectly plastic beams. *Computers and Structures*, 82, 397-411.

Ringsberg, J. W., Saglam, H., Sarder, M. A., & Ulfvarson, A. (2014). Lightweight design of offshore platform marine structures – Optimization of weight to strength utilization of corrugated shell plating. *Ships and Offshore Structures*, 9, 38-53.

Scott, M. H., & Jafari, A., V. (2017). Response sensitivity of material and geometric nonlinear force-based Timoshenko frame elements. *International Journal for Numerical Methods in Engineering*, 111(5), 474-492.

Shan, S., & Wang, G. (2008). Reliable design space and complete single-loop reliability based design optimization. *Reliability Engineering and System Safety*, 93(8), 1218-1230.

Sharifi, Y., & Paik, J. K. (2011). Ultimate strength reliability analysis of corroded steel-box girder bridges. *Thin-Walled Structures*, 49, 157-166.

Shi, G., & Wang, D. (2012). Ultimate strength model experiment regarding a container ship's hull structures. *Ships and Offshore Structures*, 7(2), 165-184.

Vaz, L. E., & Hinton, E. (1995). FE-shape sensitivity of elastoplastic response. *Structural Optimization*, 10, 231.

Wang, F., Paik, J. K., Kim, B. J., Cui, W., Hayat, T., & Ahmad, B. (2015). Ultimate shear strength of intact and cracked stiffened panels. *Thin-Walled Structures*, 88, 48-57.

Wang, L., Grandhi, R. V., & Hopkins, D. A. (1995). Structural reliability optimization using an efficient safety index calculation procedure. *International Journal for Numerical Methods in Engineering*, 38, 1721-1738.

Xu, M. C., & Guedes Soares, C. (2013). Comparisons of calculations with experiments on the ultimate strength of wide stiffened panels. *Marine Structures*, 31, 82-101.

Xu, M. C, Teixeira, A. P., & Guedes Soares, C. (2015). Reliability assessment of a tanker using the model correction factor method based on the IACS-CSR requirement for hull girder ultimate strength. *Probabilistic Engineering Mechanics*, 42, 42-53.

Youn, B. D., & Choi, K. K. (2004). A new response surface methodology for reliability-based design optimization. *Computers and Structures*, 82 (2-3), 241-256.

Yu, X., Choi, K. K., & Chang K. H. (1997). A mixed design approach for probabilistic structural durability. *Structural Optimization*, 14(3-4), 81-90.

Zhang, S. (2016). A review and study on ultimate strength of steel plates and stiffened panels in axial compression. *Ships and Offshore Structures*, 11, 81-91.

Zhao, W. (2016). Reliability analysis of ultimate compressive strength for stiffened composite panels. *Journal of Reinforced Plastic and Composites*, 35, 902-914.

A Appendix

A.1 ANNEX A

CONSTITUTIVE EQUATIONS

The cross-section geometry of the beam-column is shown in following figure:

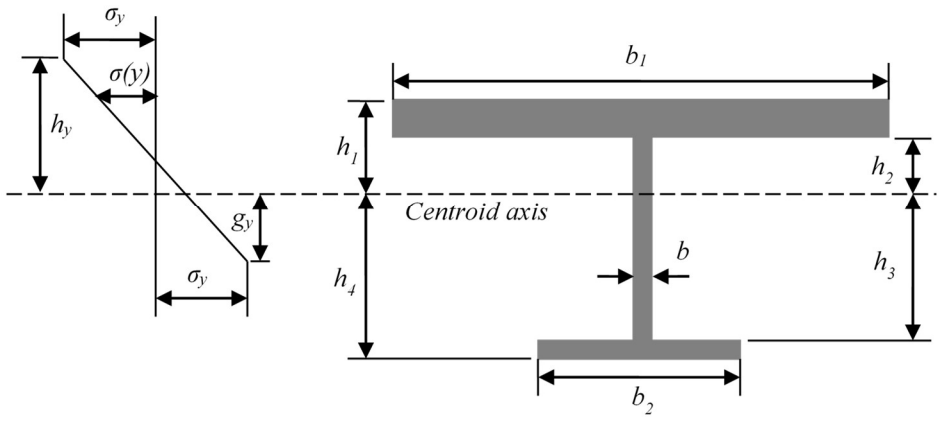

Assume the plating is on top and the stiffener is on the bottom, the dimensions $h_1, h_2, h_3, h_4, b_1, b_2$ and b are corresponding to the cross-sectional geometric parameters by following equations:

$$b_1 = b_p, b = t_w, b_2 = b_f, h_2 + h_3 = h_w, h_1 = h_2 + t_p, h_4 = h_3 + t_f$$

where the geometric parameters are plate width b, plate thickness t, web height h_w, web thickness t_w, flange width b_f and flange thickness t_f.

The distance of centroid axis to the middle of the web plate is denoted as C_t which is

$$C_t = \frac{1}{2} * \frac{(-b_f) * {t_f}^2 - b_f * t_f * h_w + b_p * t_p * h_w + b_p * {t_p}^2}{b_f * t_f + h_w * t_w + b_p * t_p}$$

h_1, h_2, h_3 and h_4 are calculated by following equations:

$h_1 = 0.5 * h_w - C_t + t_p$, $h_2 = 0.5 * h_w - C_t$, $h_3 = 0.5 * h_w + C_t$, $h_4 = 0.5 * h_w + C_t + t_f$

The stress-strain relationship of elastic-perfectly-plastic material and Euler-Bernoulli beam are

$\sigma(y) = E\varepsilon(y), \varepsilon(y) = \gamma_x - \kappa_z y, \varepsilon_y = E\sigma_y$

where E is Young's Modulus, y is the distance from centroid axis, $\varepsilon(y)$ is elastic strain, $\sigma(y)$ is elastic stress, γ_x is the strain at centroid axis, κ_z is the curvature at centroid axis, σ_y is yield stress and ε_y is yield strain.

When $\kappa_z > 0$, the boundaries of plastic zone h_y and g_y are calculated by

$h_y = \frac{\gamma_x + \varepsilon_y}{\kappa_z}, g_y = \frac{-\gamma_x + \varepsilon_y}{\kappa_z}$

When $\kappa_z > 0$, expressions of cross-sectional force P and moment M are distinguished by15 cases. The integration forms are shown below. The omitted expressions of moment can easily derived by adding the vertical distance y to each integrand from the expressions of corresponding force.

If $g_y > h_4$

Case 1: $h_y > h_1$,

$P_1 = \int_{-h_4}^{-h_3} E\varepsilon b_2 dy + \int_{-h_3}^{h_2} E\varepsilon b dy + \int_{h_2}^{h_1} E\varepsilon b_1 dy$

$M_1 = \int_{-h_4}^{-h_3} E\varepsilon \ {}_2 y dy + \int_{-h_3}^{h_2} E\varepsilon b y dy + \int_{h_2}^{h_1} E\varepsilon b_1 y dy$

Case 2: $h_1 > h_y > h_2$,

$$P_2 = \int_{-h_4}^{-h_3} E\varepsilon b_2 dy + \int_{-h_3}^{h_2} E\varepsilon b dy + \int_{h_2}^{h_y} E\varepsilon b_1 dy + \int_{h_y}^{h_1} (-\sigma_y) b_1 dy$$

$$M_2 = \int_{-h_4}^{-h_3} E\varepsilon b_2 y dy + \int_{-h_3}^{h_2} E\varepsilon b y dy + \int_{h_2}^{h_y} E\varepsilon b_1 y dy + \int_{h_y}^{h_1} (-\sigma_y) b_1 y dy$$

Case 3: $h_2 > h_y > -h_3$,

$$P_3 = \int_{-h_4}^{-h_3} E\varepsilon b_2 dy + \int_{-h_3}^{h_y} E\varepsilon b dy + \int_{h_y}^{h_2} (-\sigma_y) b dy + \int_{h_2}^{h_1} (-\sigma_y) b_1 dy$$

Case 4: $-h_3 > h_y > -h_4$,

$$P_4 = \int_{-h_4}^{h_y} E\varepsilon b_2 dy + \int_{h_y}^{-h_3} (-\sigma_y) b_2 dy + \int_{-h_3}^{h_2} (-\sigma_y) b dy + \int_{h_2}^{h_1} (-\sigma_y) b_1 dy$$

Case 5: $-h_4 > h_y$,

$$P_5 = \int_{-h_4}^{-h_3} (-\sigma_y) b_2 dy + \int_{-h_3}^{h_2} (-\sigma_y) b dy + \int_{h_2}^{h_1} (-\sigma_y) b_1 dy$$

If $h_4 > g_y > h_3$

Case 6: $h_y > h_1$,

$$P_6 = \int_{-h_4}^{-g_y} \sigma_y b_2 dy + \int_{-g_y}^{-h_3} E\varepsilon b_2 dy + \int_{-h_3}^{h_2} E\varepsilon b dy + \int_{h_2}^{h_1} E\varepsilon b_1 dy$$

Case 7: $h_1 > h_y > h_2$,

$$P_7 = \int_{-h_4}^{-g_y} \sigma_y b_2 dy + \int_{-g_y}^{-h_3} E\varepsilon b_2 dy + \int_{-h_3}^{h_2} E\varepsilon b dy + \int_{h_2}^{h_y} E\varepsilon_{\ 1} dy + \int_{h_y}^{h_1} (-\sigma_y) b_1 dy$$

Case 8: $h_2 > h_y > -h_3$,

$$P_8 = \int_{-h_4}^{-g_y} \sigma_y b_2 dy + \int_{-g_y}^{-h_3} E\varepsilon b_2 dy + \int_{-h_3}^{h_y} E\varepsilon b dy + \int_{h_y}^{h_2} (-\sigma_y) b dy + \int_{h_2}^{h_1} (-\sigma_y) b_1 dy$$

Case 9: $-h_3 > h_y > -h_4$,

$$P_9 = \int_{-h_4}^{-g_y} \sigma_y b_2 dy + \int_{-g_y}^{h_y} E\varepsilon b_2 dy + \int_{h_y}^{-h_3} (-\sigma_y) b_2 dy + \int_{-h_3}^{h_2} (-\sigma_y) b dy + \int_{h_2}^{h_1} (-\sigma_y) b_1 dy$$

If $h_3 > g_y > -h_2$

Case 10: $h_y > h_1$,

$$P_{10} = \int_{-h_4}^{-h_3} \sigma_y b_2 dy + \int_{-h_3}^{-g_y} \sigma_y b dy + \int_{-g_y}^{h_2} E\varepsilon b dy + \int_{h_2}^{h_1} E\varepsilon b_1 dy$$

Case 11: $h_1 > h_y > h_2$,

$$P_{11} = \int_{-h_4}^{-h_3} \sigma_y b_2 dy + \int_{-h_3}^{-g_y} \sigma_y b dy + \int_{-g_y}^{h_2} E\varepsilon b dy + \int_{h_2}^{h_y} E\varepsilon b_1 dy + \int_{h_y}^{h_1} (-\sigma_y) b_1 dy$$

Case 12: $h_2 > h_y > -h_3$,

$$P_{12} = \int_{-h_4}^{-h_3} \sigma_y b_2 dy + \int_{-h_3}^{-g_y} \sigma_y b dy + \int_{-g_y}^{h_y} E\varepsilon b dy + \int_{h_y}^{h_2} (-\sigma_y) b dy + \int_{h_2}^{h_1} (-\sigma_y) b_1 dy$$

If $-h_2 > g_y > -h_1$

Case 13: $h_y > h_1$,

$$P_{13} = \int_{-h_4}^{-h_3} \sigma_y b_2 dy + \int_{-h_3}^{h_2} \sigma_y b dy + \int_{h_2}^{-g_y} \sigma_y b_1 dy + \int_{-g_y}^{h_1} E\varepsilon b_1 dy$$

Case 14: $h_1 > h_y > h_2$,

$$P_{14} = \int_{-h_4}^{-h_3} \sigma_y b_2 dy + \int_{-h_3}^{h_2} \sigma_y b dy + \int_{h_2}^{-g_y} \sigma_y b_1 dy + \int_{-g_y}^{h_y} E\varepsilon b_1 dy + \int_{h_y}^{h_1} (-\sigma_y) b_1 dy$$

If $-h_1 > g_y$

Case 15:

$$P_{15} = \int_{-h_4}^{-h_3} \sigma_y b_2 dy + \int_{-h_3}^{h_2} \sigma_y b dy + \int_{h_2}^{h_1} \sigma_y b_1 dy$$

The constitutive equations of the beam-column are

$$C_x(\gamma_x, \kappa_z) + P = 0$$

$$C_z(\gamma_x, \kappa_z) - M_z = 0$$

The functions C_x and C_z can be calculated by substituting the geometric parameters and material parameters into the integration equations of the 15 cases. γ_x and κ_z are replaced by γ and κ respectively.

Case1:

$$C_x = b_1 * E * \gamma * h_1 + b * E * \gamma * h_2 - b_1 * E * \gamma * h_2 + b * E * \gamma * h_3 - b_2 * E * \gamma * h_3 + b_2 * E * \gamma * h_4 - \frac{b_1 * E * h_1^2 * \kappa}{2} - \frac{b * E * h_2^2 * \kappa}{2} + \frac{b_1 * E * h_2^2 * \kappa}{2} + \frac{b * E * h_3^2 * \kappa}{2} - \frac{b_2 * E * h_3^2 * \kappa}{2} + \frac{b_2 * E * h_4^2 * \kappa}{2}$$

$$C_z = \frac{b_1 * E * \gamma * h_1^2}{2} + \frac{b * E * \gamma * h_2^2}{2} - \frac{b_1 * E * \gamma * h_2^2}{2} - \frac{b * E * \gamma * h_3^2}{2} + \frac{b_2 * E * \gamma * h_3^2}{2} - \frac{b_2 * E * \gamma * h_4^2}{2} - \frac{b_1 * E * h_1^3 * \kappa}{3} - \frac{b * E * h_2^3 * \kappa}{3} + \frac{b_1 * E * h_2^3 * \kappa}{3} - \frac{b * E * h_3^3 * \kappa}{3} + \frac{b_2 * E * h_3^3 * \kappa}{3} - \frac{b_2 * E * h_4^3 * \kappa}{3}$$

Case 2:

$$C_x = b * E * \gamma * h_2 - b_1 * E * \gamma * h_2 + b * E * \gamma * h_3 - b_2 * E * \gamma * h_3 + b_2 * E * \gamma * h_4 + \frac{b_1 * E * \gamma^2}{2 * \kappa} - \frac{b * E * h_2^2 * \kappa}{2} + \frac{b_1 * E * h_2^2 * \kappa}{2} + \frac{b * E * h_3^2 * \kappa}{2} - \frac{b_2 * E * h_3^2 * \kappa}{2} + \frac{b_2 * E * h_4^2 * \kappa}{2} - b_1 * h_1 * S_y + \frac{b_1 * \gamma * S_y}{\kappa} + \frac{b_1 * S_y^2}{2 * E * \kappa}$$

$$C_z = \frac{b * E * \gamma * h_2^2}{2} - \frac{b_1 * E * \gamma * h_2^2}{2} - \frac{b * E * \gamma * h_3^2}{2} + \frac{b_2 * E * \gamma * h_3^2}{2} - \frac{b_2 * E * \gamma * h_4^2}{2} + \frac{b_1 * E * \gamma^3}{6 * \kappa^2} - \frac{b * E * h_2^3 * \kappa}{3} + \frac{b_1 * E * h_2^3 * \kappa}{3} - \frac{b * E * h_3^3 * \kappa}{3} + \frac{b_2 * E * h_3^3 * \kappa}{3} - \frac{b_2 * E * h_4^3 * \kappa}{3} - \frac{b_1 * \gamma * S_y^2}{2 * E * \kappa^2} - \frac{b_1 * S_y^3}{3 * E^2 * \kappa^2} - \frac{b_1 * S_y * \left(h_1^2 - \frac{\left(\gamma + \frac{S_y}{E}\right)^2}{\kappa^2} \right)}{2}$$

Case 3:

$$C_x = b * E * \gamma * h_3 - b_2 * E * \gamma * h_3 + b_2 * E * \gamma * h_4 + \frac{b*E*\gamma^2}{2*\kappa} + \frac{b*E*h_3^2*\kappa}{2} - \frac{b_2*E*h_3^2*\kappa}{2} + \frac{b_2*E*h_4^2*\kappa}{2} - b_1 * h_1 * S_y - b * h_2 * S_y + b_1 * h_2 * S_y + \frac{b*\gamma*S_y}{\kappa} + \frac{b*S_y^2}{2*E*\kappa}$$

$$C_z = -\frac{b*E*\gamma*h_3^2}{2} + \frac{b_2*E*\gamma*h_3^2}{2} - \frac{b_2*E*\gamma*h_4^2}{2} + \frac{b*E*\gamma^3}{6*\kappa^2} - \frac{b*E*h_3^3*\kappa}{3} + \frac{b_2*E*h_3^3*\kappa}{3} - \frac{b_2*E*h_4^3*\kappa}{3} - \frac{b_1*h_1^2*S_y}{2} + \frac{b_1*h_2^2*S_y}{2} - \frac{b*\gamma*S_y^2}{2*E*\kappa^2} - \frac{b*S_y^3}{3*E^2*\kappa^2} - \frac{b*S_y*\left(h_2^2 - \frac{\left(\gamma + \frac{S_y}{E}\right)^2}{\kappa^2}\right)}{2}$$

Case 4:

$$C_x = b_2 * E * \gamma * h_4 + \frac{b_2*E*\gamma^2}{2*\kappa} + \frac{b_2*E*h_4^2*\kappa}{2} - b_1 * h_1 * S_y - b * h_2 * S_y + b_1 * h_2 * S_y - b * h_3 * S_y + b_2 * h_3 * S_y + \frac{b_2*\gamma*S_y}{\kappa} + \frac{b_2*S_y^2}{2*E*\kappa}$$

$$C_z = -\frac{b_2*E*\gamma*h_4^2}{2} + \frac{b_2*E*\gamma^3}{6*\kappa^2} - \frac{b_2*E*h_4^3*\kappa}{3} - \frac{b_1*h_1^2*S_y}{2} - \frac{b*h_2^2*S_y}{2} + \frac{b_1*h_2^2*S_y}{2} + \frac{b*h_3^2*S_y}{2} - \frac{b_2*\gamma*S_y^2}{2*E*\kappa^2} - \frac{b_2*S_y^3}{3*E^2*\kappa^2} - \frac{b_2*S_y*\left(h_3^2 - \frac{\left(\gamma + \frac{S_y}{E}\right)^2}{\kappa^2}\right)}{2}$$

Case 5:

$$C_x = -\left(b_1 * h_1 * S_y\right) - b * h_2 * S_y + b_1 * h_2 * S_y - b * h_3 * S_y + b_2 * h_3 * S_y - b_2 * h_4 * S_y$$

$$C_z = -\frac{b_1 * h_1^2 * S_y}{2} - \frac{b * h_2^2 * S_y}{2} + \frac{b_1 * h_2^2 * S_y}{2} + \frac{b * h_3^2 * S_y}{2} - \frac{b_2 * h_3^2 * S_y}{2} + \frac{b_2 * h_4^2 * S_y}{2}$$

Case 6:

$$C_x = b_1 * E * \gamma * h_1 + b * E * \gamma * h_2 - b_1 * E * \gamma * h_2 + b * E * \gamma * h_3 - b_2 * E * \gamma * h_3 - \frac{b_2 * E * \gamma^2}{2 * \kappa} - \frac{b_1 * E * h_1^2 * \kappa}{2} - \frac{b * E * h_2^2 * \kappa}{2} + \frac{b_1 * E * h_2^2 * \kappa}{2} + \frac{b * E * h_3^2 * \kappa}{2} - \frac{b_2 * E * h_3^2 * \kappa}{2} + b_2 * h_4 * S_y + \frac{b_2 * \gamma * S_y}{\kappa} - \frac{b_2 * S_y^2}{2 * E * \kappa}$$

$$C_z = \frac{b_1 * E * \gamma * h_1^2}{2} + \frac{b * E * \gamma * h_2^2}{2} - \frac{b_1 * E * \gamma * h_2^2}{2} - \frac{b * E * \gamma * h_3^2}{2} + \frac{b_2 * E * \gamma * h_3^2}{2} - \frac{b_2 * E * \gamma^3}{6 * \kappa^2} - \frac{b_1 * E * h_1^3 * \kappa}{3} - \frac{b * E * h_2^3 * \kappa}{3} + \frac{b_1 * E * h_2^3 * \kappa}{3} - \frac{b * E * h_3^3 * \kappa}{3} + \frac{b_2 * E * h_3^3 * \kappa}{3} + \frac{b_2 * \gamma * S_y^2}{2 * E * \kappa^2} - \frac{b_2 * S_y^3}{3 * E^2 * \kappa^2} + \frac{b_2 * S_y * \left(-h_4^2 + \frac{\left(\gamma - \frac{S_y}{E}\right)^2}{\kappa^2} \right)}{2}$$

Case 7:

$$C_x = b * E * \gamma * h_2 - b_1 * E * \gamma * h_2 + b * E * \gamma * h_3 - b_2 * E * \gamma * h_3 + \frac{b_1 * E * \gamma^2}{2 * \kappa} - \frac{b_2 * E * \gamma^2}{2 * \kappa} - \frac{b * E * h_2^2 * \kappa}{2} + \frac{b_1 * E * h_2^2 * \kappa}{2} + \frac{b * E * h_3^2 * \kappa}{2} - \frac{b_2 * E * h_3^2 * \kappa}{2} - b_1 * h_1 * S_y + b_2 * h_4 * S_y + \frac{b_1 * \gamma * S_y}{\kappa} + \frac{b_2 * \gamma * S_y}{\kappa} + \frac{b_1 * S_y^2}{2 * E * \kappa} - \frac{b_2 * S_y^2}{2 * E * \kappa}$$

$$C_z = \frac{b*E*\gamma*h_2^2}{2} - \frac{b_1*E*\gamma*h_2^2}{2} - \frac{b*E*\gamma*h_3^2}{2} + \frac{b_2*E*\gamma*h_3^2}{2} + \frac{b_1*E*\gamma^3}{6*\kappa^2} - \frac{b_2*E*\gamma^3}{6*\kappa^2} - \frac{b*E*h_2^3*\kappa}{3} + \frac{b_1*E*h_2^3*\kappa}{3} - \frac{b*E*h_3^3*\kappa}{3} + \frac{b_2*E*h_3^3*\kappa}{3} - \frac{b_1*\gamma*S_y^2}{2*E*\kappa^2} + \frac{b_2*\gamma*S_y^2}{2*E*\kappa^2} - \frac{b_1*S_y^3}{3*E^2*\kappa^2} - \frac{b_2*S_y^3}{3*E^2*\kappa^2} + \frac{b_2*S_y*\left(-h_4^2+\frac{\left(\gamma-\frac{S_y}{E}\right)^2}{\kappa^2}\right)}{2} - \frac{b_1*S_y*\left(h_1^2-\frac{\left(\gamma+\frac{S_y}{E}\right)^2}{\kappa^2}\right)}{2}$$

Case 8:

$$C_x = b*E*\gamma*h_3 - b_2*E*\gamma*h_3 + \frac{b*E*\gamma^2}{2*\kappa} - \frac{b_2*E*\gamma^2}{2*\kappa} + \frac{b*E*h_3^2*\kappa}{2} - \frac{b_2*E*h_3^2*\kappa}{2} - b_1*h_1*S_y - b*h_2*S_y + b_1*h_2*S_y + b_2*h_4*S_y + \frac{b*\gamma*S_y}{\kappa} + \frac{b_2*\gamma*S_y}{\kappa} + \frac{b*S_y^2}{2*E*\kappa} - \frac{b_2*S_y^2}{2*E*\kappa}$$

$$C_z = -\frac{b*E*\gamma*h_3^2}{2} + \frac{b_2*E*\gamma*h_3^2}{2} + \frac{b*E*\gamma^3}{6*\kappa^2} - \frac{b_2*E*\gamma^3}{6*\kappa^2} - \frac{b*E*h_3^3*\kappa}{3} + \frac{b_2*E*h_3^3*\kappa}{3} - \frac{b_1*h_1^2*S_y}{2} + \frac{b_1*h_2^2*S_y}{2} - \frac{b*\gamma*S_y^2}{2*E*\kappa^2} + \frac{b_2*\gamma*S_y^2}{2*E*\kappa^2} - \frac{b*S_y^3}{3*E^2*\kappa^2} - \frac{b_2*S_y^3}{3*E^2*\kappa^2} + \frac{b_2*S_y*\left(-h_4^2+\frac{\left(\gamma-\frac{S_y}{E}\right)^2}{\kappa^2}\right)}{2} - \frac{b*S_y*\left(h_2^2-\frac{\left(\gamma+\frac{S_y}{E}\right)^2}{\kappa^2}\right)}{2}$$

Case 9:

$$C_x = -\left(b_1*h_1*S_y\right) - b*h_2*S_y + b_1*h_2*S_y + b_2*h_4*S_y + \frac{b*\gamma*S_y}{\kappa} + \frac{b_2*\gamma*S_y}{\kappa} + \frac{b*S_y^2}{E*\kappa} - \frac{b_2*S_y^2}{E*\kappa}$$

$$C_z = -\frac{b_1*h_1^2*S_y}{2} - \frac{b*h_2^2*S_y}{2} + \frac{b_1*h_2^2*S_y}{2} + \frac{b*h_3^2*S_y}{2} - \frac{2*b_2*S_y^3}{3*E^2*\kappa^2} + \frac{b_2*S_y*\left(-h_4^2+\frac{\left(\gamma-\frac{S_y}{E}\right)^2}{\kappa^2}\right)}{2} - \frac{b*S_y*\left(h_3^2-\frac{\left(\gamma+\frac{S_y}{E}\right)^2}{\kappa^2}\right)}{2}$$

Case 10:

$$C_x = b_1 * E * \gamma * h_1 + b * E * \gamma * h_2 - b_1 * E * \gamma * h_2 - \frac{b*E*\gamma^2}{2*\kappa} - \frac{b_1*E*h_1^2*\kappa}{2} - \frac{b*E*h_2^2*\kappa}{2} + \frac{b_1*E*h_2^2*\kappa}{2} + b * h_3 * S_y - b_2 * h_3 * S_y + b_2 * h_4 * S_y + \frac{b*\gamma*S_y}{\kappa} - \frac{b*S_y^2}{2*E*\kappa}$$

$$C_z = \frac{b_1*E*\gamma*h_1^2}{2} + \frac{b*E*\gamma*h_2^2}{2} - \frac{b_1*E*\gamma*h_2^2}{2} - \frac{b*E*\gamma^3}{6*\kappa^2} - \frac{b_1*E*h_1^3*\kappa}{3} - \frac{b*E*h_2^3*\kappa}{3} + \frac{b_1*E*h_2^3*\kappa}{3} + \frac{b_2*h_3^2*S_y}{2} - \frac{b_2*h_4^2*S_y}{2} + \frac{b*\gamma*S_y^2}{2*E*\kappa^2} - \frac{b*S_y^3}{3*E^2*\kappa^2} + \frac{b*S_y*\left(-h_3^2+\frac{\left(\gamma-\frac{S_y}{E}\right)^2}{\kappa^2}\right)}{2}$$

Case 11:

$$C_x = b * E * \gamma * h_2 - b_1 * E * \gamma * h_2 - \frac{b*E*\gamma^2}{2*\kappa} + \frac{b_1*E*\gamma^2}{2*\kappa} - \frac{b*E*h_2^2*\kappa}{2} + \frac{b_1*E*h_2^2*\kappa}{2} - b_1 * h_1 * S_y + b * h_3 * S_y - b_2 * h_3 * S_y + b_2 * h_4 * S_y + \frac{b*\gamma*S_y}{\kappa} + \frac{b_1*\gamma*S_y}{\kappa} - \frac{b*S_y^2}{2*E*\kappa} + \frac{b_1*S_y^2}{2*E*\kappa}$$

$$C_z = \frac{b*E*\gamma*h_2^2}{2} - \frac{b_1*E*\gamma*h_2^2}{2} - \frac{b*E*\gamma^3}{6*\kappa^2} + \frac{b_1*E*\gamma^3}{6*\kappa^2} - \frac{b*E*h_2^3*\kappa}{3} + \frac{b_1*E*h_2^3*\kappa}{3} + \frac{b_2*h_3^2*S_y}{2} - \frac{b_2*h_4^2*S_y}{2} + \frac{b*\gamma*S_y^2}{2*E*\kappa^2} - \frac{b_1*\gamma*S_y^2}{2*E*\kappa^2} - \frac{b*S_y^3}{3*E^2*\kappa^2} - \frac{b_1*S_y^3}{3*E^2*\kappa^2} + \frac{b*S_y*\left(-h_3^2+\frac{\left(\gamma-\frac{S_y}{E}\right)^2}{\kappa^2}\right)}{2} - \frac{b_1*S_y*\left(h_1^2-\frac{\left(\gamma+\frac{S_y}{E}\right)^2}{\kappa^2}\right)}{2}$$

Case 12:

$$C_x = -\left(b_1 * h_1 * S_y\right) - b * h_2 * S_y + b_1 * h_2 * S_y + b * h_3 * S_y - b_2 * h_3 * S_y + b_2 * h_4 * S_y + \frac{2*b*\gamma*S_y}{\kappa}$$

$$C_z = -\frac{b_1*h_1^2*S_y}{2} + \frac{b_1*h_2^2*S_y}{2} + \frac{b_2*h_3^2*S_y}{2} - \frac{b_2*h_4^2*S_y}{2} - \frac{2*b*S_y^3}{3*E^2*\kappa^2} + \frac{b*S_y*\left(-h_3^2+\frac{\left(\gamma-\frac{S_y}{E}\right)^2}{\kappa^2}\right)}{2} - \frac{b*S_y*\left(h_2^2-\frac{\left(\gamma+\frac{S_y}{E}\right)^2}{\kappa^2}\right)}{2}$$

Case 13:

$$C_x = b_1 * E * \gamma * h_1 - \frac{b_1*E*\gamma^2}{2*\kappa} - \frac{b_1*E*h_1^2*\kappa}{2} + b * h_2 * S_y - b_1 * h_2 * S_y + b * h_3 * S_y - b_2 * h_3 * S_y + b_2 * h_4 * S_y + \frac{b_1*\gamma*S_y}{\kappa} - \frac{b_1*S_y^2}{2*E*\kappa}$$

$$C_z = \frac{b_1*E*\gamma*h_1^2}{2} - \frac{b_1*E*\gamma^3}{6*\kappa^2} - \frac{b_1*E*h_1^3*\kappa}{3} + \frac{b*h_2^2*S_y}{2} - \frac{b*h_3^2*S_y}{2} + \frac{b_2*h_3^2*S_y}{2} - \frac{b_2*h_4^2*S_y}{2} + \frac{b_1*\gamma*S_y^2}{2*E*\kappa^2} - \frac{b_1*S_y^3}{3*E^2*\kappa^2} + \frac{b_1*S_y*\left(-h_2^2+\frac{\left(\gamma-\frac{S_y}{E}\right)^2}{\kappa^2}\right)}{2}$$

Case 14:

$$C_x = -\left(b_1 * h_1 * S_y\right) + b * h_2 * S_y - b_1 * h_2 * S_y + b * h_3 * S_y - b_2 * h_3 * S_y + b_2 * h_4 * S_y + \frac{2*b_1*\gamma*S_y}{\kappa}$$

$$C_z = \frac{b*h_2^2*S_y}{2} - \frac{b*h_3^2*S_y}{2} + \frac{b_2*h_3^2*S_y}{2} - \frac{b_2*h_4^2*S_y}{2} - \frac{2*b_1*S_y^3}{3*E^2*\kappa^2} + \frac{b_1*S_y*\left(-h_2^2+\frac{\left(\gamma-\frac{S_y}{E}\right)^2}{\kappa^2}\right)}{2} - \frac{b_1*S_y*\left(h_1^2-\frac{\left(\gamma+\frac{S_y}{E}\right)^2}{\kappa^2}\right)}{2}$$

Case 15:

$$C_x = b_1 * h_1 * S_y + b * h_2 * S_y - b_1 * h_2 * S_y + b * h_3 * S_y - b_2 * h_3 * S_y + b_2 * h_4 * S_y$$

$$C_z = \frac{b_1*h_1^2*S_y}{2} + \frac{b*h_2^2*S_y}{2} - \frac{b_1*h_2^2*S_y}{2} - \frac{b*h_3^2*S_y}{2} + \frac{b_2*h_3^2*S_y}{2} - \frac{b_2*h_4^2*S_y}{2}$$

A.2 ANNEX B

DERIVATIVES OF CONSTITUTIVE EQUATIONS

A.2.1 First-Order Derivatives:

Case1:

$$\frac{\partial C_x}{\partial \kappa} = -\frac{b_1*E*h_1^2}{2} - \frac{b*E*h_2^2}{2} + \frac{b_1*E*h_2^2}{2} + \frac{b*E*h_3^2}{2} - \frac{b_2*E*h_3^2}{2} + \frac{b_2*E*h_4^2}{2}$$

$$\frac{\partial C_x}{\partial \gamma} = b_1 * E * h_1 + b * E * h_2 - b_1 * E * h_2 + b * E * h_3 - b_2 * E * h_3 + b_2 * E * h_4$$

$$\frac{\partial C_z}{\partial \kappa} = -\frac{b_1*E*h_1^3}{3} - \frac{b*E*h_2^3}{3} + \frac{b_1*E*h_2^3}{3} - \frac{b*E*h_3^3}{3} + \frac{b_2*E*h_3^3}{3} - \frac{b_2*E*h_4^3}{3}$$

$$\frac{\partial C_z}{\partial \gamma} = \frac{b_1*E*h_1^2}{2} + \frac{b*E*h_2^2}{2} - \frac{b_1*E*h_2^2}{2} - \frac{b*E*h_3^2}{2} + \frac{b_2*E*h_3^2}{2} - \frac{b_2*E*h_4^2}{2}$$

Case 2:

$$\frac{\partial C_x}{\partial \kappa} = -\frac{b*E*h_2^2}{2} + \frac{b_1*E*h_2^2}{2} + \frac{b*E*h_3^2}{2} - \frac{b_2*E*h_3^2}{2} + \frac{b_2*E*h_4^2}{2} - \frac{b_1*E*\gamma^2}{2*\kappa^2} - \frac{b_1*\gamma*S_y}{\kappa^2} - \frac{b_1*{S_y}^2}{2*E*\kappa^2}$$

$$\frac{\partial C_x}{\partial \gamma} = b * E * h_2 - b_1 * E * h_2 + b * E * h_3 - b_2 * E * h_3 + b_2 * E * h_4 + \frac{b_1 * E * \gamma}{\kappa} + \frac{b_1 * S_y}{\kappa}$$

$$\frac{\partial C_z}{\partial \kappa} = -\frac{b*E*h_2^3}{3} + \frac{b_1*E*h_2^3}{3} - \frac{b*E*h_3^3}{3} + \frac{b_2*E*h_3^3}{3} - \frac{b_2*E*h_4^3}{3} - \frac{b_1*E*\gamma^3}{3*\kappa^3} + \frac{b_1*\gamma*{S_y}^2}{E*\kappa^3} + \frac{2*b_1*{S_y}^3}{3*E^2*\kappa^3} - \frac{b_1*S_y*\left(\gamma + \frac{S_y}{E}\right)^2}{\kappa^3}$$

$$\frac{\partial C_z}{\partial \gamma} = \frac{b*E*h_2^2}{2} - \frac{b_1*E*h_2^2}{2} - \frac{b*E*h_3^2}{2} + \frac{b_2*E*h_3^2}{2} - \frac{b_2*E*h_4^2}{2} + \frac{b_1*E*\gamma^2}{2*\kappa^2} - \frac{b_1*{S_y}^2}{2*E*\kappa^2} + \frac{b_1*Sy*\left(\gamma + \frac{S_y}{E}\right)}{\kappa^2}$$

Case 3:

$$\frac{\partial C_x}{\partial \kappa} = \frac{b*E*h_3^2}{2} - \frac{b_2*E*h_3^2}{2} + \frac{b_2*E*h_4^2}{2} - \frac{b*E*\gamma^2}{2*\kappa^2} - \frac{b*\gamma*S_y}{\kappa^2} - \frac{b*S_y^2}{2*E*\kappa^2}$$

$$\frac{\partial C_x}{\partial \gamma} = b * E * h_3 - b_2 * E * h_3 + b_2 * E * h_4 + \frac{b*E*\gamma}{\kappa} + \frac{b*S_y}{\kappa}$$

$$\frac{\partial C_z}{\partial \kappa} = -\frac{b*E*h_3^3}{3} + \frac{b_2*E*h_3^3}{3} - \frac{b_2*E*h_4^3}{3} - \frac{b*E*\gamma^3}{3*\kappa^3} + \frac{b*\gamma*S_y^2}{E*\kappa^3} + \frac{2*b*S_y^3}{3*E^2*\kappa^3} - \frac{b*S_y*\left(\gamma + \frac{S_y}{E}\right)^2}{\kappa^3}$$

$$\frac{\partial C_z}{\partial \gamma} = -\frac{b*E*h_3^2}{2} + \frac{b_2*E*h_3^2}{2} - \frac{b_2*E*h_4^2}{2} + \frac{b*E*\gamma^2}{2*\kappa^2} - \frac{b*S_y^2}{2*E*\kappa^2} + \frac{b*S_y*\left(\gamma + \frac{S_y}{E}\right)}{\kappa^2}$$

Case 4:

$$\frac{\partial C_x}{\partial \kappa} = \frac{b_2 * E * h_4^2}{2} - \frac{b_2 * E * \gamma^2}{2 * \kappa^2} - \frac{b_2 * \gamma * S_y}{\kappa^2} - \frac{b_2 * S_y^2}{2 * E * \kappa^2}$$

$$\frac{\partial C_x}{\partial \gamma} = b_2 * E * h_4 + \frac{b_2 * E * \gamma}{\kappa} + \frac{b_2 * S_y}{\kappa}$$

$$\frac{\partial C_z}{\partial \kappa} = -\frac{b_2 * E * h_4^3}{3} - \frac{b_2 * E * \gamma^3}{3 * \kappa^3} + \frac{b_2 * \gamma * S_y^2}{E * \kappa^3} + \frac{2 * b_2 * S_y^3}{3 * E^2 * \kappa^3} - \frac{b_2 * S_y * \left(\gamma + \frac{S_y}{E}\right)^2}{\kappa^3}$$

$$\frac{\partial C_z}{\partial \gamma} = -\frac{b_2 * E * h_4^2}{2} + \frac{b_2 * E * \gamma^2}{2 * \kappa^2} - \frac{b_2 * S_y^2}{2 * E * \kappa^2} + \frac{b_2 * S_y * \left(\gamma + \frac{S_y}{E}\right)}{\kappa^2}$$

Case 5:

$$\frac{\partial C_x}{\partial \kappa} = 0$$

$$\frac{\partial C_x}{\partial \gamma} = 0$$

$$\frac{\partial C_z}{\partial \kappa} = 0$$

$$\frac{\partial C_z}{\partial \gamma} = 0$$

Case 6:

$$\frac{\partial C_x}{\partial \kappa} = -\frac{b_1*E*h_1^2}{2} - \frac{b*E*h_2^2}{2} + \frac{b_1*E*h_2^2}{2} + \frac{b*E*h_3^2}{2} - \frac{b_2*E*h_3^2}{2} + \frac{b_2*E*\gamma^2}{2*\kappa^2} - \frac{b_2*\gamma*S_y}{\kappa^2} + \frac{b_2*S_y^2}{2*E*\kappa^2}$$

$$\frac{\partial C_x}{\partial \gamma} = b_1 * E * h_1 + b * E * h_2 - b_1 * E * h_2 + b * E * h_3 - b_2 * E * h_3 - \frac{b_2*E*\gamma}{\kappa} + \frac{b_2*S_y}{\kappa}$$

$$\frac{\partial C_z}{\partial \kappa} = -\frac{b_1*E*h_1^3}{3} - \frac{b*E*h_2^3}{3} + \frac{b_1*E*h_2^3}{3} - \frac{b*E*h_3^3}{3} + \frac{b_2*E*h_3^3}{3} + \frac{b_2*E*\gamma^3}{3*\kappa^3} - \frac{b_2*\gamma*S_y^2}{E*\kappa^3} + \frac{2*b_2*S_y^3}{3*E^2*\kappa^3} - \frac{b_2*S_y*\left(\gamma - \frac{S_y}{E}\right)^2}{\kappa^3}$$

$$\frac{\partial C_z}{\partial \gamma} = \frac{b_1*E*h_1^2}{2} + \frac{b*E*h_2^2}{2} - \frac{b_1*E*h_2^2}{2} - \frac{b*E*h_3^2}{2} + \frac{b_2*E*h_3^2}{2} - \frac{b_2*E*\gamma^2}{2*\kappa^2} + \frac{b_2*S_y^2}{2*E*\kappa^2} + \frac{b_2*S_y*\left(\gamma - \frac{S_y}{E}\right)}{\kappa^2}$$

Case 7:

$$\frac{\partial C_x}{\partial \kappa} = -\frac{b*E*h_2^2}{2} + \frac{b_1*E*h_2^2}{2} + \frac{b*E*h_3^2}{2} - \frac{b_2*E*h_3^2}{2} - \frac{b_1*E*\gamma^2}{2*\kappa^2} + \frac{b_2*E*\gamma^2}{2*\kappa^2} - \frac{b_1*\gamma*S_y}{\kappa^2} - \frac{b_2*\gamma*S_y}{\kappa^2} - \frac{b_1*S_y^2}{2*E*\kappa^2} + \frac{b_2*S_y^2}{2*E*\kappa^2}$$

$$\frac{\partial C_x}{\partial \gamma} = b*E*h_2 - b_1*E*h_2 + b*E*h_3 - b_2*E*h_3 + \frac{b_1*E*\gamma}{\kappa} - \frac{b_2*E*\gamma}{\kappa} + \frac{b_1*S_y}{\kappa} + \frac{b_2*S_y}{\kappa}$$

$$\frac{\partial C_z}{\partial \kappa} = -\frac{b*E*h_2^3}{3} + \frac{b_1*E*h_2^3}{3} - \frac{b*E*h_3^3}{3} + \frac{b_2*E*h_3^3}{3} - \frac{b_1*E*\gamma^3}{3*\kappa^3} + \frac{b_2*E*\gamma^3}{3*\kappa^3} + \frac{b_1*\gamma*S_y^2}{E*\kappa^3} - \frac{b_2*\gamma*S_y^2}{E*\kappa^3} + \frac{2*b_1*S_y^3}{3*E^2*\kappa^3} + \frac{2*b_2*S_y^3}{3*E^2*\kappa^3} - \frac{b_2*S_y*\left(\gamma - \frac{S_y}{E}\right)^2}{\kappa^3} - \frac{b_1*S_y*\left(\gamma + \frac{S_y}{E}\right)^2}{\kappa^3}$$

$$\frac{\partial C_z}{\partial \gamma} = \frac{b*E*h_2^2}{2} - \frac{b_1*E*h_2^2}{2} - \frac{b*E*h_3^2}{2} + \frac{b_2*E*h_3^2}{2} + \frac{b_1*E*\gamma^2}{2*\kappa^2} - \frac{b_2*E*\gamma^2}{2*\kappa^2} - \frac{b_1*S_y^2}{2*E*\kappa^2} + \frac{b_2*S_y^2}{2*E*\kappa^2} + \frac{b_2*S_y*\left(\gamma - \frac{S_y}{E}\right)}{\kappa^2} + \frac{b_1*S_y*\left(\gamma + \frac{S_y}{E}\right)}{\kappa^2}$$

Case 8:

$$\frac{\partial C_x}{\partial \kappa} = \frac{b*E*h_3^2}{2} - \frac{b_2*E*h_3^2}{2} - \frac{b*E*\gamma^2}{2*\kappa^2} + \frac{b_2*E*\gamma^2}{2*\kappa^2} - \frac{b*\gamma*S_y}{\kappa^2} - \frac{b_2*\gamma*S_y}{\kappa^2} - \frac{b*S_y^2}{2*E*\kappa^2} + \frac{b_2*S_y^2}{2*E*\kappa^2}$$

$$\frac{\partial C_x}{\partial \gamma} = b*E*h_3 - b_2*E*h_3 + \frac{b*E*\gamma}{\kappa} - \frac{b_2*E*\gamma}{\kappa} + \frac{b*S_y}{\kappa} + \frac{b_2*S_y}{\kappa}$$

$$\frac{\partial C_z}{\partial \kappa} = -\frac{b*E*h_3^3}{3} + \frac{b_2*E*h_3^3}{3} - \frac{b*E*\gamma^3}{3*\kappa^3} + \frac{b_2*E*\gamma^3}{3*\kappa^3} + \frac{b*\gamma*S_y^2}{E*\kappa^3} - \frac{b_2*\gamma*S_y^2}{E*\kappa^3} + \frac{2*b*S_y^3}{3*E^2*\kappa^3} + \frac{2*b_2*S_y^3}{3*E^2*\kappa^3} - \frac{b_2*S_y*\left(\gamma - \frac{S_y}{E}\right)^2}{\kappa^3} - \frac{b*S_y*\left(\gamma + \frac{S_y}{E}\right)^2}{\kappa^3}$$

$$\frac{\partial C_z}{\partial \gamma} = -\frac{b*E*h_3^2}{2} + \frac{b_2*E*h_3^2}{2} + \frac{b*E*\gamma^2}{2*\kappa^2} - \frac{b_2*E*\gamma^2}{2*\kappa^2} - \frac{b*S_y^2}{2*E*\kappa^2} + \frac{b_2*S_y^2}{2*E*\kappa^2} + \frac{b_2*S_y*\left(\gamma - \frac{S_y}{E}\right)}{\kappa^2} + \frac{b*S_y*\left(\gamma + \frac{S_y}{E}\right)}{\kappa^2}$$

Case 9:

$$\frac{\partial C_x}{\partial \kappa} = -\left(\frac{b*\gamma*S_y}{\kappa^2}\right) - \frac{b_2*\gamma*S_y}{\kappa^2} - \frac{b*S_y^2}{E*\kappa^2} + \frac{b_2*S_y^2}{E*\kappa^2}$$

$$\frac{\partial C_x}{\partial \gamma} = \frac{b*S_y}{\kappa} + \frac{b_2*S_y}{\kappa}$$

$$\frac{\partial C_z}{\partial \kappa} = \frac{4*b_2*S_y^3}{3*E^2*\kappa^3} - \frac{b_2*S_y*\left(\gamma - \frac{S_y}{E}\right)^2}{\kappa^3} - \frac{b*S_y*\left(\gamma + \frac{S_y}{E}\right)^2}{\kappa^3}$$

$$\frac{\partial C_z}{\partial \gamma} = \frac{b_2*S_y*\left(\gamma - \frac{S_y}{E}\right)}{\kappa^2} + \frac{b*S_y*\left(\gamma + \frac{S_y}{E}\right)}{\kappa^2}$$

Case 10:

$$\frac{\partial C_x}{\partial \kappa} = -\frac{b_1*E*h_1^2}{2} - \frac{b*E*h_2^2}{2} + \frac{b_1*E*h_2^2}{2} + \frac{b*E*\gamma^2}{2*\kappa^2} - \frac{b*\gamma*S_y}{\kappa^2} + \frac{b*S_y^2}{2*E*\kappa^2}$$

$$\frac{\partial C_x}{\partial \gamma} = b_1 * E * h_1 + b * E * h_2 - b_1 * E * h_2 - \frac{b*E*\gamma}{\kappa} + \frac{b*S_y}{\kappa}$$

$$\frac{\partial C_z}{\partial \kappa} = -\frac{b_1*E*h_1^3}{3} - \frac{b*E*h_2^3}{3} + \frac{b_1*E*h_2^3}{3} + \frac{b*E*\gamma^3}{3*\kappa^3} - \frac{b*\gamma*S_y^2}{E*\kappa^3} + \frac{2*b*S_y^3}{3*E^2*\kappa^3} - \frac{b*S_y*\left(\gamma - \frac{S_y}{E}\right)^2}{\kappa^3}$$

$$\frac{\partial C_z}{\partial \gamma} = \frac{b_1*E*h_1^2}{2} + \frac{b*E*h_2^2}{2} - \frac{b_1*E*h_2^2}{2} - \frac{b*E*\gamma^2}{2*\kappa^2} + \frac{b*S_y^2}{2*E*\kappa^2} + \frac{b*S_y*\left(\gamma - \frac{S_y}{E}\right)}{\kappa^2}$$

Case 11:

$$\frac{\partial C_x}{\partial \kappa} = -\frac{b*E*h_2^2}{2} + \frac{b_1*E*h_2^2}{2} + \frac{b*E*\gamma^2}{2*\kappa^2} - \frac{b_1*E*\gamma^2}{2*\kappa^2} - \frac{b*\gamma*S_y}{\kappa^2} - \frac{b_1*\gamma*S_y}{\kappa^2} + \frac{b*S_y^2}{2*E*\kappa^2} - \frac{b_1*S_y^2}{2*E*\kappa^2}$$

$$\frac{\partial C_x}{\partial \gamma} = b * E * h_2 - b_1 * E * h_2 - \frac{b*E*\gamma}{\kappa} + \frac{b_1*E*\gamma}{\kappa} + \frac{b*S_y}{\kappa} + \frac{b_1*S_y}{\kappa}$$

$$\frac{\partial C_z}{\partial \kappa} = -\frac{b*E*h_2^3}{3} + \frac{b_1*E*h_2^3}{3} + \frac{b*E*\gamma^3}{3*\kappa^3} - \frac{b_1*E*\gamma^3}{3*\kappa^3} - \frac{b*\gamma*S_y^2}{E*\kappa^3} + \frac{b_1*\gamma*S_y^2}{E*\kappa^3} + \frac{2*b*S_y^3}{3*E^2*\kappa^3} + \frac{2*b_1*S_y^3}{3*E^2*\kappa^3} - \frac{b*S_y*\left(\gamma - \frac{S_y}{E}\right)^2}{\kappa^3} - \frac{b_1*S_y*\left(\gamma + \frac{S_y}{E}\right)^2}{\kappa^3}$$

$$\frac{\partial C_z}{\partial \gamma} = \frac{b*E*h_2^2}{2} - \frac{b_1*E*h_2^2}{2} - \frac{b*E*\gamma^2}{2*\kappa^2} + \frac{b_1*E*\gamma^2}{2*\kappa^2} + \frac{b*S_y^2}{2*E*\kappa^2} - \frac{b_1*S_y^2}{2*E*\kappa^2} + \frac{b*S_y*\left(\gamma - \frac{S_y}{E}\right)}{\kappa^2} + \frac{b_1*S_y*\left(\gamma + \frac{S_y}{E}\right)}{\kappa^2}$$

Case 12:

$$\frac{\partial C_x}{\partial \kappa} = \frac{-2*b*\gamma*S_y}{\kappa^2}$$

$$\frac{\partial C_x}{\partial \gamma} = \frac{2*b*S_y}{\kappa}$$

$$\frac{\partial C_z}{\partial \kappa} = \frac{4*b*S_y^3}{3*E^2*\kappa^3} - \frac{b*S_y*\left(\gamma - \frac{S_y}{E}\right)^2}{\kappa^3} - \frac{b*S_y*\left(\gamma + \frac{S_y}{E}\right)^2}{\kappa^3}$$

$$\frac{\partial C_z}{\partial \gamma} = \frac{b*S_y*\left(\gamma - \frac{S_y}{E}\right)}{\kappa^2} + \frac{b*S_y*\left(\gamma + \frac{S_y}{E}\right)}{\kappa^2}$$

Case 13:

$$\frac{\partial C_x}{\partial \kappa} = -\frac{b_1 * E * h_1^2}{2} + \frac{b_1 * E * \gamma^2}{2 * \kappa^2} - \frac{b_1 * \gamma * S_y}{\kappa^2} + \frac{b_1 * S_y^2}{2 * E * \kappa^2}$$

$$\frac{\partial C_x}{\partial \gamma} = b_1 * E * h_1 - \frac{b_1 * E * \gamma}{\kappa} + \frac{b_1 * S_y}{\kappa}$$

$$\frac{\partial C_z}{\partial \kappa} = -\frac{b_1 * E * h_1^3}{3} + \frac{b_1 * E * \gamma^3}{3 * \kappa^3} - \frac{b_1 * \gamma * S_y^2}{E * \kappa^3} + \frac{2 * b_1 * S_y^3}{3 * E^2 * \kappa^3} - \frac{b_1 * S_y * \left(\gamma - \frac{S_y}{E}\right)^2}{\kappa^3}$$

$$\frac{\partial C_z}{\partial \gamma} = \frac{b_1 * E * h_1^2}{2} - \frac{b_1 * E * \gamma^2}{2 * \kappa^2} + \frac{b_1 * S_y^2}{2 * E * \kappa^2} + \frac{b_1 * S_y * \left(\gamma - \frac{S_y}{E}\right)}{\kappa^2}$$

Case 14:

$$\frac{\partial C_x}{\partial \kappa} = \frac{-2 * b_1 * \gamma * S_y}{\kappa^2}$$

$$\frac{\partial C_x}{\partial \gamma} = \frac{2 * b_1 * S_y}{\kappa}$$

$$\frac{\partial C_z}{\partial \kappa} = \frac{4 * b_1 * S_y^3}{3 * E^2 * \kappa^3} - \frac{b_1 * S_y * \left(\gamma - \frac{S_y}{E}\right)^2}{\kappa^3} - \frac{b_1 * S_y * \left(\gamma + \frac{S_y}{E}\right)^2}{\kappa^3}$$

$$\frac{\partial C_z}{\partial \gamma} = \frac{b_1 * S_y * \left(\gamma - \frac{S_y}{E}\right)}{\kappa^2} + \frac{b_1 * S_y * \left(\gamma + \frac{S_y}{E}\right)}{\kappa^2}$$

Case 15:

$$\frac{\partial C_x}{\partial \kappa} = 0$$

$$\frac{\partial C_x}{\partial \gamma} = 0$$

$$\frac{\partial C_z}{\partial \kappa} = 0$$

$$\frac{\partial C_z}{\partial \gamma} = 0$$

A.2.2 Second-Order Derivatives:

Case 1:

$$\frac{\partial^2 C_x}{\partial \kappa^2} = 0$$

$$\frac{\partial^2 C_x}{\partial \gamma^2} = 0$$

$$\frac{\partial^2 C_x}{\partial \kappa \partial \gamma} = 0$$

$$\frac{\partial^2 C_z}{d\kappa^2} = 0$$

$$\frac{\partial^2 C_z}{\partial \gamma^2} = 0$$

$$\frac{\partial^2 C_z}{\partial \kappa \partial \gamma} = 0$$

Case 2:

$$\frac{\partial^2 C_x}{\partial \kappa^2} = \frac{b_1 * E * \gamma^2}{\kappa^3} - \frac{b_1 * S_y^2}{E * \kappa^3} + \frac{2 * b_1 * S_y * \left(\gamma + \frac{S_y}{E}\right)}{\kappa^3}$$

$$\frac{\partial^2 C_x}{\partial \gamma^2} = \frac{b_1 * E}{\kappa}$$

$$\frac{\partial^2 C_x}{\partial \kappa \partial \gamma} = -\left(\frac{b_1 * E * \gamma}{\kappa^2}\right) - \frac{b_1 * S_y}{\kappa^2}$$

$$\frac{\partial^2 C_z}{d\kappa^2} = \frac{b_1 * E * \gamma^3}{\kappa^4} - \frac{3 * b_1 * \gamma * S_y^2}{E * \kappa^4} - \frac{2 * b_1 * S_y^3}{E^2 * \kappa^4} + \frac{3 * b_1 * S_y * \left(\gamma + \frac{S_y}{E}\right)^2}{\kappa^4}$$

$$\frac{\partial^2 C_z}{\partial \gamma^2} = \frac{b_1 * E * \gamma}{\kappa^2} + \frac{b_1 * S_y}{\kappa^2}$$

$$\frac{\partial^2 C_z}{\partial \kappa \partial \gamma} = -\left(\frac{b_1 * E * \gamma^2}{\kappa^3}\right) + \frac{b_1 * S_y^2}{E * \kappa^3} - \frac{2 * b_1 * S_y * \left(\gamma + \frac{S_y}{E}\right)}{\kappa^3}$$

Case 3:

$$\frac{\partial^2 C_x}{\partial \kappa^2} = \frac{b * E * \gamma^2}{\kappa^3} - \frac{b * S_y^2}{E * \kappa^3} + \frac{2 * b * S_y * \left(\gamma + \frac{S_y}{E}\right)}{\kappa^3}$$

$$\frac{\partial^2 C_x}{\partial \gamma^2} = \frac{b * E}{\kappa}$$

$$\frac{\partial^2 C_x}{\partial \kappa \partial \gamma} = -\left(\frac{b * E * \gamma}{\kappa^2}\right) - \frac{b * S_y}{\kappa^2}$$

$$\frac{\partial^2 C_z}{d\kappa^2} = \frac{b*E*\gamma^3}{\kappa^4} - \frac{3*b*\gamma*S_y^2}{E*\kappa^4} - \frac{2*b*S_y^3}{E^2*\kappa^4} + \frac{3*b*S_y*\left(\gamma + \frac{S_y}{E}\right)^2}{\kappa^4}$$

$$\frac{\partial^2 C_z}{\partial\gamma^2} = \frac{b*E*\gamma}{\kappa^2} + \frac{b*S_y}{\kappa^2}$$

$$\frac{\partial^2 C_z}{\partial\kappa\partial\gamma} = -\left(\frac{b*E*\gamma^2}{\kappa^3}\right) + \frac{b*S_y^2}{E*\kappa^3} - \frac{2*b*S_y*\left(\gamma + \frac{S_y}{E}\right)}{\kappa^3}$$

Case 4:

$$\frac{\partial^2 C_x}{\partial\kappa^2} = \frac{b_2*E*\gamma^2}{\kappa^3} - \frac{b_2*S_y^2}{E*\kappa^3} + \frac{2*b_2*S_y*\left(\gamma + \frac{S_y}{E}\right)}{\kappa^3}$$

$$\frac{\partial^2 C_x}{\partial\gamma^2} = \frac{b_2*E}{\kappa}$$

$$\frac{\partial^2 C_x}{\partial\kappa\partial\gamma} = -\left(\frac{b_2*E*\gamma}{\kappa^2}\right) - \frac{b_2*S_y}{\kappa^2}$$

$$\frac{\partial^2 C_z}{d\kappa^2} = \frac{b_2*E*\gamma^3}{\kappa^4} - \frac{3*b_2*\gamma*S_y^2}{E*\kappa^4} - \frac{2*b_2*S_y^3}{E^2*\kappa^4} + \frac{3*b_2*S_y*\left(\gamma + \frac{S_y}{E}\right)^2}{\kappa^4}$$

$$\frac{\partial^2 C_z}{\partial \gamma^2} = \frac{b_2 * E * \gamma}{\kappa^2} + \frac{b_2 * S_y}{\kappa^2}$$

$$\frac{\partial^2 C_z}{\partial \kappa \partial \gamma} = -\left(\frac{b_2 * E * \gamma^2}{\kappa^3}\right) + \frac{b_2 * S_y^2}{E * \kappa^3} - \frac{2 * b_2 * S_y * \left(\gamma + \frac{S_y}{E}\right)}{\kappa^3}$$

Case 5:

$$\frac{\partial^2 C_x}{\partial \kappa^2} = 0$$

$$\frac{\partial^2 C_x}{\partial \gamma^2} = 0$$

$$\frac{\partial^2 C_x}{\partial \kappa \partial \gamma} = 0$$

$$\frac{\partial^2 C_z}{d \kappa^2} = 0$$

$$\frac{\partial^2 C_z}{\partial \gamma^2} = 0$$

$$\frac{\partial^2 C_z}{\partial \kappa \partial \gamma} = 0$$

Case 6:

$$\frac{\partial^2 C_x}{\partial \kappa^2} = -\left(\frac{b_2 * E * \gamma^2}{\kappa^3}\right) + \frac{b_2 * S_y^2}{E * \kappa^3} - \frac{2 * b_2 * S_y * \left(-\gamma + \frac{S_y}{E}\right)}{\kappa^3}$$

$$\frac{\partial^2 C_x}{\partial \gamma^2} = -\left(\frac{b_2 * E}{\kappa}\right)$$

$$\frac{\partial^2 C_x}{\partial \kappa \partial \gamma} = \frac{b_2 * E * \gamma}{\kappa^2} - \frac{b_2 * S_y}{\kappa^2}$$

$$\frac{\partial^2 C_z}{d\kappa^2} = -\left(\frac{b_2 * E * \gamma^3}{\kappa^4}\right) + \frac{3 * b_2 * \gamma * S_y^2}{E * \kappa^4} - \frac{2 * b_2 * S_y^3}{E^2 * \kappa^4} + \frac{3 * b_2 * S_y * \left(\gamma - \frac{S_y}{E}\right)^2}{\kappa^4}$$

$$\frac{\partial^2 C_z}{\partial \gamma^2} = -\left(\frac{b_2 * E * \gamma}{\kappa^2}\right) + \frac{b_2 * S_y}{\kappa^2}$$

$$\frac{\partial^2 C_z}{\partial \kappa \partial \gamma} = \frac{b_2 * E * \gamma^2}{\kappa^3} - \frac{b_2 * S_y^2}{E * \kappa^3} - \frac{2 * b_2 * S_y * \left(\gamma - \frac{S_y}{E}\right)}{\kappa^3}$$

Case 7:

$$\frac{\partial^2 C_x}{\partial \kappa^2} = \frac{b_1 * E * \gamma^2}{\kappa^3} - \frac{b_2 * E * \gamma^2}{\kappa^3} - \frac{b_1 * S_y^2}{E * \kappa^3} + \frac{b_2 * S_y^2}{E * \kappa^3} - \frac{2 * b_2 * S_y * \left(-\gamma + \frac{S_y}{E}\right)}{\kappa^3} + \frac{2 * b_1 * S_y * \left(\gamma + \frac{S_y}{E}\right)}{\kappa^3}$$

$$\frac{\partial^2 C_x}{\partial \gamma^2} = \frac{b_1 * E}{\kappa} - \frac{b_2 * E}{\kappa}$$

$$\frac{\partial^2 C_x}{\partial \kappa \partial \gamma} = -\left(\frac{b_1 * E * \gamma}{\kappa^2}\right) + \frac{b_2 * E * \gamma}{\kappa^2} - \frac{b_1 * S_y}{\kappa^2} - \frac{b_2 * S_y}{\kappa^2}$$

$$\frac{\partial^2 C_z}{d \kappa^2} = \frac{b_1 * E * \gamma^3}{\kappa^4} - \frac{b_2 * E * \gamma^3}{\kappa^4} - \frac{3 * b_1 * \gamma * S_y^2}{E * \kappa^4} + \frac{3 * b_2 * \gamma * S_y^2}{E * \kappa^4} - \frac{2 * b_1 * S_y^3}{E^2 * \kappa^4} - \frac{2 * b_2 * S_y^3}{E^2 * \kappa^4} + \frac{3 * b_2 * S_y * \left(\gamma - \frac{S_y}{E}\right)^2}{\kappa^4} + \frac{3 * b_1 * S_y * \left(\gamma + \frac{S_y}{E}\right)^2}{\kappa^4}$$

$$\frac{\partial^2 C_z}{\partial \gamma^2} = \frac{b_1 * E * \gamma}{\kappa^2} - \frac{b_2 * E * \gamma}{\kappa^2} + \frac{b_1 * S_y}{\kappa^2} + \frac{b_2 * S_y}{\kappa^2}$$

$$\frac{\partial^2 C_z}{\partial \kappa \partial \gamma} = -\left(\frac{b_1 * E * \gamma^2}{\kappa^3}\right) + \frac{b_2 * E * \gamma^2}{\kappa^3} + \frac{b_1 * S_y^2}{E * \kappa^3} - \frac{b_2 * S_y^2}{E * \kappa^3} - \frac{2 * b_2 * S_y * \left(\gamma - \frac{S_y}{E}\right)}{\kappa^3} - \frac{2 * b_1 * S_y * \left(\gamma + \frac{S_y}{E}\right)}{\kappa^3}$$

Case 8:

$$\frac{\partial^2 C_x}{\partial \kappa^2} = \frac{b*E*\gamma^2}{\kappa^3} - \frac{b_2*E*\gamma^2}{\kappa^3} - \frac{b*S_y^2}{E*\kappa^3} + \frac{b_2*S_y^2}{E*\kappa^3} - \frac{2*b_2*S_y*\left(-\gamma + \frac{S_y}{E}\right)}{\kappa^3} + \frac{2*b*S_y*\left(\gamma + \frac{S_y}{E}\right)}{\kappa^3}$$

$$\frac{\partial^2 C_x}{\partial \gamma^2} = \frac{b*E}{\kappa} - \frac{b_2*E}{\kappa}$$

$$\frac{\partial^2 C_x}{\partial \kappa \partial \gamma} = -\left(\frac{b*E*\gamma}{\kappa^2}\right) + \frac{b_2*E*\gamma}{\kappa^2} - \frac{b*S_y}{\kappa^2} - \frac{b_2*S_y}{\kappa^2}$$

$$\frac{\partial^2 C_z}{d\kappa^2} = \frac{b*E*\gamma^3}{\kappa^4} - \frac{b_2*E*\gamma^3}{\kappa^4} - \frac{3*b*\gamma*S_y^2}{E*\kappa^4} + \frac{3*b_2*\gamma*S_y^2}{E*\kappa^4} - \frac{2*b*S_y^3}{E^2*\kappa^4} - \frac{2*b_2*S_y^3}{E^2*\kappa^4} + \frac{3*b_2*S_y*\left(\gamma - \frac{S_y}{E}\right)^2}{\kappa^4} + \frac{3*b*S_y*\left(\gamma + \frac{S_y}{E}\right)^2}{\kappa^4}$$

$$\frac{\partial^2 C_z}{\partial \gamma^2} = \frac{b*E*\gamma}{\kappa^2} - \frac{b_2*E*\gamma}{\kappa^2} + \frac{b*S_y}{\kappa^2} + \frac{b_2*S_y}{\kappa^2}$$

$$\frac{\partial^2 C_z}{\partial \kappa \partial \gamma} = -\left(\frac{b*E*\gamma^2}{\kappa^3}\right) + \frac{b_2*E*\gamma^2}{\kappa^3} + \frac{b*S_y^2}{E*\kappa^3} - \frac{b_2*S_y^2}{E*\kappa^3} - \frac{2*b_2*S_y*\left(\gamma - \frac{S_y}{E}\right)}{\kappa^3} - \frac{2*b*S_y*\left(\gamma + \frac{S_y}{E}\right)}{\kappa^3}$$

Case 9:

$$\frac{\partial^2 C_x}{\partial \kappa^2} = \frac{-2*b_2*S_y*\left(-\gamma+\frac{S_y}{E}\right)}{\kappa^3} + \frac{2*b*S_y*\left(\gamma+\frac{S_y}{E}\right)}{\kappa^3}$$

$$\frac{\partial^2 C_x}{\partial \gamma^2} = 0$$

$$\frac{\partial^2 C_x}{\partial \kappa \partial \gamma} = -\left(\frac{b*S_y}{\kappa^2}\right) - \frac{b_2*S_y}{\kappa^2}$$

$$\frac{\partial^2 C_z}{d\kappa^2} = \frac{-4*b_2*S_y^3}{E^2*\kappa^4} + \frac{3*b_2*S_y*\left(\gamma-\frac{S_y}{E}\right)^2}{\kappa^4} + \frac{3*b*S_y*\left(\gamma+\frac{S_y}{E}\right)^2}{\kappa^4}$$

$$\frac{\partial^2 C_z}{\partial \gamma^2} = \frac{b*S_y}{\kappa^2} + \frac{b_2*S_y}{\kappa^2}$$

$$\frac{\partial^2 C_z}{\partial \kappa \partial \gamma} = \frac{-2*b_2*S_y*\left(\gamma-\frac{S_y}{E}\right)}{\kappa^3} - \frac{2*b*S_y*\left(\gamma+\frac{S_y}{E}\right)}{\kappa^3}$$

Case 10:

$$\frac{\partial^2 C_x}{\partial \kappa^2} = -\left(\frac{b*E*\gamma^2}{\kappa^3}\right) + \frac{b*S_y^2}{E*\kappa^3} - \frac{2*b*S_y*\left(-\gamma+\frac{S_y}{E}\right)}{\kappa^3}$$

$$\frac{\partial^2 C_x}{\partial \gamma^2} = -\left(\frac{b*E}{\kappa}\right)$$

$$\frac{\partial^2 C_x}{\partial \kappa \partial \gamma} = \frac{b*E*\gamma}{\kappa^2} - \frac{b*S_y}{\kappa^2}$$

$$\frac{\partial^2 C_z}{d\kappa^2} = -\left(\frac{b*E*\gamma^3}{\kappa^4}\right) + \frac{3*b*\gamma*S_y^2}{E*\kappa^4} - \frac{2*b*S_y^3}{E^2*\kappa^4} + \frac{3*b*S_y*\left(\gamma - \frac{S_y}{E}\right)^2}{\kappa^4}$$

$$\frac{\partial^2 C_z}{\partial \gamma^2} = -\left(\frac{b*E*\gamma}{\kappa^2}\right) + \frac{b*S_y}{\kappa^2}$$

$$\frac{\partial^2 C_z}{\partial \kappa \partial \gamma} = \frac{b*E*\gamma^2}{\kappa^3} - \frac{b*S_y^2}{E*\kappa^3} - \frac{2*b*S_y*\left(\gamma - \frac{S_y}{E}\right)}{\kappa^3}$$

Case 11:

$$\frac{\partial^2 C_x}{\partial \kappa^2} = -\left(\frac{b*E*\gamma^2}{\kappa^3}\right) + \frac{b_1*E*\gamma^2}{\kappa^3} + \frac{b*S_y^2}{E*\kappa^3} - \frac{b_1*S_y^2}{E*\kappa^3} - \frac{2*b*S_y*\left(-\gamma + \frac{S_y}{E}\right)}{\kappa^3} + \frac{2*b_1*S_y*\left(\gamma + \frac{S_y}{E}\right)}{\kappa^3}$$

$$\frac{\partial^2 C_x}{\partial \gamma^2} = -\left(\frac{b*E}{\kappa}\right) + \frac{b_1*E}{\kappa}$$

$$\frac{\partial^2 C_x}{\partial \kappa \partial \gamma} = \frac{b*E*\gamma}{\kappa^2} - \frac{b_1*E*\gamma}{\kappa^2} - \frac{b*S_y}{\kappa^2} - \frac{b_1*S_y}{\kappa^2}$$

$$\frac{\partial^2 C_z}{d\kappa^2} = -\left(\frac{b*E*\gamma^3}{\kappa^4}\right) + \frac{b_1*E*\gamma^3}{\kappa^4} + \frac{3*b*\gamma*S_y^2}{E*\kappa^4} - \frac{3*b_1*\gamma*S_y^2}{E*\kappa^4} - \frac{2*b*S_y^3}{E^2*\kappa^4} - \frac{2*b_1*S_y^3}{E^2*\kappa^4} + \frac{3*b*S_y*\left(\gamma - \frac{S_y}{E}\right)^2}{\kappa^4} + \frac{3*b_1*S_y*\left(\gamma + \frac{S_y}{E}\right)^2}{\kappa^4}$$

$$\frac{\partial^2 C_z}{\partial \gamma^2} = -\left(\frac{b*E*\gamma}{\kappa^2}\right) + \frac{b_1*E*\gamma}{\kappa^2} + \frac{b*S_y}{\kappa^2} + \frac{b_1*S_y}{\kappa^2}$$

$$\frac{\partial^2 C_z}{\partial \kappa \partial \gamma} = \frac{b*E*\gamma^2}{\kappa^3} - \frac{b_1*E*\gamma^2}{\kappa^3} - \frac{b*S_y^2}{E*\kappa^3} + \frac{b_1*S_y^2}{E*\kappa^3} - \frac{2*b*S_y*\left(\gamma - \frac{S_y}{E}\right)}{\kappa^3} - \frac{2*b_1*S_y*\left(\gamma + \frac{S_y}{E}\right)}{\kappa^3}$$

Case 12:

$$\frac{\partial^2 C_x}{\partial \kappa^2} = \frac{-2*b*S_y*\left(-\gamma + \frac{S_y}{E}\right)}{\kappa^3} + \frac{2*b*S_y*\left(\gamma + \frac{S_y}{E}\right)}{\kappa^3}$$

$$\frac{\partial^2 C_x}{\partial \gamma^2} = 0$$

$$\frac{\partial^2 C_x}{\partial \kappa \partial \gamma} = \frac{-2*b*S_y}{\kappa^2}$$

$$\frac{\partial^2 C_z}{d\kappa^2} = \frac{-4*b*S_y^3}{E^2*\kappa^4} + \frac{3*b*S_y*\left(\gamma - \frac{S_y}{E}\right)^2}{\kappa^4} + \frac{3*b*S_y*\left(\gamma + \frac{S_y}{E}\right)^2}{\kappa^4}$$

$$\frac{\partial^2 C_z}{\partial\gamma^2} = \frac{2*b*S_y}{\kappa^2}$$

$$\frac{\partial^2 C_z}{\partial\kappa\partial\gamma} = \frac{-2*b*S_y*\left(\gamma - \frac{S_y}{E}\right)}{\kappa^3} - \frac{2*b*S_y*\left(\gamma + \frac{S_y}{E}\right)}{\kappa^3}$$

Case 13:

$$\frac{\partial^2 C_x}{\partial\kappa^2} = -\left(\frac{b_1*E*\gamma^2}{\kappa^3}\right) + \frac{b_1*S_y^2}{E*\kappa^3} - \frac{2*b_1*S_y*\left(-\gamma + \frac{S_y}{E}\right)}{\kappa^3}$$

$$\frac{\partial^2 C_x}{\partial\gamma^2} = -\left(\frac{b_1*E}{\kappa}\right)$$

$$\frac{\partial^2 C_x}{\partial\kappa\partial\gamma} = \frac{b_1*E*\gamma}{\kappa^2} - \frac{b_1*S_y}{\kappa^2}$$

$$\frac{\partial^2 C_z}{d\kappa^2} = -\left(\frac{b_1*E*\gamma^3}{\kappa^4}\right) + \frac{3*b_1*\gamma*S_y^2}{E*\kappa^4} - \frac{2*b_1*S_y^3}{E^2*\kappa^4} + \frac{3*b_1*S_y*\left(\gamma - \frac{S_y}{E}\right)^2}{\kappa^4}$$

$$\frac{\partial^2 C_z}{\partial \gamma^2} = -\left(\frac{b_1 * E * \gamma}{\kappa^2}\right) + \frac{b_1 * S_y}{\kappa^2}$$

$$\frac{\partial^2 C_z}{\partial \kappa \partial \gamma} = \frac{b_1 * E * \gamma^2}{\kappa^3} - \frac{b_1 * S_y^2}{E * \kappa^3} - \frac{2 * b_1 * S_y * \left(\gamma - \frac{S_y}{E}\right)}{\kappa^3}$$

Case 14:

$$\frac{\partial^2 C_x}{\partial \kappa^2} = \frac{-2 * b_1 * S_y * \left(-\gamma + \frac{S_y}{E}\right)}{\kappa^3} + \frac{2 * b_1 * S_y * \left(\gamma + \frac{S_y}{E}\right)}{\kappa^3}$$

$$\frac{\partial^2 C_x}{\partial \gamma^2} = 0$$

$$\frac{\partial^2 C_x}{\partial \kappa \partial \gamma} = \frac{-2 * b_1 * S_y}{\kappa^2}$$

$$\frac{\partial^2 C_z}{d \kappa^2} = \frac{-4 * b_1 * S_y^3}{E^2 * \kappa^4} + \frac{3 * b_1 * S_y * \left(\gamma - \frac{S_y}{E}\right)^2}{\kappa^4} + \frac{3 * b_1 * S_y * \left(\gamma + \frac{S_y}{E}\right)^2}{\kappa^4}$$

$$\frac{\partial^2 C_z}{\partial \gamma^2} = \frac{2 * b_1 * S_y}{\kappa^2}$$

$$\frac{\partial^2 C_z}{\partial \kappa \partial \gamma} = \frac{-2*b_1*S_y*\left(\gamma - \frac{S_y}{E}\right)}{\kappa^3} - \frac{2*b_1*S_y*\left(\gamma + \frac{S_y}{E}\right)}{\kappa^3}$$

Case 15:

$$\frac{\partial^2 C_x}{\partial \kappa^2} = 0$$

$$\frac{\partial^2 C_x}{\partial \gamma^2} = 0$$

$$\frac{\partial^2 C_x}{\partial \kappa \partial \gamma} = 0$$

$$\frac{\partial^2 C_z}{d \kappa^2} = 0$$

$$\frac{\partial^2 C_z}{\partial \gamma^2} = 0$$

$$\frac{\partial^2 C_z}{\partial \kappa \partial \gamma} = 0$$

A.3 ANNEX C

ADDITIONAL RESULTS OF RBDO

Load = 2.0E5 N COV = 0.01	Design variable (mm)						Ultimate load (N)	Objective function	Reliability index	Probability of failure
	b	t	h_w	t_w	b_f	t_f	P_u	Area (mm^2)	β_0	P_f
Lower limit $\bar{X}_{min}$	200.0	10.0	80.0	5.0	30.0	5.0	2.7616E5	2550.00	1.4356	0.0756
Upper limit $\bar{X}_{max}$	400.0	15.0	120.0	10.0	50.0	10.0	1.1077E6	7700.00	7.92386	1.1512E-15
Initial value $\bar{X}_0$	300.0	12.5	100.0	7.5	40.0	7.5	6.1657E5	4800.00	5.8010	3.2965E-9
Deterministic optimum design	200.0	10.0	120.0	7.7	50.0	10.0	6.1657E5	3425.95	6.3484	1.0881E-10
RBDO design	200.0	10.0	120.0	5.0	49.3	10.0	5.4545E5	3093.11	5.8010	3.2965E-9
RBDO with different reliability limit	200.0	10.0	88.1	5.0	30.0	5.0	3.0488E5	2590.68	2.0	0.0228
	200.0	10.0	103.2	5.0	30.0	5.0	3.5440E5	2665.94	3.0	0.0013
	200.0	10.0	120.0	5.0	30.0	5.0	4.0690E5	2751.24	4.0	3.1671E-5
	200.0	10.0	120.0	5.0	50.0	9.9	5.4608E5	2897.60	5.0	2.8665E-7
	200.0	10.0	120.0	5.8	50.0	10.0	5.6821E5	3197.05	6.0	9.8659E-10
	200.0	10.0	120.0	8.5	50.0	10.0	6.3617E5	3525.13	6.5	4.0160E-11
	200.0	12.4	120.0	10.0	50.0	10.0	7.4023E5	4187.83	7.0	1.2798E-12
	254.3	15.0	120.0	10.0	50.0	10.0	9.0207E5	5513.80	7.5	3.1909E-14

Load = 2.0E5 N COV = 0.2	Design variable (mm)						Ultimate load (N)	Objective function	Reliability index	Probability of failure
	b	t	h_w	t_w	b_f	t_f	P_u	Area (mm^2)	β_0	P_f
Lower limit $\bar{X}_{min}$	200.0	10.0	80.0	5.0	30.0	5.0	2.7616E5	2550.00	1.0713	0.142
Upper limit $\bar{X}_{max}$	400.0	15.0	120.0	10.0	50.0	10.0	1.1077E6	7700.00	7.0903	6.6906E-13
Initial value $\bar{X}_0$	300.0	12.5	100.0	7.5	40.0	7.5	6.1657E5	4800.00	4.4827	3.6857E-6
Deterministic optimum design	200.0	10.0	120.0	7.7	50.0	10.0	6.1657E5	3425.95	5.0725	1.9633E-7
RBDO with same reliability limit	200.0	10.0	120.0	5.1	50.0	10.0	5.5037E5	3107.43	4.4827	3.6857E-6
RBDO with different reliability limit	200.0	10.0	100.1	5.0	30.0	5.0	3.4525E5	2650.34	2.0	0.0228
	200.0	10.0	120.0	5.0	30.0	6.0	4.2155E5	2781.35	3.0	0.0013
	200.0	10.0	120.0	5.0	37.9	10.0	5.0522E5	2978.95	4.0	3.1671E-5
	200.0	10.0	120.0	7.3	50.0	10.0	6.0612E5	3377.55	5.0	2.8665E-7
	200.0	10.0	120.0	9.8	50.0	10.0	6.6847E5	3681.34	5.5	1.8990E-8
	200.0	13.2	120.0	10.0	50.0	10.0	7.6185E5	4343.01	6.0	9.8659E-10
	241.4	15.0	120.0	10.0	50.0	10.0	8.8098E5	5320.29	6.5	4.0160E-11